# Chemical Investigations of Graphene

**A THESIS**
**SUBMITTED FOR DEGREE OF**

## Master of Science [Engg.]

**By**
**Gopalakrishnan K.**


**Chemistry and Physics of Materials Unit**

**Jawaharlal Nehru Centre for Advanced Scientific Research**

**(A Deemed University)**

**Bangalore-560064**

**August-2012**

**Dedicated**

**To**

**GRANDMA**

# Declaration

I hereby declare that the matter embodied in this thesis entitled ***"Chemical Investigations of Graphene"*** is the result of investigations carried out by me under the supervision of Prof. C. N. R. Rao, FRS at the Chemistry and Physics of Materials Unit, Jawaharlal Nehru Centre for Advanced Scientific Research, Bangalore, India and that it has not been submitted elsewhere for the award of any degree or diploma.

In keeping with the general practice in reporting scientific observations, due acknowledgement has been made whenever the work described is based on the findings of other investigators.

_____

Gopalakrishnan K.

# CERTIFICATE

I hereby certify that the matter embodied in this thesis entitled ***"Chemical Investigations of Graphene"*** has been carried out by Mr. Gopalakrishnan K. at the Chemistry and Physics of Materials Unit, Jawaharlal Nehru Centre for Advanced Scientific Research, Bangalore, India under my supervision and that it has not been submitted elsewhere for the award of any degree or diploma.

_____

Prof. C. N. R. Rao, FRS

(Research Supervisor)

# Acknowlegments

I am extremely thankful to Prof. C. N. R. Rao, FRS and I take this opportunity to express my immense gratitude to him. He not only introduced me to the fascinating field of Material Science but also has helped me with his invaluable guidance and constant encouragement. He has taught me the various facts of science, the way of understanding the problem and how to maintain levelheaded approach when problems do not work.

My deepest thanks to Mrs. Indumati Rao and Mr. Sanjay for their affection and hospitality.

I would like to express my sincere thanks to Dr. A. Govindaraj who has helped me a great deal in carrying out the various experiments. It has been a good learning experience working with him in the lab.

I am grateful to the administration of JNCASR, especially present and past CPMU chairmen, Prof. S. Balasubramanian and Prof. G. U. Kulkarni, chairman of NCU Prof. C. N. R. Rao, for allowing me to use all the facilities in JNCASR required for my experimental work.

I am thankful to Usha Madam, Anil, Vasu, Selvi, Dr. Karthik, (TEM), Dr. Basavaraj (VEECO), Kishore (XPS) and Mahesh for their help with the various characterization techniques. I thank Srinath for his technical help.

I would like to thank Dr. A. Gomathi, Dr. K. S. Subrahmanyam, Dr. L. S. Panchakarla, Dr. Prashant Kumar, Dr. Joshi, Dr. Shashi, Dr. Barun Das and Mr. Moses for working with me in different research problems.

I would like thank Mr. K. V. Rao for elemental analysis and GC-MS.

I thank Mrs. Shashi, Mrs. Sudha, Mrs. Aruna (ICMS), Mr. Gowda and Mr. Victor for their help.

I am thankful to all academic staff members (Mrs. Sukanya, Dr. Princy) and administrative staff for their support, in particular senior administrative officer A.N. Jayachandra.

I am thankful to all computer lab staff members for their help.

I am thankful to all work shop members (Arogyanathan, Moorthy and Sunil).

I would like to thank all my past and present lab mates, Dr. Gomathi, Dr. Subrahmanyam, Dr. Leela, Dr. Rakesh, , Dr. Neenu, Dr. Anupama, Dr. Prashant, , Dr. Sandeep, Dr. Barun, Basant, Dr. Claudy, Dr. Latte, Dr. Jyoti, Dr. Kalyan, Ramakrishna, Urmi, Nitesh, Moses, Dr. Sashi, Dr. Sundarayya, Dr. Biswas, Dr. Naidu, Pramoda, Sunita, Rana, Govind, Ram, Utham, Monali and Ajmala, for their constant cheerful company and help in various occasions.

I would like to thank Mrs. G. L. Vidaya Barathi, my teacher, who has been giving constant encouragement and suggestions in my life.

I thank all my lab mates and friends from the core of my heart for their fruitful discussions.

Above all, I would like to thank my family, specially my parents, my aunt, uncle, and my grandmother for all the love, affection and support they gave. They stood by me whenever I felt depressed and led me to find out the correct way.

# PREFACE

The thesis consists of five chapters of which the first chapter is a brief overview of graphene. Chapter 2 deals with chlorination and bromination of graphene and shows how a reversible chemical storage of halogens can be achieved in graphene. Synthesis of nitrogen-doped graphene by the urea route is presented in Chapter 3. This chapter also consists of synthesis of acid-functionalized graphene with interesting acidic properties.

In Chapter 4, selectivity in the photocatalytic activity of the nanocomposites of $TiO_2$nanoparticles with N- and B-doped graphenes is described. The catalytic activity of the nanocomposites with N- and B-doped graphene is found to be high with electron acceptor and donor molecules respectively. Interaction of electron-donor and -acceptor molecules with chemically doped graphene has been studied by Raman spectroscopy and presented in Chapter 5.

# CONTENTS

**3.1 Nitrogen doped graphene**



**3.2 Acid-functionalized graphene**



**CHAPTER 4: SELECTIVITY IN THE PHOTOCATALYTIC PROPERTIES OF THE COMPOSITES OF $TiO_2$ NANOPARTICLES WITH B- AND N-DOPED GRAPHENES**

# CHAPTER 1

# GRAPHENE: AN OVERVIEW

## 1.1 Nature of graphene and related aspects

### 1.1.1 Allotropes of carbon

Carbon is one of the most interesting elements in the periodic table and it plays a unique role in nature. Carbon has the ability to form very long chains of interconnecting C-C bonds which is known as catenation. Due to catenation, carbon forms the highest number of compounds compared to any other element. The capability of carbon atoms to form complicated networks[1] is fundamental to organic chemistry and forms the basis for the existence of life. Elemental carbon forms many allotropes (Figure 1) such as diamond, graphite, fullerenes[2-4] and nanotubes.[5]

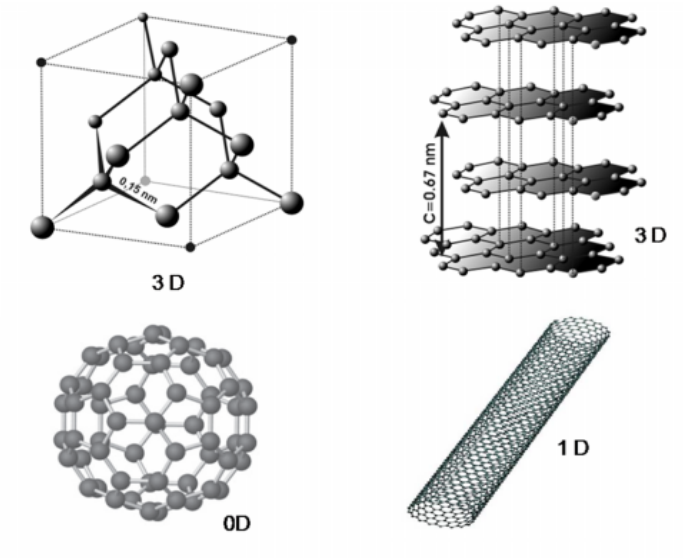


**Figure 1.** *3D, 1D and 0D allotropes of carbon.*

### 1.1.2 Brief history of graphene

The two-dimensional form of carbon called graphene (or '2D graphite') is the mother of all graphitic forms. It is a single-layer of carbon atoms tightly packed into a honeycomb lattice which can be either wrapped up into 0D fullerenes, rolled into 1D nanotubes or stacked into 3D graphite (Figure 2). Although there has been a great surge in graphene research recently, graphene-related materials produced from graphite oxide (GO) were already reported in 1962, and the chemical modifications of graphite were performed as early as 1840. In the 1940s[6] a number of theoretical studies suggested that the graphitic layers in their isolated form might exhibit extraordinary characteristics.

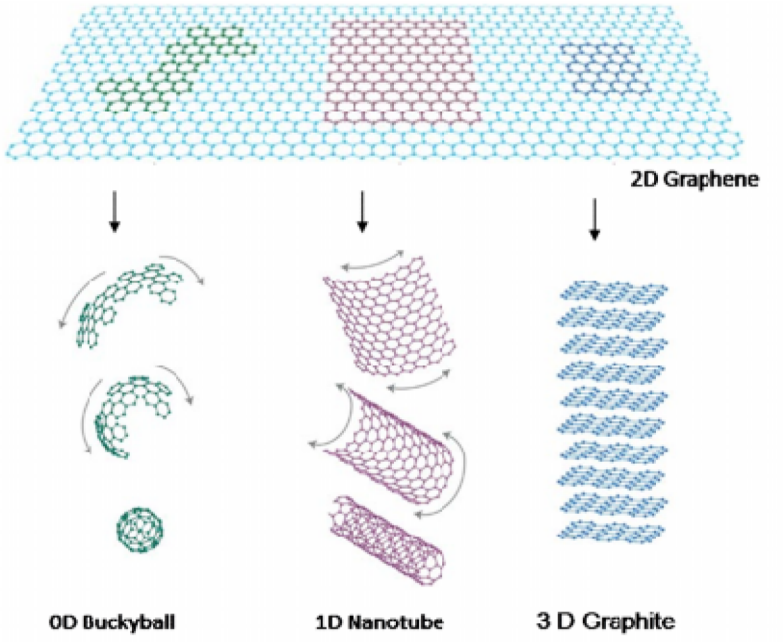


**Figure 2.** *Mother of all graphitic forms. (From ref. [14]).*

Following the theoretical studies, later, several researchers made attempts to prepare graphene by employing different procedures like thermal deflagration of GO, mechanical

exfoliation of GO followed by reduction,[7] sublimation of silicon from single crystals of silicon carbide (0001),[8] and by micromechanical approach.[9,10] Most of these procedures resulted in multi-layered graphene and the products were not characterized properly. In 2004 Geim and co-workers employed the same "micro-mechanical approach" reported by Roscoe *et al*.[10] and found that the approach enables the generation of extremely thin graphene films with a single layer or few layers.[11-13] The graphene samples have been characterized by a variety of microscopic and other physical techniques like atomic force microscopy (AFM), transmission electron microscopy (TEM), scanning tunnelling microscopy (STM) and Raman spectroscopy.[14] It has been showed that graphene is a two-dimensional semi-metal with a tiny overlap between valence and conductance bands. Graphene exhibits a strong ambipolar electric field effect with very high concentrations of electrons and holes, up to $10^{13}/cm^2$ and room-temperature mobilities of ~10,000 $cm^2/V.s$ (Figure 3).[11] It is interesting that single-layer graphene placed on a silicon wafer with a 300 nm thick layer of $SiO_2$, becomes visible in an optical microscope.[15]

### 1.1.3 Types of graphene

Graphene can be classified as three types: single-, double- and few- (3 to <10) layer graphenes. Films containing more than 10 layers can be considered as thin films of graphite. It was shown that the electronic structure of graphene rapidly evolves with the number of layers, approaching the 3D limit of graphite at 10 layers.[16] Moreover, only single- and bi- layer graphenes have simple electronic spectra: they are both zero-gap

semiconductors (they can also be referred to as zero-overlap semimetals) with a single type of electrons and holes.

After more than two layers, the spectra become increasingly complicated by the overlapping of the conduction and valence bands[16] and thus by the appearance of several types of charge carriers.

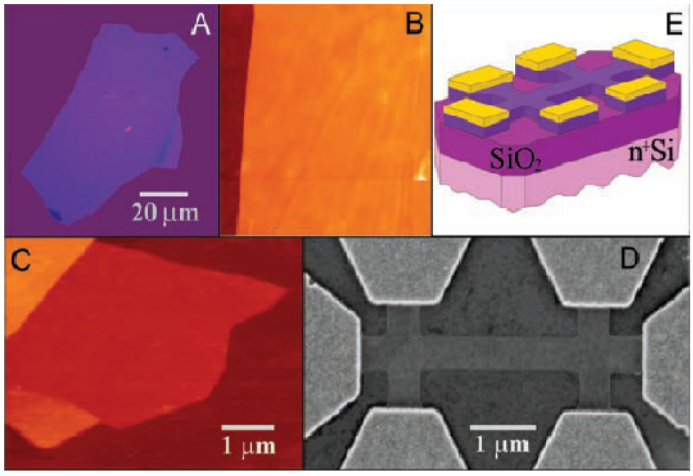


**Figure 3.** *Graphene films. (A) Photograph (in normal white light) of a relatively large multilayer graphene flake with thickness ~3 nm on top of an oxidized Si wafer. (B) Atomic force microscope (AFM) image of 2 μm by 2 μm area of this flake near its edge. Colors: dark brown, $SiO_2$ surface; orange, 3 nm height above the $SiO_2$ surface. (C) AFM image of single-layer graphene. Colors: dark brown, $SiO_2$ surface; brown-red (central area), 0.8 nm height; yellow-brown (bottom left), 1.2 nm; orange (top left), 2.5 nm. Notice the folded part of the film near the bottom, which exhibits a differential height of ~0.4 nm. (D) Scanning electron microscope image of an experimental device prepared from FLG. (E) Schematic view of the device in (D). (From ref. [11]).*

### 1.1.4 Synthesis of Graphene

At the beginning, the graphene fabrication is micromechanical cleavage from graphite, it is also the method that graphene was first isolated for property study. This way is often referred to as a scotch-tape technique, which relies on destroying Van der Waals force between graphite layers. Geim's group first isolated graphene from platelets of highly oriented pyrolytic graphite (HOPG).[11] The next method for graphene fabrication is chemical cleavage from graphite, which is an improvement of micromechanical cleavage. Graphene made from chemical cleavage can reap larger quantities. The single sheet is fabricated from graphite oxide. Due to the existence of oxide groups, the atomic planes of graphite are partially detached by intercalation. After ultrasonication for several hours, these samples are exfoliated to create stable aqueous dispersions of individual sheets. After deposition, graphene oxide can be reduced to graphene either by means of chemical or by thermal annealing.[17] Although the thickness is not consistent, which varies between one and four layers of carbon, the optical properties still match to those of graphene fabricated by micromechanical cleavage method. The small scale size, in tens of microns however, hinders the application of graphene by this method.

The graphene grown epitaxially on SiC substrates and patterned via standard lithographic procedures has been proposed as a platform for carbon-based nanoelectronics and molecular electronics in recent studies.[18,19] The epitaxial graphene was produced on the Si terminated (0001) facet of single-crystal 6H-SiC by thermal desorption of Si.[20] After the surface is oxidized or reduced in $H_2$, samples are heated by electron bombardment in ultrahigh vacuum ($1.33 \times 10^{-8}$ Pa) to 1000°C and remove the oxide. Then, samples are

heated again to temperatures in the range of 1250°C to 1450°C for 1–20 min. After these processes, thin graphene layers are formed, and the layer thickness is determined predominantly by the temperature.[18] The shortcoming of the epitaxial graphene on SiC is presence of large number of defects in the layer besides it hard to transfer to other substrates.

Chemical vapour deposition (CVD) has the potential for large-area production. Graphene made by CVD on silicon wafer with nickel layer as catalyst has achieved the lateral dimensions centimetre in size. Groups at MIT and in Korea[21,22] have developed a simple method to grow and transfer the high-quality stretchable graphene films using CVD technology on nickel layer. The mechanism is based on precipitation of cabron, where Ni and C atoms form a solid solution in CVD after heating. Since the solubility of C in Ni is temperature-dependent, C atoms precipitate and form graphene layer on the Ni surface upon sharply cooling the sample[22] and the layer of graphene depends on the concentration of C precipitated on Ni. However, Li et al.[23] recently fabricated graphene films on copper foils. They concluded that the thickness of graphene films were independent on exposing time, and the low solubility of carbon in copper made this growth process self-limiting. The precipitation mechanism did not work on copper substrate. Therefore, the mechanism of CVD growth of graphene needs additional experiments to be carried out to fully understand the process.

Arc-discharge is the most efficient method of making few-layer graphene has been developed by Rao et al.[24] Arc-discharge between two graphite electrodes was done in a stainless steel chamber that was filled with hydrogen and helium mixtures at different proportions, without any catalyst. Soot materials with web like appearance were formed

on the inner walls of the reaction chamber and around the cathode after the evaporation of graphite anode. This method gives graphene containing 2-3 layers.

### 1.1.5 Stability of graphene

Graphene is the two-dimensional counterpart of three dimensional graphite, exhibiting high crystal quality and ballistic conduction. But according to some earlier reports, perfect two-dimensional crystals cannot exist in free state.[26-30] This discrepancy can be resolved by considering the graphene structures studied so far to be an integral part of a larger, three-dimensional structure, either supported by a substrate or embedded in a three dimensional matrix.[31-33] But surprisingly, individual graphene sheets (Figure 4) freely suspended on a micro fabricated scaffold in vacuum or in air have also been reported.[34] At first more than 70 years ago, Peierls[27,28] and Landau[35,36] raised questions about the existence of a strictly two-dimensional (2D) crystal. They showed that, in the standard harmonic approximation,[37] thermal fluctuations destroy the long-range order which leads to the melting of 2D lattice at any finite temperature. Later, Mermin and Wagner proved that a magnetic long-range order could not exist in one and two dimensions[35] and later extended the proof to crystalline order in 2D.[30] Importantly, number of experiments on thin films were in agreement with the theory, showing that below a certain thickness, typically of dozens of atomic layers, the films segregate into islands or decompose unless they constitute an inherent part of a three-dimensional (3D) system.[38,39] However, although the theory does not allow perfect crystals in 2D space, it does not forbid nearly perfect 2D crystals in 3D space. Indeed, a detailed analysis of the 2D crystal problem beyond the harmonic approximation has led to the conclusion[40-42] that the interaction between bending and of stretching long-wavelength phonons could in principle stabilize

atomically thin membranes through their deformation in the third dimension.[42]

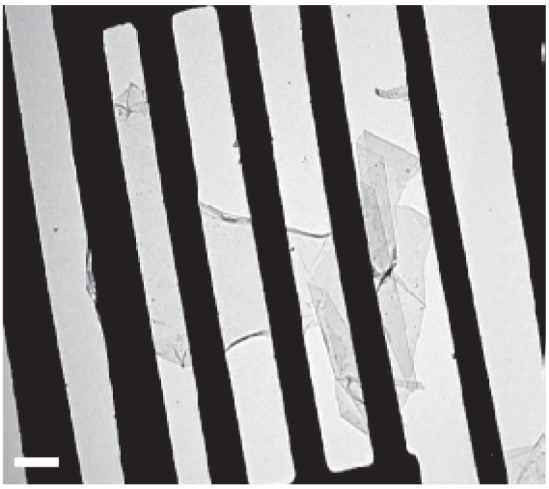

**Figure 4.** *TEM image of a suspended graphene membrane. (Scale bar, 500 nm) (From ref. [33]).*

### 1.1.6 Electronic structure

Graphene honeycomb lattice is composed of two equivalent carbon sublattices A and B, as shown in Figure 5a. Figure 5b shows the first Brillouin zone of graphene, with the high-symmetry points M, K, K' and Γ marked. Note that K and K' are two inequivalent points in the Brillouin zone. The s, $p_x$ and $p_y$ orbitals of carbon atoms form σ bonds with neighboring carbon atoms. The π electrons in the $p_z$ orbital, one from each carbon, form the bonding π and the anti-bonding π* bands of graphene. Dispersion relation of these π-electrons is described by the tight binding model, incorporating only the first nearest neighbour interactions [Eq.(1)]:[43,44]

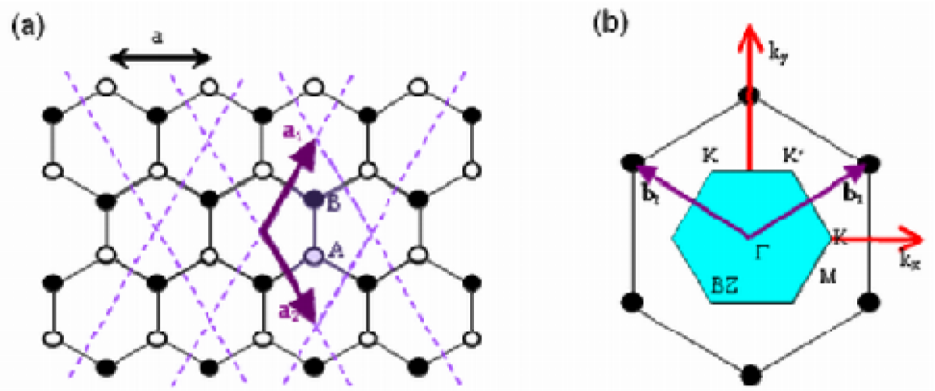


**Figure 5** *a) Graphene lattice.* $\vec{a}_1$ *and* $\vec{a}_2$ *are the unit vectors. (b) Reciprocal lattice of graphene. Shaded hexagon is the first Brillouin zone.* $\vec{b}_1$ *and* $\vec{b}_2$ *are reciprocal lattice vectors.*

. $$E^{\pm}(k_x, k_y) = \pm\gamma_0\sqrt{1+4\cos\frac{\sqrt{3}k_x a}{2}\cos\frac{k_y a}{2}+4\cos^2\frac{k_y a}{2}} \qquad (1)$$

where $a=\sqrt{3}a_{CC}$, $a_{CC}$ – ) and $\gamma_o$, the transfer integral, is the matrix element between the π-orbitals of neighboring carbon atoms and its magnitude is ~ 3eV. The – sign in Eq.1 refers to the π-band which is fully occupied in graphene and the + sign corresponds to the totally empty anti-bonding π* band. The π and π* bands touch at the K and K′ points. A Taylor expansion of Eq.1 around K or K' points yield linear dispersion bands [Eq. (2)].

$$E^{\pm}(k) = \pm\gamma\left|\vec{k}\right| \qquad (2)$$

Here, $\vec{k}$ is measured with respect to the K-point, $\gamma = \hbar v_F = \sqrt{3} a \gamma_0 / 2$ and $v_F$ is the Fermi group velocity. The linear bands, a result of graphene's crystal symmetry, are a hallmark of graphene giving rise to many of the interesting physical properties such as half - integer quantum Hall effect, Berry's phase and Klein – paradox.[45,46] Within the linear – band approximation, the constant energy contours are circles around the K and K' points. The effective Hamiltonian near the K-point can be expressed by the Dirac equation with zero mass [Eq. (3)].

$$H = \begin{pmatrix} 0 & \gamma k \\ \gamma k & 0 \end{pmatrix} = \hbar v_F \, \vec{\sigma}.\vec{k} \qquad (3)$$

Here $\vec{\sigma}$ is the 2d pseudospin Pauli matrix. Physically, this implies that the electronic states near the K- point are composed of states belonging to different sub lattices A and B and their relative contributions is taken into account using two component wave functions (spino. The eigen functions near K are given by Eq. (4)

$$\psi^{o}_{s,k}(\vec{r}) = \frac{1}{\sqrt{2}} \begin{pmatrix} 1 \\ s e^{i\theta_k} \end{pmatrix} e^{i\vec{k}.\vec{r}} \qquad (4)$$

where s = ± 1 is the band index and $\theta_{\vec{k}}$ is the polar angle of the wave vector $\vec{k}$. Eq.4 reflects that the pseudospin vector is parallel to the wave vector $\vec{k}$ in the upper band (s = 1) and is anti-parallel in the lower band (s = -1). The wave functions at K and K' are related by time-reversal symmetry. The pseudospin and Berry phase may be manipulated by application of an inhomogeneous lattice distortion. Interestingly, a non-constant lattice distortion can lead to a valley-Hall effect, analogous to the spin-Hall effect in semiconductors.[47]

The electronic dispersion of bi-layer graphene is different from that of single-layer graphene. The lattice structure of a bi-layer graphene is shown in Figure 6 (a) and (b). where the top and bottom layers are represented by solid and dashed lines and indexes 1 and 2 label the sublattices of the bottom and top layers, respectively. The $A_2$ sublattice of the top layer is exactly on top of the sublattice $B_1$ of the bottom layer. In addition to the in-plane nearest neighbour hopping energy $\gamma_0$ ($A_1$-$B_1$ or $A_2$-$B_2$), there is interlayer hopping energy $\gamma_1$ ($A_2$-$B_1$). Taking only these two energy scales and neglecting all other hopping energies ($B_2$-$A_1$, $A_2$-$A_1$ or $B_2$-$B_1$), the Hamiltonian of a bi-layer graphene near the K-point can be written as Eq. (5).

$$H = \begin{pmatrix} 0 & \gamma k & 0 & 0 \\ \gamma k & 0 & \gamma_1 & 0 \\ 0 & \gamma_1 & 0 & \gamma k \\ 0 & 0 & \gamma k & 0 \end{pmatrix} \tag{5}$$

The eigen values of this Hamiltonian are given by Eq. (6)

$$E_{sj}(k) = s\left[\left(\sqrt{\left(\frac{\gamma_1}{2}\right)^2 + (\gamma_0 k)^2}\right)(-1)^j \frac{\gamma_1}{2}\right]$$

(6)

where s = ± 1 is a band index j is a sub band index (j = 1, 2). Figure 6c shows the electronic dispersion of the bi-layer, where $\gamma_1$ is the energy separation between the two sub-bands in conduction or valence bands. There is no gap between the valence band and the conduction band. However, a gap can open on application of an electric field perpendicular to the bi-layer.[48,49]

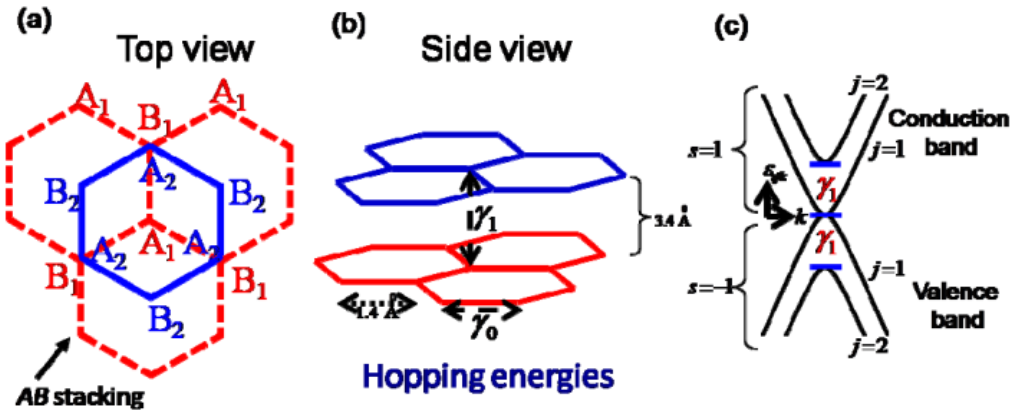


**Figure 6.** (a) *Top and (b) side view of a bi-layer graphene. $A_1$, $B_1$ are the sub lattices of the bottom layer and $A_2$, $B_2$ are sublattices of the top layer. c) Energy dispersion of a bi-layer graphene. Here* $\gamma_1$ *is the energy separation between the two sub bands.*

A band gap has been observed by angle-resolved photo-emission experiments on a chemically doped bi-layer graphene[31] where the electric field arises due to charge transfer from the dopants to the carbon atoms. A direct application of top-gate electric field to the back gated bi-layer field effect transistor gives a controlled way to manipulate the band gap, presenting a possibility of electrostatically controlled graphene-based devices.[50]

**Quantum Hall Effect:** The massless Dirac Fermion nature of carriers in single-layer graphene has interesting consequences on the energy spectrum of the Landau levels (LL) produced in the presence of a magnetic field perpendicular to the graphene layer.[51-53]

The energies of the Landau levels, indexed by integer j, are given by $E_j = \pm v_F \sqrt{2|j|e\hbar B}$. Notice that $E_j$ is proportional to $\sqrt{B}$, in contrast to conventional 2-dimensional electron-gas with parabolic bands where $E_j = \left(j + \frac{1}{2}\right)\hbar eB/m^*$. Furthermore, since the bands touch at the K and K′ points, the j=0 Landau level is shared equally between electrons and holes, whereas in parabolic bands, the first LL is shifted by $\hbar eB/2m^*$. These peculiarities of the Dirac Fermions lead to anomalous quantum hall effect (QHE) with half – integer quantization of the Hall conductivity, instead of an integer QHE. The Hall conductivity, $\sigma_{xy}$, in single-layer graphene shows a plateau quantized at $\frac{4e^2}{h}\left(j + \frac{1}{2}\right)$ as a function of carrier density, $n_s$, at a fixed magnetic field or as a function of B at a fixed $n_s$. Another interesting feature is that the splitting between the LLs (j=0 and j=1) is 240 meV at 45 T which makes the observation of QHE possible at room temperature.[54]

For bi-layer graphene, the quasi-particles are chiral but with a finite mass. The Landau levels in this case are given by $E_j = \pm\frac{\hbar eB}{m^*}\sqrt{j(j-1)}$, leading to two degenerate levels j=0 and j=1 at zero energy. This results in the absence of the zero energy plateau, $\sigma_{xy} = j.4e^2/h$, where j is an integer except j=0.[55] The opening of a gap in bi-layer graphene by the electric field is also reflected in the quantum hall plateaus.[56]

### 1.1.7 Phonons and Raman Spectroscopy

Single-layer graphene belongs to the $D_{6h}$ point group which reduces to $D_{3d}$ for the AB bi-layer and ABC tri-layer and $D_{3h}$ for the ABA tri-layer. The zero-wavevector

(q=0) optical phonons in single-layer graphene belong to the irreducible representations $E_{2g}$ (R) and $B_{2g}$, where R refer to Raman active modes. The eigen vectors of these optical modes (Figure 7a) show that the $E_{2g}$ mode (degenerate transverse optic (TO) and longitudinal optic (LO)) is an in-plane optical vibration with the frequency ~ 1582 $cm^{-1}$.[57,58] The two neighbouring atoms vibrate opposite to one another, resulting in large bond distortions. In the $B_{2g}$ mode, the carbon atoms move perpendicular to the graphene plane. For bi-layer graphene with AB stacking with 4 atoms per unit cell, the optical modes are $2E_g$ (R) + $2E_{1u}$ (IR) + $A_{2u}$ (IR) + 2 $B_{1g}$. The eigen-vectors of $E_g$ and $E_{1u}$ are shown in Figure 7b. The IR active $E_{1u}$ mode is slightly higher in frequency (~7$cm^{-1}$) as compared to the Raman $E_g$ mode.

Vibrational properties of ultra thin n-layer graphene (n=1-7) have been studied using first-principals density functional theory.[59] It is found that a low frequency optical phonon (~110 $cm^{-1}$) with out-of-plane displacements exhibits a large sensitivity to the number of layers, although the interlayer spacing does not change appreciably as n varies. This low-frequency mode is yet to be observed experimentally and can prove to be a marker for the number of layers.

Figure 8 shows the phonon dispersion of single-layer graphene using density functional theory.[52] The branch indexed as ZA refers to the out-of-plane acoustic mode which has a $q^2$-dispersion, in contrast to the linear q dispersion of the longitudinal and transverse acoustic modes. Many recent calculations have discussed the important issue of electron-phonon coupling in graphene.[60-63]

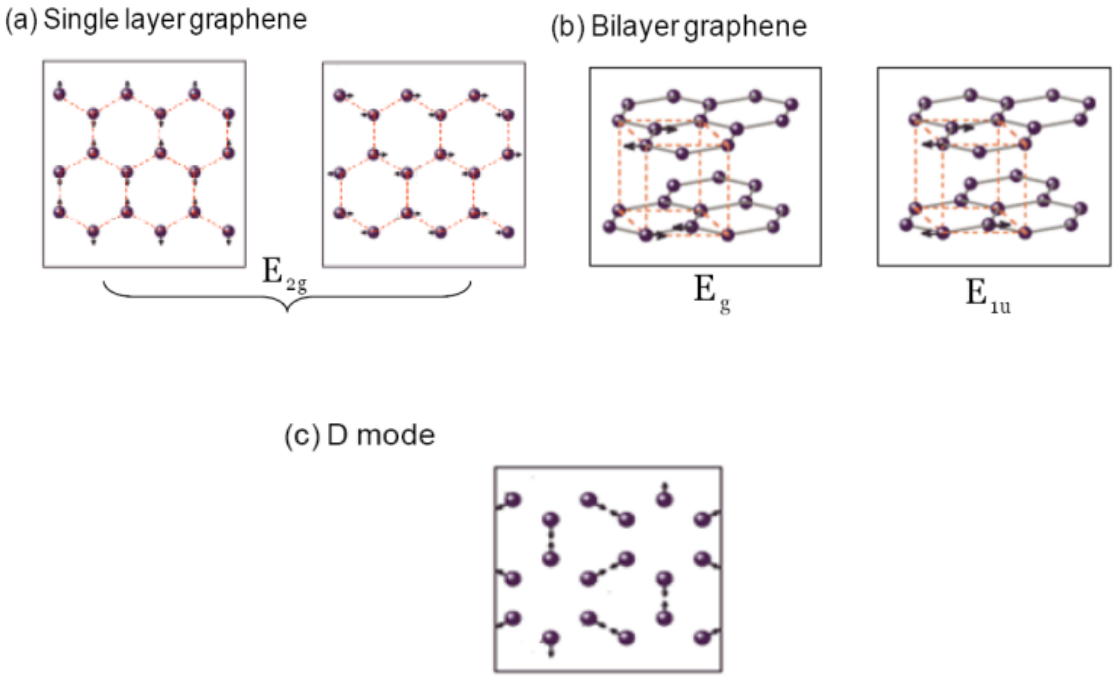


**Figure 7.** a) *Atomic displacements for the $E_{2g}$ (TO/LO) modes at Γ in monolayer graphene. (b) For bi-layer, atomic displacements of $E_g$ (R) and $E_{1u}$ (IR) modes at Γ. Here one mode for each degenerate pair is shown. (c) Atomic displacements for the highest TO mode at K. [From reference 58]*

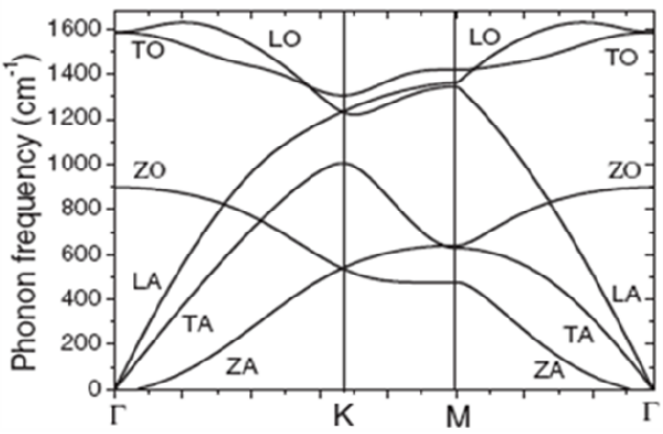


**Figure 8.** *Phonon dispersion for monolayer graphene. [From reference 58]*

The degenerate $E_{2g}$ phonon at Γ and the highest TO phonon at K have strong electron-phonon interactions, resulting in Kohn anomalies in the phonon dispersion. The Kohn anomaly refers to the anomalous screening of phonons of wavevector **q** which can connect two points $\mathbf{k_1}$ and $\mathbf{k_2}$ on the Fermi surface such that $\mathbf{k_2} = \mathbf{k_1} + \mathbf{q}$.[64] For graphene and metallic nanotubes, the Kohn anomalies occur at **q= 0** and **q = K.** The eigen vectors of the phonon modes responsible for the Raman D-band transform according to the $A_1$ and $B_1$ representations of $C_{6v}$ are shown in Figure 7c.[58] The two sublattice atoms move circularly in opposite directions.

Raman spectroscopy is a powerful probe for characterizing $sp^2$ and $sp^3$ carbon materials – be it graphite, diamond-like carbon, diamond, poly-aromatic compounds, fullerenes and carbon nanotubes. Raman fingerprints of single, bi- and few layer graphenes are different and have been investigated by several groups.[65-71] A typical Raman spectrum of single-layer graphene is shown in Figure 9. The symmetry allowed $E_{2g}$ mode at the Γ-point, usually termed as the G-mode, appears at ~1583 $cm^{-1}$. The other Raman modes seen are at ~1350 $cm^{-1}$(D-mode), 1620 $cm^{-1}$(D'-mode), 2680 (2D or $D^*$mode), 2950 (D+G), 3245(2D') and 4290 $cm^{-1}$(2D+G). The mode at ~ 1350 $cm^{-1}$, termed as the D-mode, is a disorder – activated Raman mode and is associated with the TO – branch near the K-point. Its frequency depends on the incident laser energy (~50 $cm^{-1}$/eV) and has been understood[72-76] based on the double resonance Raman process shown in Figure 10. The Raman tensor can be written in fourth order perturbation theory as Eq. (7)

$$R = \sum_{a,b,c} \frac{M_{er} M_{e-def} M_{ep} M_{er}}{\left(E - E_a - i\gamma\right)\left(E - h\omega_p^q - E_b - i\gamma\right)\left(E - h\omega_p^q - E_c - i\gamma\right)} \qquad (7)$$

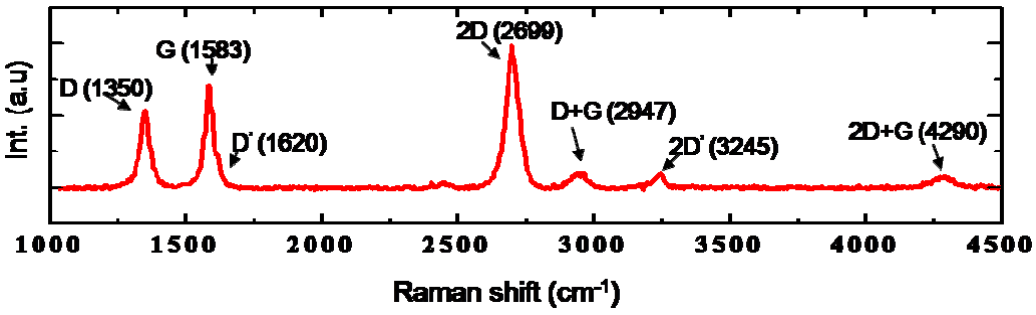


**Figure 9.** *Typical Raman spectrum of single-layer graphene prepared by mechanical exfoliation method. The excitation laser wavelength was 514.5 nm.*

Here, $E_L$ is the energy of the incident laser photon, M's are the matrix elements and γ is the life-time broadening of the intermediate electronic states a, b and c. Figure 10(a) shows the four steps involved in defect –assisted Raman process: step one is the electron – radiation interaction with matrix element $M_{er}$, the second step is the electron-phonon interaction ($M_{ep}$)

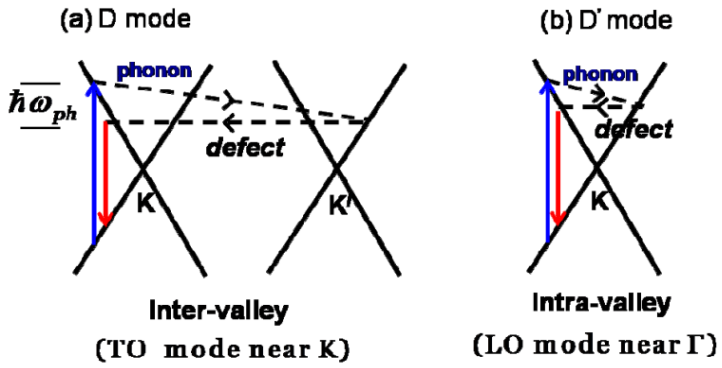


**Figure 10 (a) and (b):** *Double resonance Raman scheme for the D and D' modes. Vertical solid lines represent inter-band electronic transitions accompanied by photon absorption or emission. Dashed arrow represents phonon emission and horizontal dotted line represents the defect scattering.*

making a phonon assisted inter-valley transition, the third step is defect-assisted transition $M_{e\text{-}def}$ to take care of the momentum conservation and the fourth step is the electron-radiation interaction. In the double resonance Raman process, the phonon with wavevector **q** is so chosen that the energy denominator is minimum. A change in the incident photon energy results in choosing a phonon of different wavevector on the TO-branch and hence the shift in the D-mode frequency arises due to the dispersion of the phonon branch near the K-point of the Brillouin zone. The mode at ~1620 $cm^{-1}$, termed as D', also arises due to the double resonance process, involving intra-valley scattering involving LO phonon near the Γ – point (Figure 10b).

The mode at ~ 2680 $cm^{-1}$ is the second – order Raman scattering involving TO phonons near the K-point. It is labelled as the D* or 2D mode. Unlike the D-band, disorder is not required for the wavevector conservation because two-phonons of equal and opposite momentum can satisfy the Raman requirement of q~0. Hence, one can observe the 2D band in the Raman spectra, even though the D-mode is absent. Like the D-band, this Raman band is highly dispersive with incident photon energy (~100 $cm^{-1}$/eV), almost twice of the dispersion of the D-band. Double resonance Raman scattering shown in Figure 11(a) can quantitatively explain the dependence of the 2D Raman band frequency on the laser photon energy. It has been pointed out[72,73] that the Raman process shown in Figure 11(b), labelled fully resonant, is more dominant than the double resonance process. In bi-layer graphene, the electronic dispersion is different from that in single-layer graphene (See Figure 6c) and hence the shape of 2D band is different from that in single-layer graphene.[67,68]

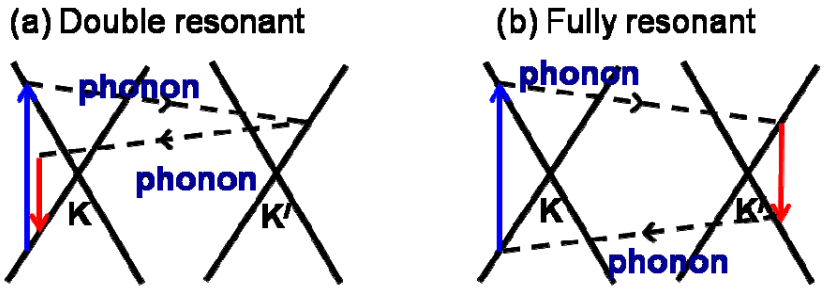


**Figure 11.** *Double resonance Raman process for the two-phonon Raman Scattering. Notation same as in Figure 10.*

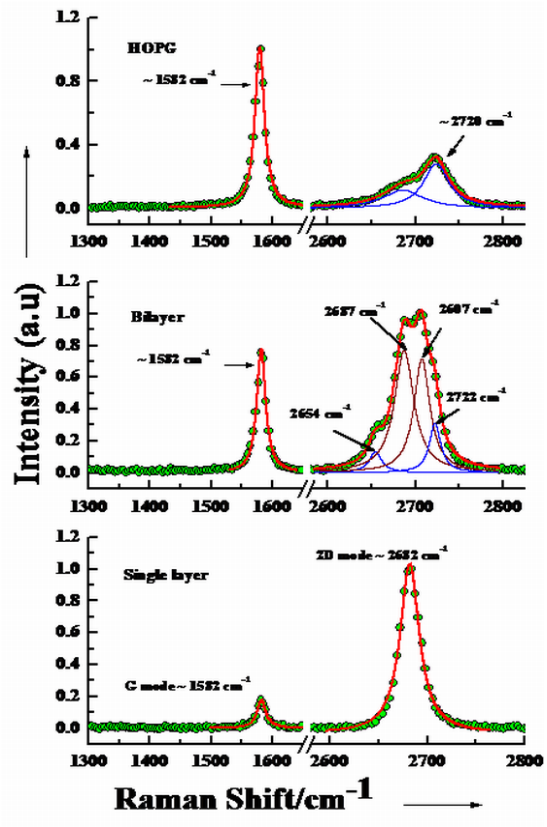


**Figure 12.** *Raman spectra of single-layer graphene and bi-layer graphene prepared by mechanical exfoliation of HOPG. Note that even though the D-mode is absent in graphene samples, the 2D mode is strong. The 2D band in bi-layer graphene is deconvoluted into 4 bands arising due to double resonance processes. [From reference 64]*

Figure 12 shows the comparative Raman spectra of mono- and bi-layer graphenes along with the spectrum of HOPG. Ferrari et al.[67] have shown that the 2D band in bi-layer graphene can be decomposed into 4 bands arising from the different phonon assisted inter-valley transitions shown in Figure 13. It is found[70] that the position of the Raman G-band in mechanically exfoliated single-layer graphene varies from 1582 $cm^{-1}$ to ~ 1594 $cm^{-1}$. The line-width also varies from ~20 $cm^{-1}$ to 14 $cm^{-1}$. Figure 14 shows the variation of the G-mode frequency $\omega_G$ and its full width at half-maximum (FWHM) as a function of the intensity ratio of the D and G modes, $I_D/ I_G$. The latter is a measure of the disorder in the sample, which can be edges, charge puddles, ripples or any other defects. The data in Figure 14 reflects the unintentional charge doping of the graphene by defects. The intensity of D-band is related to the edge chirality.[74] It is weak at the zigzag edge and strong at the arm-chair edge.

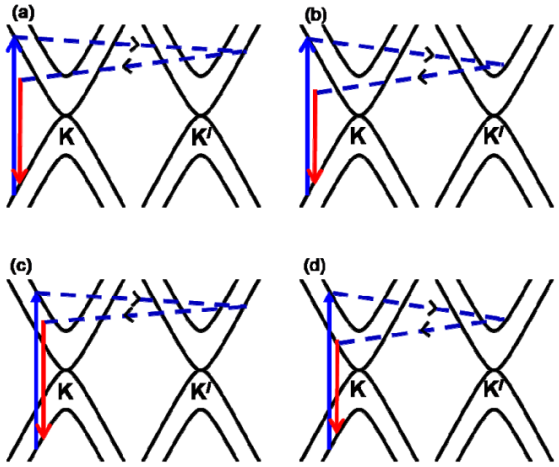


**Figure 13.** *Schematic representation of all the four possibilities in a double resonance Raman process. The solid vertical lines are electronic transitions and dotted lines represent emission of phonons.*

Raman spectra are routinely used to characterize graphene samples. The shift and splitting of Raman modes can be used to determine the strain in graphene layers. Raman spectra of epitaxial graphene layers grown on SiC show a significant blue shift of the G-band (~20 $cm^{-1}$) and 2D bands (~60 $cm^{-1}$) as compared to graphene prepared by micromechanical clevage.[76, 77] This mainly arises due to compressive strain that builds up when sample is cooled down after annealing.

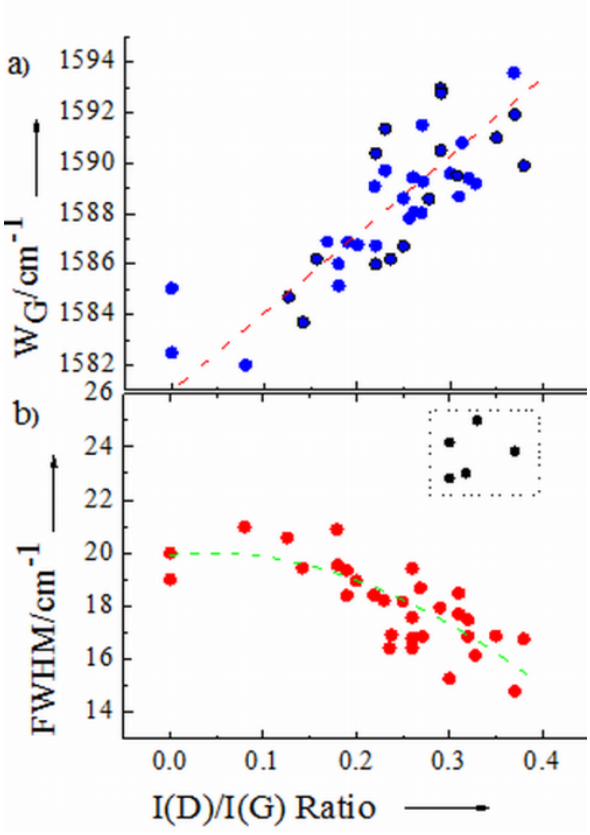


**Figure 14.** *Peak position of G-mode, $\omega_G$, and its FWHM of different samples of SG as a function of the $I_D/I_G$ ratio. The dashed lines are guide to the eye. [From reference 70]*

In graphene monolayer under uni-axial strain, the doubly degenerate $E_{2g}$ mode splits into two components – one polarized along the strain and the other perpendicular to it.[78,79] This results in splitting of the G-band into two bands $G^+$ and $G^-$ which are red shifted for the uniaxial tensile strain. The red shifts for 1% strain are ~11 $cm^{-1}$ for $G^+$ band, ~32 $cm^{-1}$ for $G^-$ band.[80] For the 2D band, the corresponding shift is ~64 $cm^{-1}$, which can also have contributions from the changes in the phonon wavevector arising from relative movement of the Dirac cones.[80] This can contribute to the asymmetric broadening of the 2D band.

### 1.1.8 Graphene nanoribbons

Depending on the width and edge configuration, graphene nanoribbons (GNRs) can be either metallic or semiconducting. GNRs narrower than 10 nm can be semiconductors regardless of the edges and excellent candidates for use in electronic devices, such as field-effect transistors.[81] Graphene nanoribbons with controlled widths were prepared by unzipping carbon nanotubes (Figure 15). In this process, multiwalled carbon nanotubes comprising 15–20 concentric cylinders were intercalated with concentrated sulphuric acid and potassium permanganate at room temperature and heated at 55–70 °C. This process yielded nanoribbons up to 4 micrometres long, with widths of 100–500 nanometres and thicknesses of 1–30 graphene layers. GNRs were also prepared by employing different procedures such as lithography, chemical and sonochemical synthetic methods, chemical vapour deposition, laser unzipping and micromechanical cleavage.[82]

### 1.1.9 Graphane

Graphane is a “hypothetical” two-dimensional polymer of carbon and hydrogen with a hexagonal network. All the carbon atoms in graphane are $sp^3$ hybridized and the hydrogen

atoms are bonded to carbon on both sides of the plane in an alternating manner. First principle density functional theory calculatios shows a binding energy comparable to other hydrocarbons such as benzene, cyclohexane, and polyethylene.

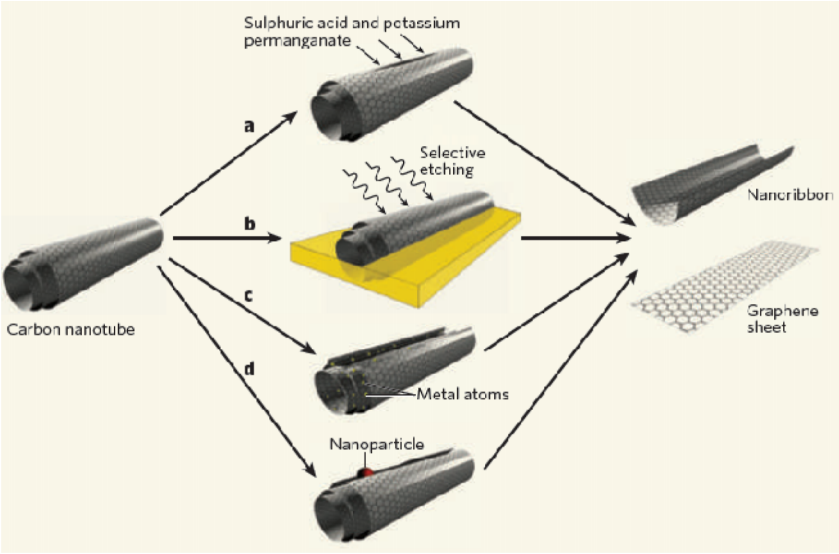


**Figure 15.** *Methods for unzipping carbon nanotubes. a) Unzipping of multiwalled carbon nanotubes by treating with sulphuric acid and potassium permanganate (an oxidizing agent) to form nanoribbons or graphene sheets. b) Argon plasma etching of nanotubes embedded polymer film. c) Insertion of alkali-metal atoms between the concentric cylinders of a multiwalled carbon nanotube, causes graphene sheets to peel off. d) A method still to be explored would use catalytic metal nanoparticles to cut along the length of a nanotube like a pair of scissors. [From reference 77]*

Hydrocarbons are the simplest organic compounds made only of carbon and hydrogen.[83] Some of them occur naturally in the form of crude oil and natural gas. Others are synthesized such as polyethylene and other plastics. They are readily oxidized to produce carbon dioxide and water with a considerable release of energy; therefore, they are usually good fuels. All known hydrocarbons, until now, are molecules that consist of a carbon backbone with hydrogen atoms attached. The backbone can be a linear chain, a ring, or combinations of both. On the contrary, graphane is the first extended two-dimensional covalently bonded hydrocarbon. Graphane is predicted to be a semiconductor, because of its novel structure and low dimensionality. There is a fully fluorinated analog, poly-(carbon monofluoride) with formula CF, which has been synthesized earlier.[84] Because fluorine is known to replace hydrogen in many hydrocarbons, the existence of this fully fluorinated form gives further support to prediction of this new academic material.

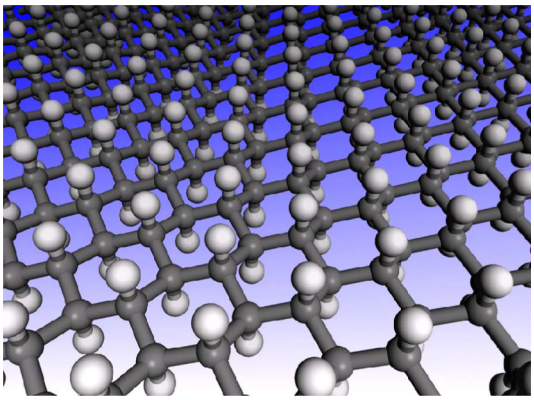

**Figure 16.** *Structure of graphane in the chair conformation. The carbon atoms are shown in gray and the hydrogen atoms in white. The figure shows the hexagonal network with carbon in the $sp^3$ hybridization. [From reference 81]*

Graphane has two favourable conformations: a chair-like conformer with the hydrogen atoms alternating on both sides of the plane and a boat-like conformer with the hydrogen atoms alternating in pairs (Figure 16). In the chair conformer, every C-C bond connects carbon atoms with hydrogen attached at opposite sides of the plane. The calculated C-C bond length of 1.52 Å is similar to the $sp^3$ bond length of 1.53 Å in diamond and is much greater than 1.42 Å characteristic of $sp^2$ carbon in graphene. The boat conformer has two different types of C-C bonds: those connecting carbons bonded to hydrogen atoms on opposite sides of the plane with a bond length of 1.52 Å and those connecting carbon atoms bonded to hydrogen atoms on the same side of the plane with a bond length of 1.56 Å, slightly longer due to H-H repulsion.[85] The C-H bond length of 1.1 Å is similar in both conformers and typical of hydrocarbon compounds. The graphane bonds are fully saturated and there is no opportunity for hydrogen bonding between the sheets.

Experimentally, Sunmin Ryu et al. have shown the reaction of single-layer graphene with hydrogen atoms generates $sp^3$ C-H bonds on the basal plane and the reduced material gets dehydrogenated on photothermal heating.[86] In their experiments graphene samples coated with hydrogen silsesquioxane (HSQ) (30 nm thick) were irradiated with 30 keV electrons at various doses (0.5~8 $mC/cm^2$). In an another approach, Elias et al.[87] have employed hydrogen plasma to hydrogenate graphene samples. In this process, graphene samples deposited on silicon substrate were exposed to a cold hydrogen plasma ignited between two aluminum electrodes. During experiments, the samples were kept 30 cm away from the discharge zone in order to minimize any possible damage by energetic ions. It has also been shown that the reaction with hydrogen is reversible, the original metallic state, the lattice spacing, and even the quantum Hall effect could be restored after annealing.

Recently, Rao et al.[88] showed that Birch-reduction of few-layer graphene gives rise to hydrogenated graphene containing up to 5 wt. % of hydrogen. Interestingly, hydrogenated graphene decomposes on heating up to 500 $^{o}$C or on laser irradiation, releasing all the hydrogen. This result demonstrates that the $sp^3$ C-H bond of hydrogenated graphene can be considered to act as a reversible chemical storage of hydrogen.

## 1.2 Applications

### 1.2.1 Batteries

Owing to its reversibility and reasonable specific capacity graphite is generally employed as anode material in Li-ion batteries (Figure 17). However, new electrode materials with higher capacity and stability need to be developed for Li-ion batteries to achieve higher energy density and durability. Graphene has been considered as one of the promising anodic materials in Li-ion batteries, as it comprises good electrical conductivity, high surface area and chemical tolerance.[89,90] Song et al.[91] have reported that graphene exhibits a relatively high reversible capacity of 672 $mAhg^{-1}$ having much enhanced cycling performance relative to graphite. The capacity and cycle performance of Li-ion battery has been further improved using graphene based hybrid nanostructures as electrodes.[92] Typical examples of those nanostructures employed are $TiO_2$, $SnO_2$, CNTs, $Co_3O_4$ and $Co(OH)_2$ (Figure 17). It was suggested that the synergetic effect between two components in the hybrid nanostructures should be responsible for the improved performance due to the maximum utilization of electrochemically active area of graphene.

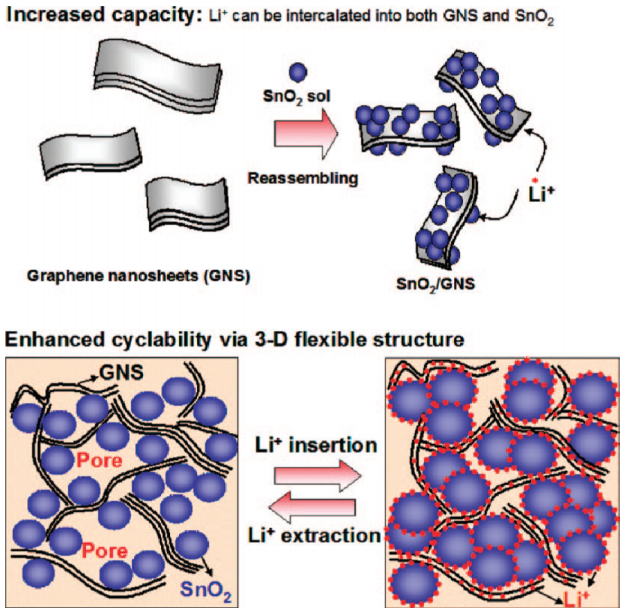


**Figure 17.** *Schematic illustration of synthesis and structure of $SnO_2$/graphene for battery application. [From reference 87]*

### 1.2.2 Composites

Graphite is soft and flaky, and cannot be used in load-bearing structures. This problem could be solved by making a composite material of graphene sheets and polymers. The manufacturing of such composites requires not only that graphene sheets be produced on a sufficient scale but that they also be incorporated, and homogeneously distributed, into various matrices. Unfortunately, owing to their hydrophilic nature, graphene oxide sheets can only be dispersed in aqueous media that are incompatible with the most organic polymers. In addition, graphite oxide is electrically insulating, unlike graphite, which limits its usefulness for the synthesis of conductive nanocomposites. It has been

demonstrated,[93,94] however, that the electrical conductivity of graphite oxide can be significantly increased by chemical reduction, presumably owing to the restoration of a graphitic network of $sp^2$ bonds. Processing of nanographene platelets to produce composites has been briefly reviewed by Jang *et al*.[95]

Polyacrylonitrile nanofibers reinforced by graphite nanoplatelets have been prepared and have improved mechanical properties.[96] Hansma *et al*.[97] indicated how a combination of adhesives and high-strength structures such as graphene and carbon nanotubes can yield strong, lightweight, and damage-resistant materials. Ramanathan *et al*.[98] reported that 1 wt% of functionalized graphene sheets in poly(acrylonitrile) increases the glass transition temperature (Tg) of the polymer by over 40 ºC and an increase of nearly 30 ºC is observed with only 0.05 wt% of graphene in poly(methyl methacrylate) (PMMA). An addition of approximately 1 wt% of graphene to PMMA leads to an increase in the elastic modulus by 80% and in the ultimate tensile strength by 20%. A comparative study by these workers shows that among all the nano-filler materials considered, single-layer functionalized graphene gives the best results. Das *et al*.[99] have studied the mechanical properties of polyvinyl alcohol (PVA) and PMMA composites reinforced by functionalized few-layer graphene by employing the nanoindentation technique. The addition of 0.6 wt% of the graphene results in a significant increase in both the elastic modulus and hardness. The crystallinity of PVA also increases with the addition of few-layer graphene. An observed improvement in the mechanical properties of the polymers is suggested to have arisen from the good mechanical interaction between the polymer and the few-layer graphene, which in turn, provides better load-transfer between the matrix and the fiber. Epoxy composites of few-layer graphene show very interesting properties which are useful for the development of thermal interface materials for electronic

packaging and advanced composites.[100] A loading of nearly 25 vol % of graphene into epoxy matrix enhances the thermal conductivity by more than 3000 times. This surpasses the performance of conventional fillers that require a loading of nearly 70 vol % to achieve the same thermal conductivity.

### 1.2.3 Sensors

In many applications, solid-state gas sensors have been widely employed due to their high sensitivity, low production costs and miniature sizes.[101,102] Recently, gas sensors using carbon nanotubes and semiconductor nanowires have also been demonstrated.[103,104] The ultimate goal of any detection method is to attain the level of sensing even single atom or molecule. Such resolution has so far been beyond the reach of any detection technique, including solid-state gas sensors known for their exceptional sensitivity. The main reason for the limitation is fluctuations due to thermal motion of charges and defects,[105] which leads to intrinsic noise exceeding the sought-after signal from individual molecules, usually by many orders of magnitude. But the micrometer-size sensors made from graphene are capable of detecting even individual molecules. Such gas sensors rely on the change in their electrical conductivity.[106] The observed change in conductivity arises due to a change in the carrier concentration of graphene, caused by adsorbed gaseous molecules acting as donors or acceptors. Some interesting properties of graphene render its sensitivity up to single atom or molecule level detection. First, as graphene is a two-dimensional (2D) material all carbon atoms in the plane are exposed to the analyte of interest.[107] Second, graphene is highly conductive with low Johnson noise (electronic noise generated by the thermal agitation of the charge carriers inside an electrical conductor at equilibrium, which happens irrespective of any applied voltage), therefore, a

little change in carrier concentration can cause a marked variation in electrical conductivity.[107] Third, graphene has very few crystal defects,[108] ensuring a low level of noise caused by thermal switching. Finally, four-probe measurements can be made on a single-crystal graphene device with ohmic electrical contacts having low resistance.[107] All these features contribute to maximize the signal-to-noise ratio to a level sufficient for detecting changes in a local concentration by less than one electron charge, e, at room temperature.

Ghosh *et al.*[109] have studied the sensor characteristics of thick films made of few-layer graphenes for $NO_2$, $H_2O$ and aliphatic alcohols. Good sensitivities were observed for $NO_2$ and $H_2O$, and the sensitivity was mainly found to be affected by boron or nitrogen doping. Gas-sensing properties of graphene sheets deposited on $LiTaO_3$ substrates have been reported.[110] Glucose sensors based on graphene have been reported.[111,112] With glucose oxidase (GOD) as an enzyme model, Shan *et al*. constructed a novel polyvinylpyrrolidone protected graphene/polyethylenimine-functionalized ionic liquid/GOD electrochemical biosensor. Through the sensor, they reported direct electron transfer of GOD, demonstrating graphene's potential application for fabrication of glucose sensors. A linear response up to 14 mM of glucose was observed by them.[112] The possibilities of single-layer graphene to act as a mass sensor and an atomic dust detector have also been indicated.[113]

Graphene chemically modified by electrodeposition of Pd nanoparticles[114] has been reported to show good response for $H_2$ sensing, as Pd has good affinity towards $H_2$. DFT calculations show that aluminum-doped graphene strongly chemisorbs CO molecules, forming Al-CO bonds. Thus, aluminum-doped graphene is expected to be a potential

candidate for the detection of CO.[115] Chemically modified graphene has been used in bioelectronics as a sensor at both the microbial and the molecular level.[116] It acts as an interface to recognize single bacteria, a label-free, reversible DNA detector, and a polarity specific molecular transistor for protein/DNA adsorption.

## References

[1] L. Pauling, *The Nature of the Chemical Bond*, Cornell University Press, Ithaca, NY, 1960.

[2] R. F. Curl, *Rev. Mod. Phys.* 1997, **69**, 691.

[3] H. Kroto, *Rev. Mod. Phys.* 1997, **69**, 703.

[4] R. E. Smalley, *Rev. Mod. Phys.* 1997, **69**, 723.

[5] S. Iijima, *Nature* 1991, **354**, 56.

[6] P. R. Wallace, *Phys. Rev.* 1947, **71**, 622.

[7] H.P. Boehm, *Angew. Chem. Int. Ed.* 2010, **49**, 9332.

[8] A. J. van Bommel, J. E. Crombeen, A. van Tooren, *Surf. Sci.* 1975, **48**, 463.

[9] X. Lu, M. Yu, H. Huang, R. S. Ruoff, *Nanotechnology* 1999, **10**, 269.

[10] C. Roscoe, J. M. Thomas, *Proc. R. Soc. London Ser. A* 1967, **297**, 397.

[11] K. S. Novoselov, A. K. Geim, S. V. Morozov, D. Jiang, Y. Zhang, S. V. Dubonos, I. V. Grigorieva, A. A. Firsov, *Science* 2004, **306**, 666.

[12] K. S. Novoselov, A. K. Geim, S. V. Morozov, D. Jiang, M. I. Katsnelson, I. V. Grigorieva, S. V. Dubonos, A. A. Firsov, *Nature* 2005, **438**, 197.

[13] C. N. R. Rao, A. K. Sood, K. S. Subrahmanyam, A. Govindaraj, *Angew. Chem. Int. Edition*, 2009, **48**, 7752.

[14] A. K. Geim, K. S. Novoselov, *Nat. Mater.* 2007, **6,** 183.

[15] P. Blake, E. W. Hill, A. H. Casrto Neto, K. S. Novoselov, D. Jiang, R. Yang, T. J. Booth, A. K. Geim, *Appl. Phys. Lett.* 2007, **91,** 063124.

[16] B. Partoens, F. M. Peeters, *Phys. Rev. B* 2006, **74**, 075404.

[17] V. C. Tung, M. J. Allen and Y. Yang, *Nature Nanotechnology*, 2009, **4**, 25.

[18] C. Berger, *J. Phys. Chem., B*, 2004, **108**, 19912.

[19] C. Berger, Z. M. Song, and X. B. Li, *Science*, 2006, **312**, 1191.

[20] C. G. Jernigan, B. L. VanMil and J. L. Tedesco, *Nano Letters*, 2009, **9**, 2605.

[21] K. S. Kim, Y. Zhao and H. Jang, *Nature*, 2009, **457**, 706.

[22] A. Reina, X. T. Jia and J. Ho, *Nano Letters*, 2009, **9,** 30.

[23] X. S. Li, W. W. Cai and J. An, *Science*, 2009, **324**, 1312.

[24] K. S. Subrahmanyam, L. S. Panchakarla, A. Govindaraj and C. N. R. Rao, *J. Phys. Chem. C*, 2009, **113** ,4257

[25] K. S. Novoselov, D. Jiang, F. Schedin, T. J. Booth, V. V. Khotkevich, S. V. Morozov, A. K. Geim, *Proc. Natl Acad. Sci. USA*, 2005, **102**, 10451.

[26] R. E. Peierls, *Helv. Phys. Acta* 1934, **7,** 81.

[27] R. E. Peierls, *Ann. Inst. Henri Poincare* 1935, **5**, 177.

[28] L. D. Landau, *Phys. Z. Sowjetunion* 1937, **11,** 26.

[29] N. D. Mermin, *Phys. Rev.* 1968, **176**, 250.

[30] C. Berger, Z. Song, X. Li, X. Wu, N. Brown, C. Naud, D. Mayou, T. Li, J. Hass, A. N. Marchenkov, E. H. Conrad, P. N. First, W. A. de Heer, *Science* 2006, **312**, 1191.

[31] T. Ohta, A. Bostwick, T. Seyller, K. Horn, E. Rotenberg, *Science* 2006, **313**, 951.

[32] S. Stankovich, D. A. Dikin, G. H. B. Dommett, K. M. Kohlhaas, E. J. Zimney, E. A. Stach, R. D. Piner, S. T. Nguyen, R. S. Ruoff, *Nature* 2006, **442**, 282.

[33] J. C. Meyer, A. K. Geim, M. I. Katsnelson, K. S. Novoselov, T. J. Booth, S. Roth, *Nature* 2007, **446**, 60.

[34] L. D. Landau, E. M. Lifshitz, *Statistical Physics Part I*, Pergamon, Oxford, 1980.

[35] L. D. Landau, *Zur Theorie der Phasenumwandlungen II. Phys. Z., Vol.* **11**, Sowjetunion 1937.

[36] M. Born, K. Huang, *Dynamical Theory of Crystal Lattices*, Clarendon, Oxford, 1954.

[37] J. A. Venables, G. D. T. Spiller, M. Hanbucken, *Rep. Prog. Phys.* 1984, **47**, 399.

[38] M. Zinke-Allmang, L. C. Feldman, M. H. Grabow, *Surf. Sci. Rep.* 1992, **16**, 377.

[39] J. W. Evans, P. A. Thiel, M. C. Bartelt, *Surf. Sci. Rep.* 2006, **1**, 61.

[40] D. R. Nelson, L. Peliti, *J. Physique* 1987, **48**, 1085.

[41] P. Le Doussal, L. Radzihovsky, *Phys. Rev. Lett.* 1992, **69**, 1209.

[42] D. R. Nelson, T. Piran, S. Weinberg, *Statistical Mechanics of Membranes and Surfaces*, World Scientific, Singapore, 2004.

[43] R. Saito, G. Dresselhaus, M. S. Dresselhaus, *Physical Properties of Carbon Nanotubes*, Imperial College Press, London, 1998.

[44] A. H. Castro Neto, F. Guinea, N. M. R. Peres, K. S. Novoselov, A. K. Geim, *Rev. Mod. Phys.* 2009, *81*, 109.

[45] M. I. Katsnelson, K. S. Novoselov, A. K. Geim, *Nat. Phys.* 2006, **2**, 620.

[46] M. I. Katsnelson, *Mater. Today* 2007, **10**, 20.

[47] P. Gosselin, A. Bérard, H. Mohrbach, S. Ghosh, *Eur. Phys. J. C* 2009, **59**, 883.

[48] E. McCann, V. I. Fal'ko, *Phys. Rev. Lett.* 2006, **96**, 086805.

[49] H. Min, B. Sahu, S. K. Banerjee, A. H. MacDonald, *Phys. Rev. B* 2007, **75**, 155115.

[50] J. B. Oostinga, H. B. Heersche, X. Liu, A. F. Morpurgo, L. M. K. Vandersypen, *Nat. Mater.* 2008, **7**, 151.

[51] K. S. Novoselov, A. K. Geim, S. V. Morozov, D. Jiang, M. I. Katsnelson, I. V. Grigorieva, S. V. Dubonos, A. A. Firsov, *Nature* 2005, **438**, 197.

[52] Y. Zhang, J. W. Tan, H. L. Stormer, P. Kim, *Nature* 2005, **438**, 201.

[53] Z. Jiang, Y. Zhang, Y. W. Tan, H. L. Stormer, P. Kim, *Solid State Commun.* 2007, **143**, 14.

[54] K. S. Novoselov, Z. Jiang, Y. Zhang, S. V. Morozov, H. L. Stormer, U. Zeitler, J. C. Maan, G. S. Boebinger, P. Kim, A. K. Geim, *Science* 2007, **315**, 1379.

[55] K. S. Novoselov, E. McCann, S. V. Morozov, V. I. Fal'ko, M. I. Katsnelson, U. Zeitler, D. Jiang, F. Schedin, A. K. Geim, *Nat. Phys.* 2006, **2**, 177.

[56] E. V. Castro, K. S. Novoselov, S. V. Morozov, N. M. R. Peres, J. M. B. Lopes dos Santos, J. Nilsson, F. Guinea, A. K. Geim, A. H. Castro Neto, *Phys. Rev. Lett.* 2007, **99**, 216802.

[57] S. Reich, C. Thomsen, *Philosophical Transactions of the Royal Society a-Mathematical Physical and Engineering Sciences* 2004, **362**, 2271.

[58] J.-A. Yan, W. Y. Ruan, M. Y. Chou, *Phys. Rev. B* 2008, **77**, 125401.

[59] S. K. Saha, U. V. Waghmare, H. R. Krishnamurthy, A. K. Sood, *Phys. Rev. B* 2008, **78**, 165421.

[60] S. Piscanec, M. Lazzeri, J. Robertson, A. C. Ferrari, F. Mauri, *Phys. Rev. B* 2007, **75**, 035427.

[61] O. Dubay, G. Kresse, *Phys. Rev. B* 2003, **67**, 035401.

[62] M. Lazzeri, F. Mauri, *Phys. Rev. Lett.* 2006, **97**, 266407.

[63] C. H. Park, F. Giustino, M. L. Cohen, S. G. Louie, *Nano Lett.* 2008, **8**, 4229.

[64] W. Kohn, *Phys. Rev. Lett.* 1959, **2**, 393.

[65] A. Gupta, G. Chen, P. Joshi, S. Tadigadapa, P. C. Eklund, *Nano Lett.* 2006, *6*, 2667.

[66] A. C. Ferrari, *Solid State Commun.* 2007, **143**, 47.

[67] A. C. Ferrari, J. C. Meyer, V. Scardaci, C. Casiraghi, M. Lazzeri, F. Mauri, S. Piscanec, D. Jiang, K. S. Novoselov, S. Roth, A. K. Geim, *Phys. Rev. Lett.* 2006, **97**, 187401.

[68] M. A. Pimenta, G. Dresselhaus, M. S. Dresselhaus, L. G. Cancado, A. Jorio, R. Saito, *Phys. Chem. Chem. Phys.* 2007, **9**, 1276.

[69] D. Graf, F. Molitor, K. Ensslin, C. Stampfer, A. Jungen, C. Hierold, L. Wirtz, *Nano Lett.* 2007, **7**, 238.

[70] A. Das, B. Chakraborty, A. Sood, *Bull. Mater. Sci.* 2008, **31**, 579.

[71] Z. Ni, Y. Wang, T. Yu, Z. Shen, *Nano Res.* 2008, **1**, 273.

[72] D. M. Basko, *Phys. Rev. B* 2008, **78**, 125418.

[73] D. M. Basko, *Phys. Rev. B* 2007, **76**, 081405.

[74] Y. You, Z. Ni, T. Yu, Z. Shen, *Appl. Phy. Lett.* 2008, **93**, 163112.

[76] J. Rohrl, M. Hundhausen, K. V. Emtsev, T. Seyller, R. Graupner, L. Ley, *Appl. Phy. Lett.* 2008, **92**, 201918.

[77] N. Ferralis, R. Maboudian, C. Carraro, *Phys. Rev. Lett.* 2008, **101**, 156801.

[78] Z. H. Ni, H. M. Wang, Y. Ma, J. Kasim, Y. H. Wu, Z. X. Shen, *ACS Nano* 2008, **2**, 1033.

[79] T. Yu, Z. H. Ni, C. L. Du, Y. M. You, Y. Y. Wang, Z. X. Shen, *J. Phys. Chem. C* 2008, **112**, 12602.

[80] T. M. G. Mohiuddin, A. Lombardo, R. R. Nair, A. Bonetti, G. Savini, R. Jalil, N. Bonini, D. M. Basko, C. Galiotis, N. Marzari, K. S. Novoselov, A. K. Geim, A. C. Ferrari, *Phys. Rev. B* 2009, **79**, 205433.

[81] M. Terrones, *Nature* 2009, **458,** 845.

[82] S. Guo, S. Dong, *Chem. Soc. Rev.* 2011, **40**, 2644.

[83] G. A. Olah, Á. Molnár, *Hydrocarbon Chemistry*, Wiley-Interscience, Hoboken, NJ, USA, 2003.

[84] N. Watanabe, T. Nakajima, H. Touhara, *Graphite fluorides* Elsevier, Amsterdam, 1988.

[85] J. O. Sofo, A. S. Chaudhari, G. D. Barber, *Phys. Rev. B* 2007, **75**, 153401.

[86] S. Ryu, M. Y. Han, J. Maultzsch, T. F. Heinz, P. Kim, M. L. Steigerwald, L. E. Brus, *Nano Lett.* 2008, **8**, 4597.

[87] D. C. Elias, R. R. Nair, T. M. G. Mohiuddin, S. V. Morozov, P. Blake, M. P. Halsall, A. C. Ferrari, D. W. Boukhvalov, M. I. Katsnelson, A. K. Geim, K. S. Novoselov, *Science* 2009, **323**, 610.

[88] K. S. Subrahmanyam, P. Kumar, U. Maitra, A. Govindaraj, K. P. S. S. Hembram, U. V. Waghmare and C. N. R. Rao, *Proc. Natl. Acad. Sci.*, 2011, **108**, 2674.

[89] X. Wang, L. J. Zhi, K. Mullen, *Nano Lett.* 2008, **8**, 323.

[90] S. Gilje, S. Han, M. Wang, K. L. Wang, R. B. Kaner, *Nano Lett.* 2007, **7**, 3394.

[91] P. Guo, H. Song, X. Chen, *Electrochem.Commun.* 2009, **11**, 1320.

[92] S. M. Paek, E. Yoo, I. Honma, *Nano Lett.* 2009, **9**, 72.

[93] S. Stankovich, R. D. Piner, X. Q. Chen, N. Q. Wu, S. T. Nguyen, R. S. Ruoff, *J. Mater. Chem.* 2006, **16**, 155.

[94] N. A. Kotov, I. Dekany, J. H. Fendler, *Adv. Mater.* 1996, **8**, 637.

[95] J. Lu, L. T. Drzal, R. M. Worden, I. Lee, *Chem. Mater.* 2007, **19**, 6240.

[96] J. J. Mack, L. M. Viculis, A. Ali, R. Luoh, G. Yang, H. T. Hahn, F. K. Ko, R. B. Kaner, *Adv. Mater.* 2005, **17**, 77.

[97] P K Hansma, P. J. Turner, R. S. Ruoff, *Nanotechnology* 2007, **18**, 044026.

[98] T. Ramanathan, A. A. Abdala, StankovichS, D. A. Dikin, M. Herrera Alonso, R. D. Piner, D. H. Adamson, H. C. Schniepp, ChenX, R. S. Ruoff, S. T. Nguyen, I. A. Aksay, R. K. Prud'Homme, L. C. Brinson, *Nat. Nanotechnol.* 2008, **3**, 327.

[99] B. Das, K. Eswar Prasad, U. Ramamurty, C. N. R. Rao, *Nanotechnology* 2009, **20**, 125705.

[100] A. Yu, P. Ramesh, M. E. Itkis, E. Bekyarova, R. C. Haddon, *J. Phys. Chem. C* 2007, **111**, 7565.

[101] P. T. Moseley, *Meas. Sci. Technol.* 1997, **8**, 223.

[102] S. Capone, *J. Optoelect. Adv. Mater.* 2003, **5**, 1335.

[103] C. X. Cong, T. Yu, Z. H. Ni, L. Liu, Z. X. Shen, W. Huang, *J. Phys. Chem. C* 2009, **113**, 6529.

[104] P. G. Collins, K. Bradley, M. Ishigami, A. Zettl, *Science* 2000, **287**, 1801.

[105] P. Dutta, P. M. Horn, *Rev. Mod. Phys.* 1981, **53**, 497.

[106] C. Lee, X. Wei, J. W. Kysar, J. Hone, *Science* 2008, *321*, 385.

[107] F. Schedin, A. K. Geim, S. V. Morozov, E. W. Hill, P. Blake, M. I. Katsnelson, K. S. Novoselov, *Nat. Mater.* 2007, **6**, 652.

[108] K. S. Nonoselov, E. McCann, S. V. Morozov, V. I. Fal'ko, M. I. Katsnelson, U. Zeitler, D. Jiang, F. Schedin, A. K. Geim, *Nat. Phys.* 2006, **2**, 177.

[109] A. Ghosh, D. J. Late, L. S. Panchakarla, A. Govindaraj, C. N. R. Rao, *J. Exp. Nanosci.* 2009, **4**, 313.

[110] R. Arsat, M. Breedon, M. Shafiei, P. G. Spizziri, S. Gilje, R. B. Kaner, K. Kalantarzadeh, W. Wlodarski, *Chem. Phys.Lett.* 2009, **467**, 344.

[111] J. Lu, I. Do, L. T. Drzal, R. M. Worden, I. Lee, *ACS Nano* 2008, **2**, 1825.

[112] C. Shan, H. Yang, J. Song, D. Han, A. Ivaska, L. Niu, *Anal. Chem.* 2009, **81**, 2378.

[113] A. Sakhaee-Pour, M. T. Ahmadian, A. Vafai, *Solid State Commun.* 2008, **145**, 168.

[114] R. S. Sundaram, C. Gómez-Navarro, K. Balasubramanian, M. Burghard, K. Kern, *Adv. Mater.* 2008, **20,** 3050.

[115] Z. M. Ao, J. Yang, S. Li, Q. Jiang, *Chem. Phys.Lett.* 2008, **461**, 276.

[116] N. Mohanty, V. Berry, *Nano Lett.* 2008, **8**, 4469.

# CHAPTER 2

# REVERSIBLE CHEMICAL STORAGE OF HALOGENS IN FEW-LAYER GRAPHENE


## Summary*

Few-layer graphene can be chlorinated up to 56 wt. % by irradiation with UV light in liquid chlorine medium. Spectroscopic studies reveal the presence of $sp^3$ C-Cl bonds in the chlorinated graphenes. They, however, decompose readily on heating to 500 °C or on irradiation with UV or laser radiation releasing all the chlorine. Laser-induced dechlorination of graphene showed appreciable photothermal effects. Similarly, we could brominate few-layer graphene up to 25 wt. % wherein the $sp^3$ C-Br bond dissociates on heating to 500 $^oC$ giving out bromine. The present study shows the possible use of few-layer graphene for chemical storage of halogens.


***** A paper based on this work has been published in *RSC Advances (2012)* and *Macromol. Chem. Phys. (2012).*

## Chapter 2

### 2.1 Introduction

Halogens are notable as being the only group in the periodic table (Group 17) in which the elements exist in all three states of matter at room temperature. In ascending order of size, the halogens are fluorine, chlorine, bromine, iodine and astatine. All of the halogens exist as diatomic molecules when pure elements. Fluorine and chlorine are gaseous and more toxic than other halogens and are stored in containers with great complexity and these containers may burst when exposed to elevated temperatures. Fluorine and chlorine can react with and corrode some forms of rubber and metal coatings. Fluorine is especially problematic, as the element will react with most other materials. Even storage materials like glass can react with fluorine and create dangerous results. Bromine is a liquid at standard temperature and pressure, and so storage and transport doesn't involve the same level of hazard as the gaseous halogens. Iodine is a solid at standard conditions and less dangerous than the other halogens and storing is very easy. Astatine is a solid and is considered the rarest substance in Earth. There is only a tiny amount in existence, unlike the other four halogens that are produced in much larger quantities due to their large applications.

Chlorine will combine directly with almost all other elements. Large amounts are used yearly for making chlorinated organic compounds, bleaches, and inorganic compounds. Organic compounds, ones which have a skeleton of carbon atoms bonded to each other, can contain halogen atoms connected to the carbon atoms. Low molecular weight organic chlorine compounds are liquids and are good solvents for many purposes. They dissolve starting materials for chemical reactions, and are effective for cleaning such different items as computer parts and clothing (dry cleaning). These uses are now being phased out because of problems that the compounds cause in Earth's atmosphere.

Halogens have variety of applications; chlorine containing organic polymers are also widely employed. Polymers are large molecules made of many small units that hook together. One is polyvinyl chloride (PVC), from which plastic tubings and many other plastic products are made. Neoprene is a synthetic rubber made with another chlorine-containing polymer. Neoprene is resistant to the effects of heat, oxidation, and oils, and so is widely used in automobile parts.

Many medicines are organic molecules containing chlorine, and additional chlorine compounds form intermediate steps in the synthesis of a variety of others. Most crop protection chemicals, herbicides, pesticides, and fungicides have chlorine in them. Freon refrigerants are chlorofluorocarbons (CFCs). These perform well because they are volatile, that is they evaporate easily, but they are not flammable. Freon 12, one of the most common, is $CCl_2F_2$ two chlorine atoms and two fluorine atoms bonded to a carbon atom.

Chlorine is part of several compounds, such as the insecticide DDT, that are soluble in fats and oils rather than in water. These compounds tend to accumulate in the fatty tissues of biological organisms. Some of these compounds are carcinogens, substances that cause cancer. DDT and other pesticides, polychlorinated biphenyls (PCBs), and dioxins are substances that are no longer manufactured. However, they are still present in the environment, and disposal of materials containing these compounds is a problem.

The next heaviest element in the halogen family is bromine, named from a Greek word for stink, because of its strong and disagreeable odour. It was first isolated as an element in 1826. Bromine is a reddish-brown liquid that vaporizes easily. The vapours are irritating to the eyes and throat. Elemental bromine is made by oxidation, removal of

electrons from bromide ions in brine. Brines in Arkansas and Michigan are fairly rich in bromide. Other worldwide sources are the Dead Sea and ocean water. There are a variety of applications for bromine compounds. The major use at one time was in ethylene dibromide, an additive in leaded gasoline. This need has declined with the phase-out of leaded fuel. Several brominated organic compounds have wide utilization as pesticides or disinfectants. Currently, the largest volume organic bromine product is methyl bromide, a fumigant. Some medicines contain bromine, as do some dyes. Halons, or halogenated carbon compounds, have been utilized as flame retardants. The most effective compound containing bromine, for example, halon 1301 is $CBrF_3$. Inorganic bromine compounds function in water sanitation and silver bromide is used in photographic film. Bromine also appears in quartz-halide light bulbs.

### 2.1.1 Storage of halogens

Though halogens have a variety of applications storing is a major issue. Since chlorine is a harmful gas, it must be stored in a sealed container. Chlorine gas which is gaseous at ordinary temperatures, generally stored in a special cylinder. For the purpose of overcoming storing difficulty, methods other than the techniques for directly liquefying the halogen are being researched. Heretofore, there has been used one method in which the halogen is converted into a complex compound with an amine and is stored in a liquid state, [1] and another method (a hydrate method) in which has been cooled to several degrees centigrade or less and is stored in the form of a solid hydrate such as $Cl_2.6H_2O$ or $Br_2.10H_2O$. [2] These methods involve reactions such as complexing reactions and hydrating reactions, and thus in these cases, to form and decompose a complex or hydrate

heat energy corresponding to the heat of each reaction mush be eliminated from the system. As for the hydrate method, the halogen cannot be stored securely, unless solid hydrate continuously maintained in a cold state during the storage.

Antimony pentachloride **is** used as a storage material for chlorine chemically. It is prepared by passing chlorine gas into molten antimony trichloride.

$$SbCl_3 + Cl_2 \rightarrow SbCl_5$$

It liberates chlorine when heated to 300 $^oC$.

$$SbCl_5 \rightarrow SbCl_3 + Cl_2 \uparrow$$

Even phosphorous pentachloride also used as storage material for chlorine.

### 2.1.2 Graphene, a new storage material

Single and few few-layer graphene attracted attention as promising storage media. Graphene is a lightweight, chemically stable and exhibits attractive physico-chemical properties for hydrogen adsorption. Theoretical studies regarding chemically modified graphene suggest that it can absorb up to 8 wt. % of hydrogen, which is close to the objectives of the US Department of Energy for hydrogen storage (9 wt% by 2015). For practical use as a storage medium, hydrogen should be released when needed, possibly without heating the device to high temperatures (several hundred centigrades).

Recently, Rao et al.[3] showed that Birch-reduction of few-layer graphene gives rise to hydrogenated graphene containing up to 5 wt. % of hydrogen. Interestingly, hydrogenated graphene decomposes on heating up to 500 $^oC$ or on laser irradiation, releasing all the hydrogen. This result demonstrates that the $sp^3$ C-H bond of hydrogenated graphene can

be considered to act as a reversible chemical storage of hydrogen. Reversible fluorination of graphene has also been reported by Zhu et al.[4]

## 2.2 Scope of the present investigations

Storage of chlorine in high pressure cylinders and tanks is well known. It will be interesting if there is an alternative way of storing chlorine. They are few ways of storing halogens like hydrate method or by making complexes with amines. These methods have their own demerits. Recently, graphene, a noble material has found to be a good candidate for storing hydrogen. Interestingly, hydrogenated graphene decomposes on heating up to 500 $^{o}$C or on laser irradiation, releasing all the hydrogen. This shows that the $sp^3$ C-H bond of hydrogenated graphene can be considered to act as a reversible chemical storage of hydrogen. In the light of this observation, we felt that it would be of interest to carry out chlorination of graphene and examine the nature of the chlorinated product. It would be interesting to explore whether chlorinated graphene decomposes on heating or on laser irradiation. When excimer laser is irradiated upon chlorinated graphene the C-Cl bond is cleaved to give back graphene. Such photoinitiated chemical transformations are exothermic in nature and therefore release heat. Such heat can be measure from the rise of temperature of the solution. We have therefore carried out chlorination of graphene and examined the stability of the chlorinated product. We have also carried out a similar study on the bromination of graphene.

## 2.3 Experimental section

### 2.3.1 Synthesis of Few-layer graphene

Few-layer graphene (G) was prepared by the arc evaporation of graphite in a water-cooled stainless steel chamber filled with a mixture of hydrogen (200 Torr) and helium (500 Torr) without using any catalyst.[5] In a typical experiment, a graphite rod (Alfa Aesar with 99.999% purity, 6 mm in diameter and 50 mm long) was used as the anode and another graphite rod (13 mm in diameter and 60 mm in length) was used as the cathode. The arc-discharge current (during the evaporation of anode) was in the 100-150 A range, with a maximum open circuit voltage of 60 V. The graphene obtained by this method contains 2-4 layers.

### 2.3.2 Synthesis of chlorinated graphene (G-Cl)

Graphene (15 mg) was taken in 30 mL of carbon tetrachloride (spectroscopic grade) and sonicated for 20 min using a ultrasonicator. The suspension obtained was transferred to a 500 mL quartz vessel which was fitted with a condenser maintained at -77 $^{o}$C. The reaction chamber was purged with high pure nitrogen (99.9999%) for 30 min and chlorine gas was passed through the chamber. The gaseous chlorine condensed in the quartz vessel (see Figure 1). The quartz vessel containing around 20 mL of liquid chlorine was heated to 250 $^{o}$C with simultaneous irradiation of UV light (Philips 250 Watt High pressure Hg vapor lamp) for 1.5 h. The solvent and excess chlorine was removed, leaving a transparent film on the walls of the quartz vessel. The solid was dispersed in absolute alcohol under ultrasonication, filtered and washed with distilled water and absolute alcohol. The filtrate was then re-dispersed in 40 ml of distilled water, ultrasonicated for 2 min and centrifuged. The black supernatant obtained was separated and filtered

using a polyvinylidene fluoride (PVDF) membrane (200 nm pore size). The yield from 15 mg graphene sample was around 3-4 mg.

### 2.3.3 Synthesis of brominated graphene (G-Br)

In the case of bromination, 12 mg of graphene was taken in the quartz vessel, to which 20 mL of liquid bromine was added. The mixture was sonicated for 10 min using an ultrasonicator. To this 0.5 g of carbon tetrabromide was added. The quartz vessel was then heated to 250 $^{o}$C with simultaneous irradiation of UV light just as in chlorination. The excess bromine was removed and the product washed with sodium thiosulphate. The solid residue was then washed with water and absolute alcohol several times to remove

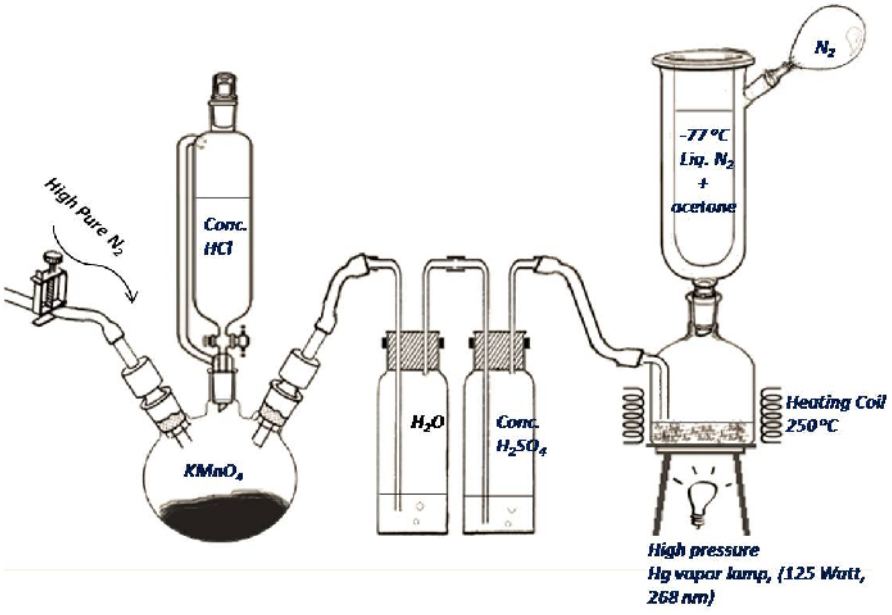


**Figure 1.** *Experimental setup used for chlorination of graphene*

sodium thiosulphate and then dispersed in 40 mL distilled water and centrifuged. The black supernatant obtained was separated and filtered using a PVDF membrane (200 nm pore size). The yield from 12 mg sample was around 2-3 mg.

### 2.3.4 Photothermal experiment

Chlorinated graphene (3 mg) was dispersed in $CCl_4$ and taken in a quartz vessel. The solution was irradiated using the set up show in Figure 2. The temperature of the solutions is recorded every minute using a thermal sensor and this was continued for 45 min. Lambda physik KrF excimer laser ($\lambda$ = 248 nm, $\tau$ = 30 ns, rep. rate = 5 Hz) was employed for this purpose. It is necessary to have a good dispersion of the graphene material in the solvent in order to spread the heat uniformly throughout the solution. Solvents to might get heated on laser radiation. It is, therefore, necessary to measure separately the effect of irradiation the solvent alone.

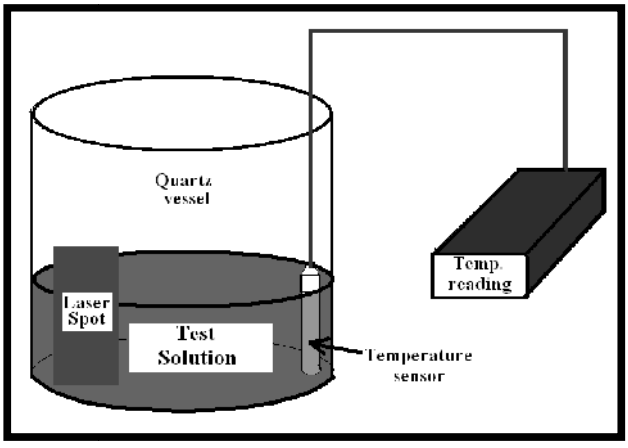


**Figure 2.** *Schematic of the experimental set-up for measurement of the heat evolved during laser-induced chemical transformation.*

## Chapter 2

### Characterization techniques

The halogenated samples were characterized by energy dispersive X-ray spectroscopy (EDAX), X-ray photoelectron spectroscopy (XPS), transmission electron microscopy (TEM), Raman spectroscopy, atomic force microscopy (AFM), thermogravimetric analysis (TGA) and infra-red spectroscopy. They were heated to different temperatures in the 200°-600 °C range and the products subjected to EDAX analysis and other methods of characterization. To study the laser induced transformation of the chlorinated graphene, the chlorinated graphene samples were first spin-coated on a NaCl crystal and dried slowly to evaporate all solvent present on the crystal. For laser irradiation, the NaCl crystal (coated with the sample) was tightly affixed (covered) with a quartz plate so that material could not get delaminated from the substrate. Lambda physik KrF excimer laser ($\lambda$ = 248 nm, $\tau$ = 30 ns, rep. rate = 5 Hz) was employed for this purpose. The aluminum metal slit (beam shaper), which usually gives a rectangular beam, was removed while laser irradiation was carried out. This makes laser energy almost uniform throughout the area where the sample is present. Excimer laser beam direction was aligned normal to the substrate. Laser beam energy of 370 mJ was employed to achieve the dechlorination of graphene.

EDAX spectrum was recorded by employing FEI NOVA NANOSEM 600. X-ray photoelectron spectra was recored with a Omicron nanotechnology spectrometer. To record IR spectra, the chlorinated graphene samples were spin-coated on a NaCl crystal and spectra recorded using a Bruker IFS 66V/S. TGA of the samples was carried out in a flowing argon atmosphere or in air with a heating rate of 10° per minute using a Mettler-

Toledo-TG-850 apparatus. TEM images were obtained with a JEOL JEM 3010 instrument fitted with a Gatan CCD camera operating at an accelerating voltage of 300 kV. Raman spectra were recorded at different locations of the sample using Jobin Yvon LabRam HR spectrometer with 632 nm Ar laser. AFM measurements were performed using Bruker-Innova atomic force microscope.

### 2.4 Results and discussion

We have carried out halogenation studies on few-layer graphene since the presence of more than one layer is expected to favor the hydrogenation reaction.[3] We have used graphene samples with 2-4 layers for the present study. The graphene (G) sample was characterized by employing transmission electron microscopy (TEM), atomic force microscopy (AFM), X-ray photoelectron spectroscopy (XPS), Raman spectroscopy and infrared spectroscopy. Brunauer-Emmett-Teller (BET) surface area of the graphene was around 200 $m^2/g$. The Raman spectrum showed the characteristic D (1323 $cm^{-1}$), G (1572 $cm^{-1}$), D' (1600 $cm^{-1}$) and the 2D (2641 $cm^{-1}$) bands.[6,7] The D and D'-bands are defect-induced features and are absent in defect-free samples. The G-band corresponds to the $E_{2g}$ mode of graphene and arises from the vibration of $sp^2$ bonded carbon atoms. The 2D band originates from second order double resonant Raman scattering and varies with the number of layers.

Chlorination of graphene was carried out by irradiation with UV light in liquid chlorine medium and the product examined by various techniques mentioned earlier. We show typical EDAX analysis of a chlorinated sample (G-Cl) in Figure 3 (a). We could chlorinate graphene by this means up to 56 wt. % (30 at. %). It should be noted that

maximum possible chlorination 74.7 wt. %. We have estimated the composition of G-Cl by employing XPS (Figure 3 (b)) as well. The X-ray photoelectron (XP) spectrum shows a is signal around 284.6 eV, assigned to C 1s and features due to chlorine 2p at 201.2 eV (see inset of Figure 3 (b)). Deconvolution of the C1s feature could be carried with three features centered at 284.6, 285.8 and 287.6 eV corresponding to $sp^2$ hybridized carbon, $sp^3$ hybridized carbon and C-Cl respectively.[8] The composition of the sample was determined by the ratio of C-Cl peak intensity in Cl 2p to the C1s peak intensity taking into account the atomic sensitivity factors of Cl 2p and C 1s.[9,10] This gave an estimate of 30 at. % of chlorine in agreement with EDAX analysis.

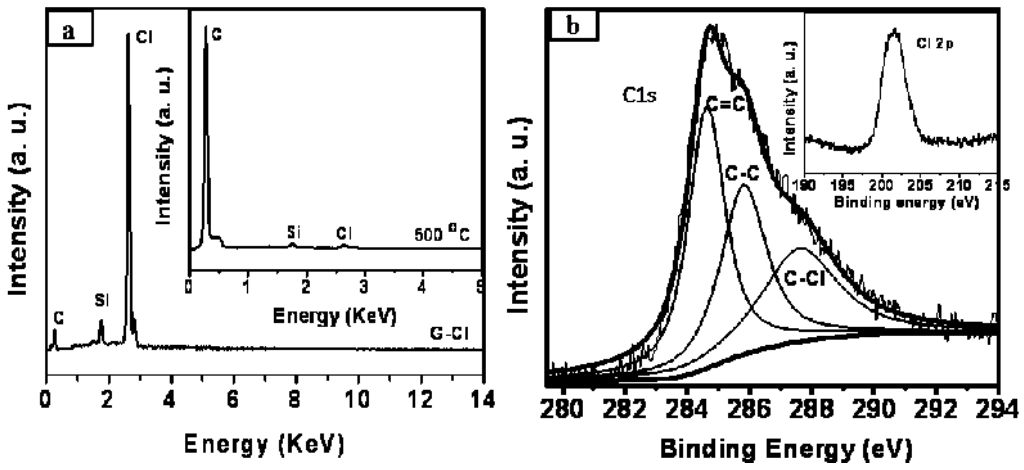


**Figure 3** *(a) EDAX spectrum of chlorinated graphene (G-Cl). Inset shows the EDAX spectrum after heating G-Cl at 500 $^oC$ for 4 h. (b) C1s core level XP spectrum of G-Cl. Inset shows the Cl 2p signal in XPS.*

The infrared spectrum of the chlorinated sample shows a band at 790 $cm^{-1}$ due to the C-Cl stretching vibration as shown in Figure 4 (a).[11] Thermogravimetric analysis supports the EDAX and XPS results.

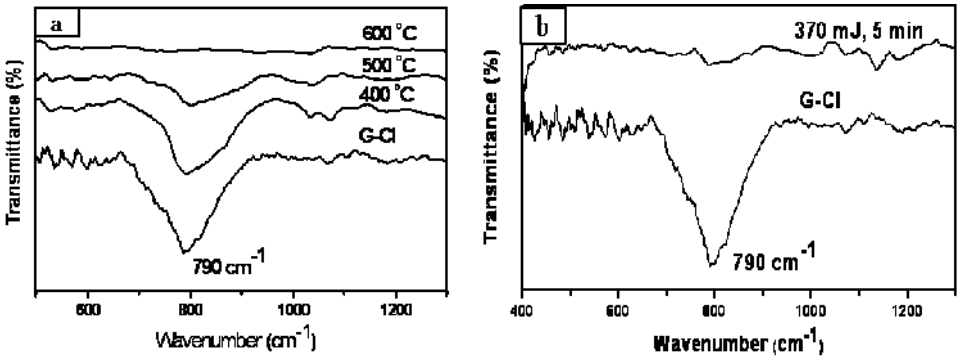


**Figure 4***(a) IR spectra of G-Cl heated for 4h at 400 °C, 500 °C and 600 °C. (b) IR spectra of G-Cl and G-Cl subjected to laser radiation (370 mJ, 5 min).*

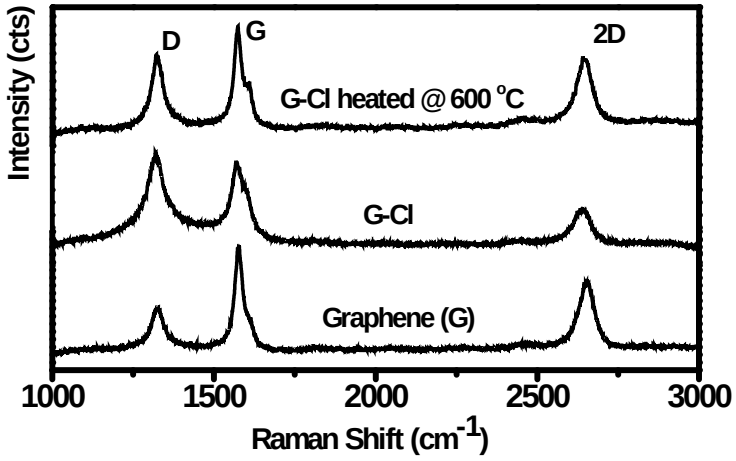


**Figure 5.** *Raman spectra of graphene (G), chlorinated graphene (G-Cl) and G-Cl heated at 600 °C*

The chlorinated graphene (G-Cl) sample is stable under ambient condition and can be stored for long periods. We have examined the thermal stability of G-Cl in detail. In Figure 4(a), we show the infrared spectra of the chlorinated sample heated to different temperatures. We observe a decrease in C-Cl band intensity on heating progressively and completely disappears above 500 $^{o}$C. In Figure 5 we show the Raman spectra of graphene (G), chlorinated graphene (G-Cl) and G-Cl heated at 600 $^{o}$C. The Raman spectrum of the chlorinated sample shows an increase in the intensity of the D band relative to that of the G-band. On chlorination, due to the C-Cl $sp^3$ bond formation and breaking of C=C $sp^2$ translational symmetry, intensity of D band increases and 2D band decrease, thus resulting in increased defects in graphene lattice (due to $sp^3$ C-Cl bond formation). The Raman data of graphene and functionalized graphene is given in Table 1.

| **Sample** | **D band ($cm^{-1}$)** | **G-Band ($cm^{-1}$)** | **2D band ($cm^{-1}$)** | **$I_D/I_G$** | **$I_{2D}/I_G$** |
|---|---|---|---|---|---|
| Graphene | 1323 | 1568 | 2649 | 0.4 | 0.6 |
| G-Cl | 1320 | 1570 | 2645 | 1.1 | 0.4 |
| G-Cl at 600 $^{o}$C | 1323 | 1572 | 2644 | 0.7 | 0.6 |

**Table 1.** *The Raman data of graphene and functionlized graphene*

In Figure 6 we show the loss of chlorine from the chlorinated graphene with increase in temperature. The EDAX spectrum of the sample heated to 500 $^{o}$C also shows the disappearance of the chlorine signal (see inset of Figure 3 (a)). Clearly all the chlorine is eliminated on heating G-Cl to 500 $^{o}$C.

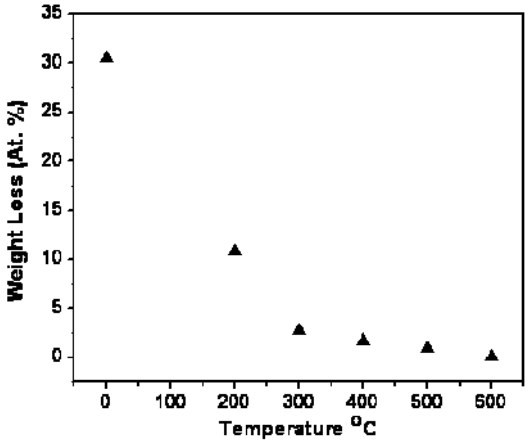


**Figure 6.** *Loss of chlorine from chlorinated graphene with increase in temperature*

We could also remove chlorine in G-Cl on irradiation with a laser (Lambda physik KrF excimer laser (λ = 248 nm, τ = 30 ns, rep. rate = 5 Hz, laser energy = 370 mJ)). We show the effect of laser irradiation in Figure 4 (b) which shows the absence of the C-Cl stretching band in the infrared spectrum on irradiation for 5 min.

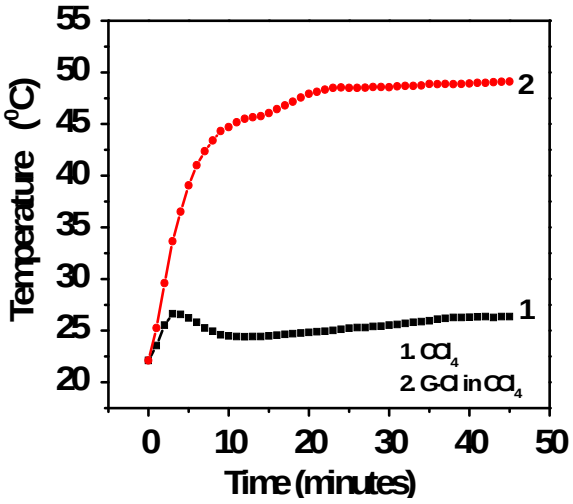


**Figure 7.** *Changes in temperature of the solution with laser irradiation tme for chlroinated graphene (G-Cl)*

Dechlorination by laser irradiation shows photothermal effect. Thus, G-Cl dispersed in carbon tetrachloride shows an increase in temperature by 26 $^{o}$C on irradiation (Figure 7). The Raman spectrum of the dechlorinated sample showed a decrease in the relative intensity of the D-band to the value in the starting graphene sample (Figure 5).

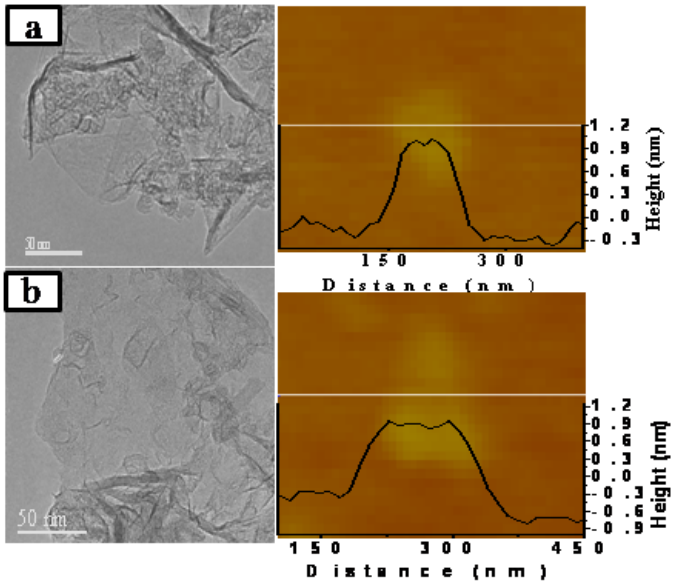


**Figure 8.** *TEM images of (a) graphene and (b) dechlorinated graphene. AFM images of these samples are shown alongside*

Interestingly, the nature of graphene was not affected on chlorination and dechlorination. In Figure 8 we compare the TEM images of the starting graphene sample and of the dechlorinated sample. AFM images of the two samples are also comparable. The dechlorinated samples can be chlorinated again satisfactorily. We have also carried out bromination of graphene.

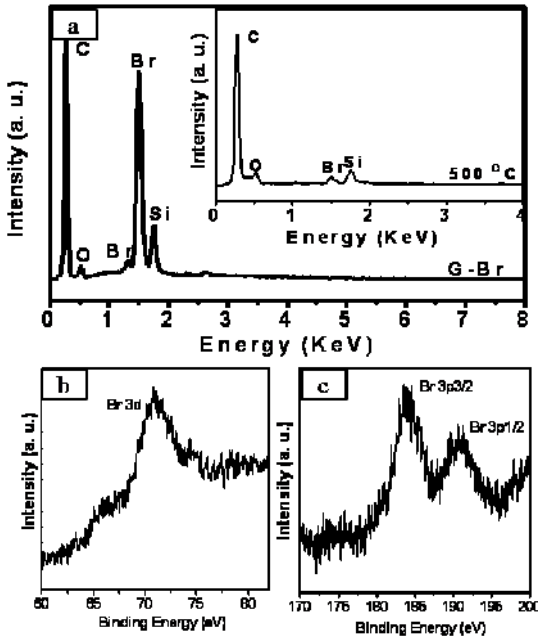


**Figure 9** (*a) EDAX spectrum of brominated graphene (G-Br). Inset shows the EDAX spectrum after heating at 500 $^{o}$C for 4 h. Core level XP spectra of G-Br show (b) Br 3d and (c) Br 3p signals.*

Figure 9 (a) shows a typical EDAX spectrum of graphene (G-Br) containing 25 wt. % (4.8 at. %). XPS analysis of the brominated sample shows Br 3d, $3p^{3/2}$ and $3p^{1/2}$ features at 70.9, 183.9 and 190.8 eV respectively as shown in Figures 9 (b) and (c).[12,13] Bromine in the samples could be eliminated to heating at 500 $^{o}$C as evidenced by the EDAX spectrum given in the inset of Figure 9 (a).

## 2.5 Conclusions

The present study demonstrates that one can achieve chlorination of few-layer graphene at least up to 56 wt. % by UV irradiation in liquid-chlorine medium. It may be possible to attain higher chlorine content by other means. The chlorinated graphene consists of $sp^3$ C-Cl bonds which are stable at room temperature. However, the chlorine can be removed on heating to around 500 $^oC$ or by laser irradiation. Clearly, dechlorination is associated with a small barrier just as the decomposition of hydrogenated graphene.[3] The strain in the chlorinated sample appears to drive the dechlorination to form the more stable graphene. It is noteworthy that chlorination of graphene is reversible. The present study demonstrates that few-layer graphene can be used to store chlorine and bromine.

## 2.6 References

[1] A. Popov, R. Rygg, *J. Am. Chem. Soc.*,1957, **79**, 4622.

[2] A. M. Berman, R. C. Walker, D. J. Aller, *U.S. Pat. No.* **4001036.**

[3] K. S. Subrahmanyam, P. Kumar, U. Maitra, A. Govindaraj, K. P. S. S. Hembram, U. V. Waghmare, C. N. R. Rao, *Proc. Natl. Acad. Sci.*, 2011, **108**, 2674.

[4] S.Tang, S. Zhang, J. Phys. Chem. C, 2011, **115**, 16644.

[5] K. S. Subrahmanyam, L. S. Panchakarla, A. Govindaraj, C. N. R. Rao, *J. Phys. Chem. C*, 2009, **113** ,4257

[6] M. A. Pimenta, G. Dresselhaus, M. S. Dresselhaus, L. G. Cancado, A. Jorio, R. Saito, *Phys. Chem. Chem. Phys.*, 2007, **9**, 1276.

[7] A. Das, S. Pisana, B. Chakraborty, S. Piscanec, S.K. Saha, U.V. Waghmare, K.S. Novoselov, H.R. Krishnamurthy, A.K. Geim, A.C. Ferrari, A.K. Sood, *Nat. Nanotechnol.*, 2008, **3**, 2010.

[8] H. Yu, Z. Zhang, Z. Wang, Z. Jiang, J. Liu, L. Wang, D. Wan, T. Tang, *J. Phys. Chem. C*, 2010, **114**, 13226.

[9] E. Papirer, R. Lacroix, J.-B. Donnet, G. Nansé, P. Fioux, *Carbon*, 1995, **33**, 63.

[10] B. Li, L. Zhou, D. Wu, H. Peng, K. Yan, Y. Zhou, Z. Liu, *ACS Nano*, 2011, **5**, 5957.

[11] C. N. R. Rao, *Chemical Applications of Infrared Spectroscopy*, Academic Press, New York, 1963.

[12] J. F. Colomer, R. Marega, H. Traboulsi, M. Meneghetti, G. V. Tendeloo, D. Bonifazi, *Chem. Mater.*, 2009, **21**, 4747.

[13] J. F. Friedrich, S. Wettmarshausen, S. Hanelt, R. Mach, R. Mix, E. B. Zeynalov, A. M -Plath, *Carbon*, 2010, **48**, 3884.

# CHAPTER 3

# SYNTHESIS AND CHARACTERIZATION OF NITROGEN-DOPED GRAPHENE AND ACID- FUNCTIONALIZED GRAPHENE


## Summary

Two-dimensional graphene exhibits fascinating electronic properties as exemplified by ballistic electronic conduction and occurrence of quantum Hall effect at room temperature. Electronic applications of graphene, however, get limited because of the band gap. It becomes necessary to tune the band gap by chemical modification or doping. Doping can modify the electronic structure of graphene significantly. Graphene can be doped electrochemically, through molecular charge-transfer and with elements like nitrogen and boron causing marked changes in the Raman spectrum. We found a easy way of doping graphene with nitrogen using urea as nitrogen source. We have obtained 7 wt. % of nitrogen content as found by with elemental analysis and X-ray photoelectron spectroscopy. The graphene samples generally had 2-4 layers estimated by atomic force microscopy and transmission electron microscopy. The N-doping in graphenes causes a stiffening of the G-band in the Raman spectra. We notice a slight increase in the thermal stability of the nitrogen doped graphene samples as compare to the pure graphene.

Liquid mineral acids were replaced by solid acids for the production of fine chemicals by acid-catalysed in liquid phase reactions. The solid acids have advantages of heterogeneous

catalysts which are very easy to separate from the reaction medium and can be reused. Sulfonic acid functionalized graphene (G-$SO_3H$) shows promising applications in acid-catalysed reactions. We have synthesized highly functionalized graphene using concentrated sulphuric acid and nitric mixture. We have estimated the acid sites of the functionalized graphene using acid-base titrations. Thermogravimetric curves shows that the sulfonic acid groups are stable up to 550 $^{o}$C. Catalytic ability in the esterification of acetic acid with 1-butanol show that G-$SO_3H$ is a highly active, very stable, and excellently recyclable catalyst.

# 3.1 Nitrogen-doped graphene

## 3.1.1 Introduction

Tuning physicochemical properties by chemical modification of materials becomes necessary in many applications.[1] One way of achieving this control is by elemental doping, a method effectively used in semiconductor silicon technology.[2, 3] For example, nitrogen atoms in silicon lock dislocations to increase mechanical strength. Effects of doping silicon with phosphorous and other elements with different oxidation states have been well documented. Chemical substitution (doping) brings about significant changes in carbon materials as well. In particular, substitution of boron or nitrogen in carbon nanostructures renders them p-type or n-type respectively. Doping also affects the Raman spectra and other properties of carbon nanostructures.[1]

### Nitrogen doping of graphene and carbon nanotubes

Different routes have been reported to dope graphene and carbon nanotubes (CNTs). In as early as 1997, substitution of carbon by nitrogen in multi-walled carbon nanotubes (MWNTs) was achieved by the pyrolysis of aza-aromatics (pyridine, triazine).[4] The nitrogen content decreased with increasing temperature of pyrolysis; the estimated nitrogen content being around 5, 3.5, and 3 at.% in nanotubes prepared by the pyrolysis of pyridine at 973, 1123 and 1273 K respectively. Good yields of N-doped MWNTs are obtained by carrying the pyrolysis of a mixture of pyridine and $Fe(CO)_5$ in flowing $Ar+H_2$.[4] In this

procedure, the iron particles formed by the decomposition of $Fe(CO)_5$ act as nucleating centres for the growth of carbon nanotubes. N-doped MWNTs were also be prepared by pyrolyzing pyridine over Co nanoparticles at 1000 $^oC$.[5] Pyrolysis of ferrocene-melamine mixtures at 900-1000 $^oC$ in the presence of Ar produces large arrays of aligned CNx nanotubes.[6] Incorporation of 2-10 at.% N in MWNTs was achieved by this procedure. The electronic density of states (DOS) of $CN_x$ nanotubes obtained from scanning tunneling spectroscopy (STS) exhibits strong features in the band close to the Fermi level (0.18 eV). Based on tight-binding and ab-initio calculations, it is found that pyridine-like N is responsible for introducing donor states close to the Fermi Level. $CN_x$-CNT intramolecular junctions have been produced via chemical vapour deposition with ferrocene and melamine.[7] N-doped single-walled carbon nanotubes (N-SWNTs) have been prepared by the arc-discharge method by introducing a nitrogen-rich precursor into the anode along with the catalyst and graphite.[8] The nitrogen source is melamine or boron nitride. Up to 1 at.% of nitrogen has been incorporated in SWNTs by this method. Water plasma chemical vapor deposition of methane and ammonia is employed to prepare N-SWNTs on $SiO_2$/Si substrates.[9] Up to 4 at.% nitrogen can be incorporated in SWNTs by this means. SWNTs obtained by this route are small in diameter and are semiconducting in nature. The density of nanotubes formed monotonically decreases with the increase in ammonia content. N-SWNTs are not formed under high doses of ammonia. N-SWNTs with a defined diameter range can be prepared by chemical decomposition of a 100% benzylamine vapour using ceramic supported bimetallic catalysts (Mo, Fe).[10] A maximum nitrogen content of 2 at.% is

obtained by this procedure. The amount of nitrogen incorporated in the nanotubes varies with the temperature employed. N-doped DWNTs are synthesized by chemical vapor deposition of methane and ammonia over the bi-metallic catalyst, $Mo_{0.1}Fe_{0.9}Mg_{13}O$.[11, 12]

There are several reports on the preparation of nitrogen-doped graphene. Graphene has been doped with nitrogen by interaction with ammonia. Panchakarla et al.[13] carried the doping in gas phase and obtained a doping of 1 at. % of nitrogen. Dai et al.[14] reported 5 at. % of nitrogen by reacting graphene oxide with ammonia, Geng et al.[15] have obtained 2.8 at. % of nitrogen content by heating graphene with ammonia at 900 $^{o}$C. Yu et al.[16] obtained 8.9 % of nitrogen by a CVD process using a mixture of methane, hydrogen and ammonia at 800 $^{o}$C. Nitrogen doping in graphene has also been carried out by plasma reaction,[17, 18] solvothermal synthesis,[19] pyrolysis of graphene oxide with melamine,[20] and by wet chemical reaction of graphene oxide with dicyandiamide.[21] Reaction of graphene oxide with urea gives 1.2 at. % of nitrogen according to Lei et al.[22] Sun et al.,[23] however, report 10.1 at. % nitrogen by the hydrothermal reaction of graphene oxide with urea. Nitrogen-doped graphene has also been prepared on a large scale from sym-triazine.[24] We have carried out nitrogenation of reduced graphene oxide and few-layer graphene by the high-temperature reaction with urea at different graphene:urea weight ratios.

### 3.1.2 Scope of the present investigations

Graphene have many possible applications in nanoelectronics, supercapacitors and lithium secondary batteries. Electronic applications of graphene, however, get limited because of the band gap. It becomes necessary to tune the band-gap by chemical modification or doping.

Doping of graphene through molecular charge-transfer caused by electron-donor and –acceptor molecules also gives rise to significant changes in the electronic structure of graphenes composed of a few layers, as evidenced by changes in the Raman and photoelectron spectra. Charge-transfer by donor and acceptor molecules softens and stiffens the G-band, respectively.

The difference between electrochemical doping and doping through molecular charge-transfer is noteworthy. Secondly, opening the band-gap in graphene is essential for facilitating its applications in electronics. With this motivation, we have done nitrogenation of graphene using urea. We have done X-ray photoelectron spectroscopy for the nitrogen doped graphene samples to understand the nature of nitrogen in the graphene matrix.

### 3.1.3 Experimental section

**Synthesis of Reduced Graphene oxide (RGO)**

Reduced graphene oxide (RGO) was prepared along with graphene oxide (GO). GO was synthesized by Hummer's method.[25] In a typical experiment 15 ml of conc. sulfuric acid was taken in a round bottomed flask which was pre-cooled in an ice bath. To this, 300 mg of potassium nitrate (SD-fine chemicals) and 300 mg of graphite power (Alfa Aesar 99.9995 %) was added and stirred. To this mixture, 2 grams of potassium permanganate was added slowly and the resulting mixture stirred for 30 min at 40 $^{o}$C. The mixture was diluted with 30 mL of water and the temperature was raised to 80 $^{o}$C, followed by addition of 4 mL of 30 %

of hydrogen peroxide. The solution turned brown and the final product (GO) obtained was washed with de-ionized water and dried in vacuum at 50 $^{o}$C for 12 h. In order to prepare reduced graphene oxide (RGO), GO was taken in 200 mL de-ionized water and sonicated for 2 h. After this, 7 mL of hydrazine hydrate was added and the mixture refluxed 12h. The obtained product was washed several times with de-ionized water and vacuum dried.

**Synthesis of Few-layer graphene**

Few-layer graphene (HG) was prepared by the arc evaporation of graphite in a water-cooled stainless steel chamber filled with a mixture of hydrogen (200 torr) and helium (500 torr) without using any catalyst.[26] In a typical experiment, a graphite rod (Alfa Aesar with 99.999% purity, 6 mm in diameter and 50 mm long) was used as the anode and another graphite rod (13 mm in diameter and 60 mm in length) was used as the cathode. The arc-discharge current was in the 100- 150 A range, with a maximum open circuit voltage of 60 V. The graphene obtained by this method i.e., arc evaporation of graphite contains 2-4 layers.

**Synthesis of nitrogen-doped graphene**

To prepare nitrogen-doped graphene samples, RGO or HG (30 mg) was dispersed in 50 mL absolute ethanol, to which urea (300 mg) was added. The aqueous mixture was sonicated for 2 h, followed by evaporation of ethanol at 50 $^{o}$C to give a grey powder. The powder was finely milled, made into a pellet and transferred to a quartz boat and heated to different temperatures ranging from 700 to 900 $^{o}$C for 90 min in a nitrogen atmosphere. The mass ratios between graphene samples and urea were varied such as 1:3, 1:6 and 1:10. The products were re-dispersed in water and sonicated for 2 hours. After sonication, the product

was centrifuged and washed several times with de-ionized water to remove residual species which are adsorbed on the surfaces of graphene.

**Characterization techniques**

X-ray photoelectron spectra (XPS) of the nitrogen doped samples were recorded with an Omicron nanotechnology spectrometer. Thermogravimetric analysis (TGA) of the samples was carried out in a flowing argon atmosphere or in air with a heating rate of 10 $^{o}$C per minute using a Mettler-Toledo-TG-850 apparatus. TEM images were obtained with a JEOL JEM 3010 TEM instrument fitted with a Gatan CCD camera operating at an accelerating voltage of 300 kV. Raman spectra were recorded at different locations of the sample using Jobin Yvon LabRam HR spectrometer with 632 nm Ar laser. AFM measurements were performed using an Bruker-Innova atomic force microscope.

### 3.1.4 Results and discussion

We have carried out the reaction of RGO as well as of pure graphene (HG) with urea at different temperatures between 700 and 900 $^{o}$C by varying the graphene:urea (G:U) weight ratio from 1:3 to 1:10. The reaction products were characterized by XPS as well as by elemental analysis. The nitrogen content of the doped graphene samples are found to increase with the increase in urea content in the reaction mixture. Thus, reaction with G:U ratios of 1:6 and 1:10 at 900 $^{o}$C gave 4 and 7 wt. % of nitrogen respectively as found both with

elemental analysis (Table 1) and XPS. The nitrogen content was maximum in the samples prepared with 1:10 G:U ratio at 900 $^{o}$C and least for the sample prepared at 700 $^{o}$C, the latter having a nitrogen content of around 2.1 wt. %. Reaction of HG at 900 $^{o}$C gave a nitrogen content of ~ 2 wt. % when the G:U ratio was 1:10. Unlike the nitrogenated RGO (N-RGO), nitrogenated graphene (N-HG) had no oxygen functionalities. The oxygen functionalities in RGO give rise to reactions with the amino groups of urea to form C-N bonds and afford greater doping. That is why reaction of GO gives even greater % of nitrogen than RGO on reaction with urea. HG without any oxygen functionalities does not give rise to high nitrogen contents which is evidenced from XP survey spectra (Figure 1)

| ***Samples*** | ***900 $^{o}$C*** | ***800 $^{o}$C*** | ***700 $^{o}$C*** |
|---|---|---|---|
| | ***N (wt.%)*** | ***N (wt.%)*** | ***N (wt.%)*** |
| RGO:Urea (1:10) | 7.0 | 2.5 | 2.1 |
| RGO:Urea (1:6) | 4.7 | 2.1 | 1.7 |
| RGO:Urea (1:3) | 4.2 | 1.7 | 1.4 |

**Table 1** *Elemental analysis data of N-Doped RGO prepared at different temperatures*

XPS, a powerful tool to identify the element's states in bulk material have been used to prove the existence of C=N and other existing forms of nitrogen. We have carried out detailed study of the N (1s) spectra in order to understand the nature of nitrogen in N-RGO and

N-HG. In Figures 2 (a) and (b) we show the N (1s) spectra of products (N-RGO) of the reaction carried out at 900 and 800 $^{o}$C with G:U ratio of 1:10 respectively. The N 1s peak could be deconvoluted into three features. The peak at a binding energy of 398.3 eV corresponds to pyridinic nitrogen and the peak at 400.1 eV corresponds pyrrolic nitrogen. The peak at 401.9 eV corresponds to graphitic nitrogen. We see the pyridinic nitrogen is maximum in the sample prepared at 900 $^{o}$C and the pyrrolic nitrogen is maximum in the sample prepared at 800 $^{o}$C.

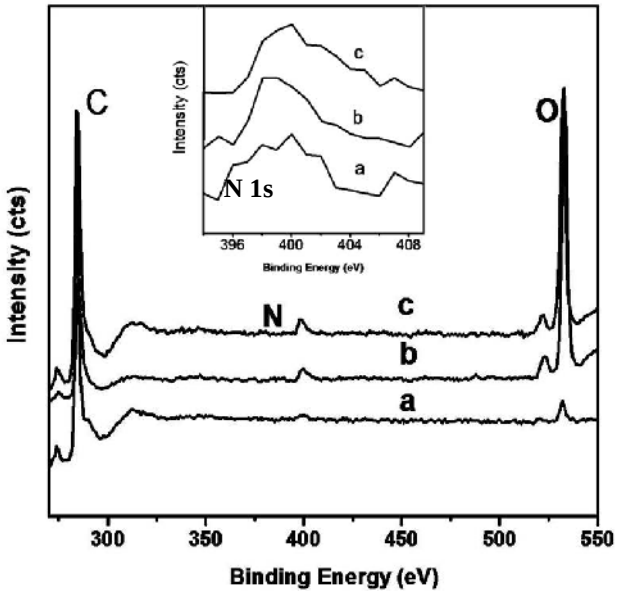


**Figure 1** *XPS Spectrum of N-Doped Graphene: (a) N-HG (1:10) at 900 $^{o}$C (b) N-RGO (1:10) at 800$^{o}$C (c) N-RGO (1:10) at 900 $^{o}$C (inset shows the N 1s core level spectra).*

Bonding of the three different nitrogens are shown in the scheme below. In Figure 2 (c) we show the N 1s spectra of N-HG prepared at 900 $^{o}$C (G:U of 1:10). The spectra was deconvoluted into three peaks 398.2 eV, 400.1 eV and 401.7 eV due to pyridinic, pyrrolic

and graphitic nitrogens respectively. Pyridinic nitrogen content is highest in this sample as well.

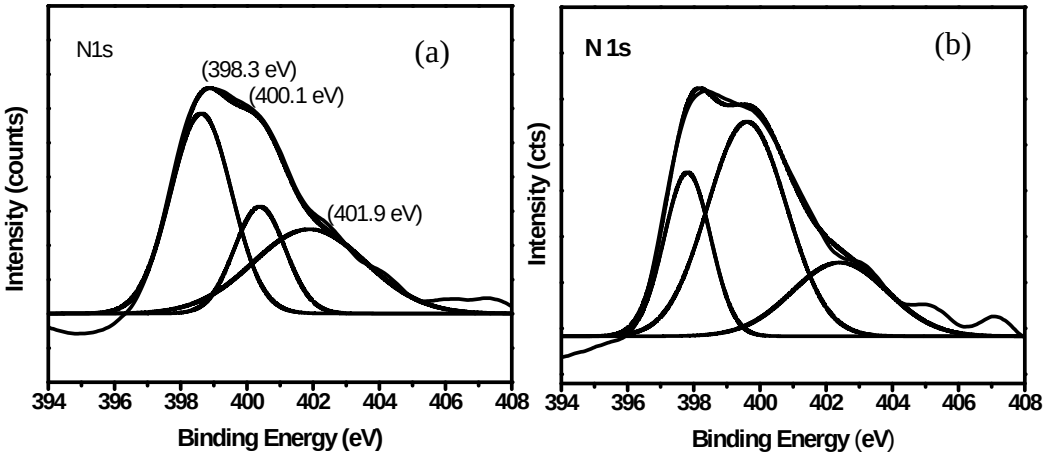


**Figure 2** *N1s core level XP spectrum of N- RGO (1:10) at (a) 900 $^{o}$C (b) 800 $^{o}$C.*

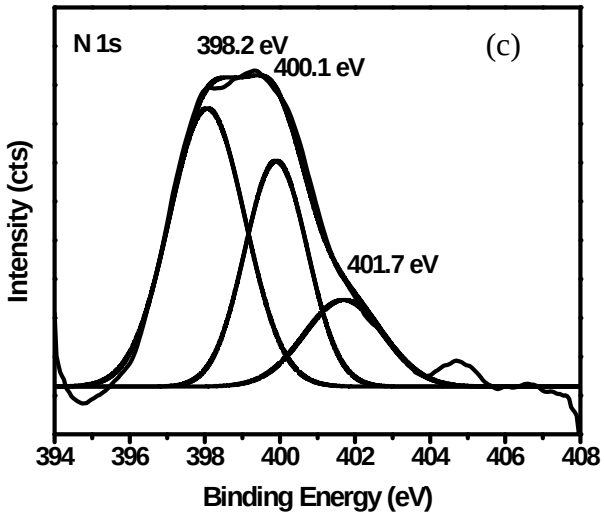


**Figure 2** (c) *N1s core level XP spectrum of N- HG (1:10) at 900 $^{o}$C.*

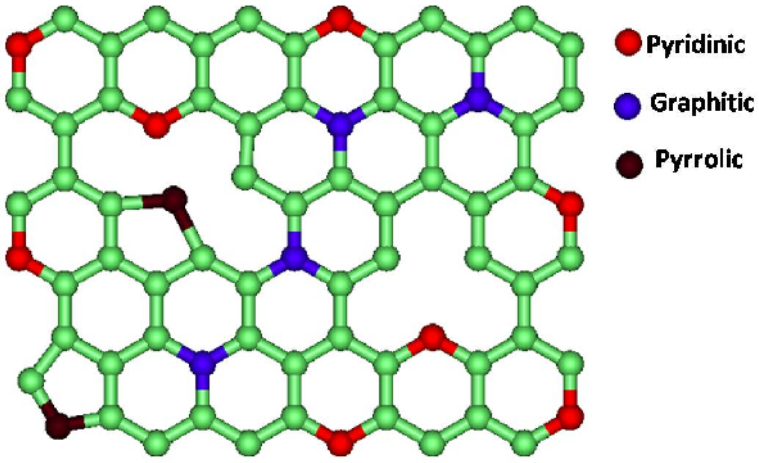


**Scheme:** *Bonding of different nitrogens in N-doped graphene samples*

In order to evaluate the degree of structural deformations of the graphene and N-graphene samples, Raman spectroscopy was carried out (Figure 3). The D band, at approximately 1340 $cm^{-1}$ for RGO and 1326 $cm^{-1}$ for HG, is disorder induced, attributable to structural defects and other disordered structures on the graphitic plane. The G-band, at approximately 1590 $cm^{-1}$ of RGO and 1570 $cm^{-1}$ for HG, is commonly observed for all graphitic structures.

G-band can be attributed to the $E_{2g}$ vibrational mode present in the $sp^2$ bonded graphitic carbons. The intensity ratio of D band to G band, namely the $I_D/I_G$ ratio, provides the measurement for the amount of structural defects. In Figure 3 (a) we show the Raman spectra of the RGO and RGO reacted with urea with different G:U ratios at 900 $^0$C. The G-band position shifts to higher frequency with increase in G:U ratio or the increase in the nitrogen content in the product. RGO shows the G-band at 1590 $cm^{-1}$ while N-RGO prepared with

1:10 G:U shows the G-band at 1597 $cm^{-1}$. The D-band position is essentially insensitive to nitrogen content. The $I_D/I_G$ ratio slightly decreases from 1.8 in RGO to 1.4 in N-RGO prepared with a G:U of 1:10. The G-band of N-HG also shifts towards higher frequency relative to HG (Figure 3(b)). The increase in the G-band frequency is around 5 $cm^{-1}$. HG shows G-band at 1570 $cm^{-1}$ and the N-HG show the G-band at 1575 $cm^{-1}$. There is no significant change in the $I_D/I_G$ ratio.

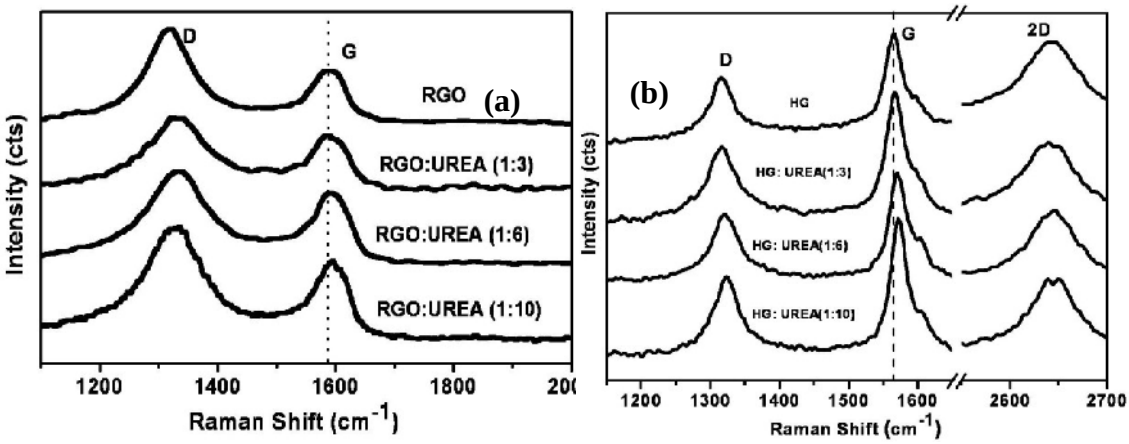


**Figure 3***(a) Raman spectra of RGO and N-RGO prepared at 900 $^oC$ with different weight ratios of urea. (b) Raman spectra of HG and N-HG prepared at 900 $^oC$ with different weight ratios of urea.*

In Figure 4 we show the Raman shifts of G-band of N-Doped RGO prepared with different concentration of urea at different temperatures. It clearly shows that the G-band position shifts towards higher frequency with respect to the nitrogen content as well as the reaction temperature.

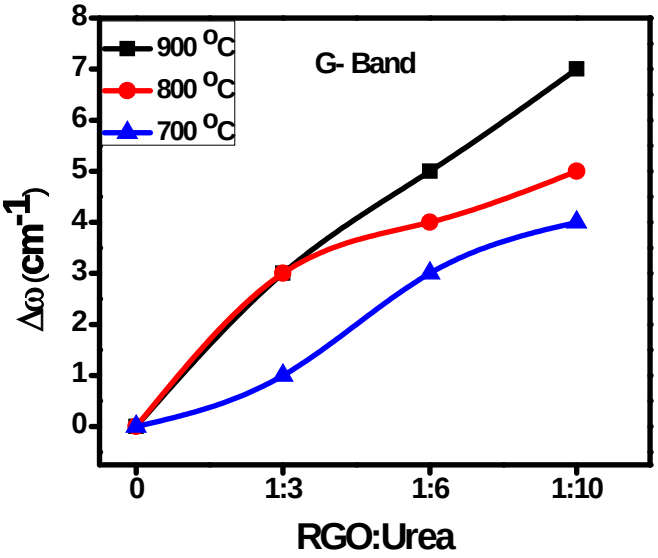


**Figure 4** *Raman shifts of G-band of N-Doped RGO prepared with different concentration of urea at different temperatures*

We have shown typical TEM and AFM images of N-RGO and N-HG in Figure 5. The TEM image of N-HG in Figure 5 (a) reveals the presence of 2-4 layers, consistent with the AFM image shown alongside. The TEM and the AFM images of N-RGO show that it has 4-5 layers.

In Figure 6(a) we show the TGA curve of N-RGO (G:U of 1:10) samples prepared at 900 $^{o}$C and 800 $^{o}$C along with the TGA curve for RGO. In Figure 6(b), we show the TGA curve of N-HG (G:U of 1:10) prepared at 900 $^{o}$C. We notice a slight increase in the thermal stability of the nitrogen doped samples.

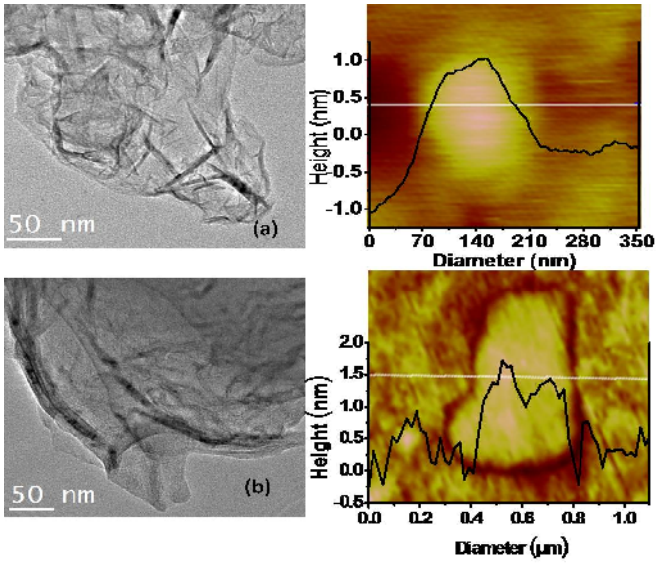


**Figure 5** *TEM images of (a) N-HG (b) N-RGO. AFM images of these samples are shown alongside.*

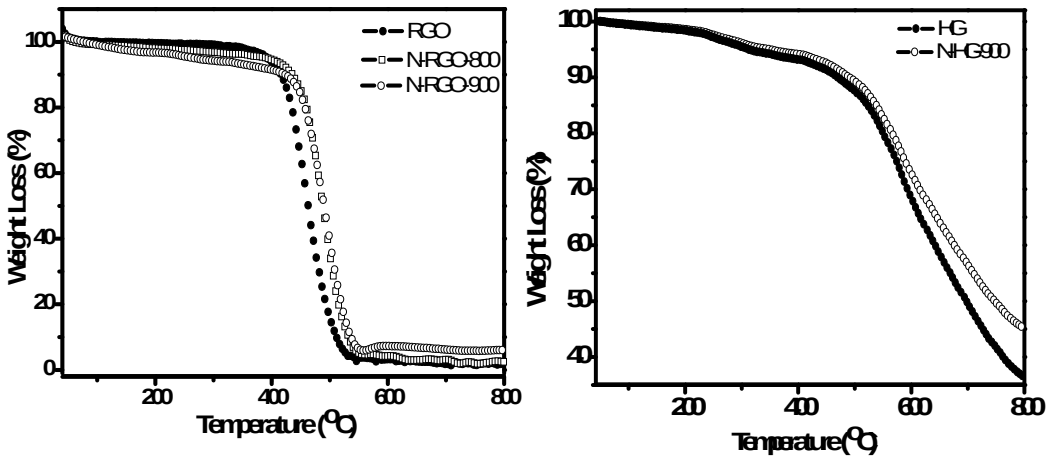


**Figure 6.** *TGA curves of (a) RGO, N- RGO at 800 °C and 900 °C (b) HG and N-HG at 900 °C.*

### 3.1.5 Conclusions

In conclusion, N-doped graphenes were synthesized by heating graphene and urea at different temperatures. The nitrogen content in the graphene lattice can reach ~7 wt. % which can be tuned by changing the ratio of graphene and urea as well as at different temperatures. Oxygen-containing functional groups in RGO and amino-groups of urea are suggested to be essential to form C-N bonds and helps in greater doping. Raman spectra of doped graphene show increase in G-band frequency with respect to urea concentrations and temperature.

## 3.2 Acid-functionalized graphene

### 3.2.1 Introduction

Organic transformations can be performed in both homogenous and heterogeneous phase. In homogenous reactions the distribution of the active sites is uniform and, consequently, molecules can collide without any difficulty. The reaction proceeds quickly with great efficiency and the rate-determining step is regulated by thermodynamics. The main disadvantage of homogenous catalytic reactions is that upon working up the reaction mixture, the catalysts cannot be regenerated or reused. As a result, they accumulate as waste. Homogenous catalytic processes, therefore, are not very advantageous either from the economic or the environmental point of view.

The replacement for homogenous catalysts strongly motivates scientist. A possible solution is to fix the catalytically active sites on various solid supports so the chemical reaction takes place under heterogeneous conditions. Heterogeneous catalysts, compared to their homogenous counterparts, have several advantages. First, the separation of catalyst from the reaction mixture can easily be performed by simple filtration or decantation. The application of heterogeneous catalysts is particularly useful from the industrial point of view. They proceed with high efficiency that is with high activity and selectivity. A further very important feature is that heterogeneous catalysts can be regenerated and reused for several catalytic cycles; which makes their application highly economical. In addition to these advantages, however, drawbacks have also to be

mentioned. Namely, the distribution of active sites is not uniform and, therefore, some of the active site cannot be reached by the reactants. Another problem is the non-uniform strength of the active sites, and hindered diffusion is often encountered in heterogeneous systems.

Most of the catalytic reactions are electrophilic in nature. Electrophilic catalysts applied in homogenous reactions (HF, $H_2SO_4$, $HNO_3$, trifluoromethanesulfonic acid) have additional drawbacks. Depending on the acid strength of various catalysts they can be used in a wide variety of reactions. Due to the strong acidic character of these catalysts they are very corrosive and poisonous.[27] Furthermore, technological applications can also be expanded using fluid and fixed-bed reactors. With the possibility of regeneration, manufacturing can be even more economical.

**Sulfonic acid functionalized catalytic materials**

Solid acids like Zeolites and mesoporous silicas (MCM and SBA materials) acts as heterogeneous catalysts for acid-catalysed reactions. These catalysts have weak acid sites and are not much efficient. Catalytically active acidic sites are mainly located in the pores of the catalysts, surface modification of the active sites helps to increase the catalytic activity. Considerable attention has been focused on tailoring the chemical composition these porous materials to increase their potential for catalytic applications. This could be accomplished either by post-synthesis grafting or direct co-condensation of tetraalkoxysiloxane and one or more organoalkoxysilanes.[28] Organic functionalization of silicates permits precise control over the surface properties, modification of the hydrophilic/hydrophobic of the surface, alteration of the surface reactivity, protection of the surface from attack, modification of the bulk properties of the materials and at the same time stabilizing the materials towards hydrolysis.[29] For example, mesoporous silica

having surfaced-bonded thiol groups showed high adsorption for heavy metals such as $Hg^{2+}$, $Ag^{+}$ ions from contaminated solutions.[30] Sulfonic acid groups grafted on mesoporous materials exhibited high catalytic activity for selective formation of bulky organic molecules.[31] The acid-synthesized sulfonic-functionalized products reported here have large uniform pore sizes, high surface areas, good mesoscopic order, high thermal and hydrothermal stabilities, and relatively high acid strengths, all of which are appealing properties for prospective catalytic applications. Thus these organo-functionalized mesoporous silica materials with controlled functionality and hydrophobicity are both physically robust and hold potential to perform complex separations, highly selective catalysis and organic-inorganic host-guest chemistry.[32] Even, sulfonic acid functionalized porous carbon and carbon nanotubes are known.[33,34]

### 3.2.2 Scope of the present investigations

Acid catalysts are essential for production of fine chemicals in industrial hydrocarbon chemistry. Traditional liquid-acid catalysts such as sulphuric acid, trifluoromethanesulfonic acid, etc., are highly efficient but non-recyclable. It is also costly and difficult to separate the liquid-acid catalysts from the homogeneous reaction mixture, thus resulting in abundant non-recyclable acid waste. Many solid acid catalysts like sulfonic acid functionalized mesoporous silicas and carbon have shown great potential to replace traditional liquid acids as recyclable and environmentally-safe acid catalysts. Graphene has excellent electrical properties, a large surface area and a two-dimensional structure providing an excellent platform to anchor a large amount of acidic

functional groups with accessible active sites. Thus, we functionalized graphene with sulfonic acid groups in order to use in acid-catalysed reactions.

### 3.2.3 Experimental

**Synthesis of Few-layer graphene**

Few-layer graphene (G) was prepared by the arc evaporation of graphite in a water-cooled stainless steel chamber filled with a mixture of hydrogen (200 torr) and helium (500 torr) without using any catalyst. In a typical experiment, a graphite rod (Alfa Aesar with 99.999% purity, 6 mm in diameter and 50 mm long) was used as the anode and another graphite rod (13 mm in diameter and 60 mm in length) was used as the cathode. The discharge current was in the 100- 150 A range, with a maximum open circuit voltage of 60 V. The graphene so obtained by the evaporation of anode contains 2-4 layers.[35]

**Synthesis of acid-functionalized graphene**

To synthesize acid functionalized graphene; 50 mg of graphene (G) was taken in a round bottomed flask. To this conc. sulfuric acid and conc. nitric acid (3:2) was added and refluxed for 90 min to obtain a clear colorless solution. Excess acid mixture was distilled off using vacuum pump to give a white residue, in contrast to the black graphene that we started with (Figure 1). The white solid was washed extensively with distilled water and dried under vacuum.

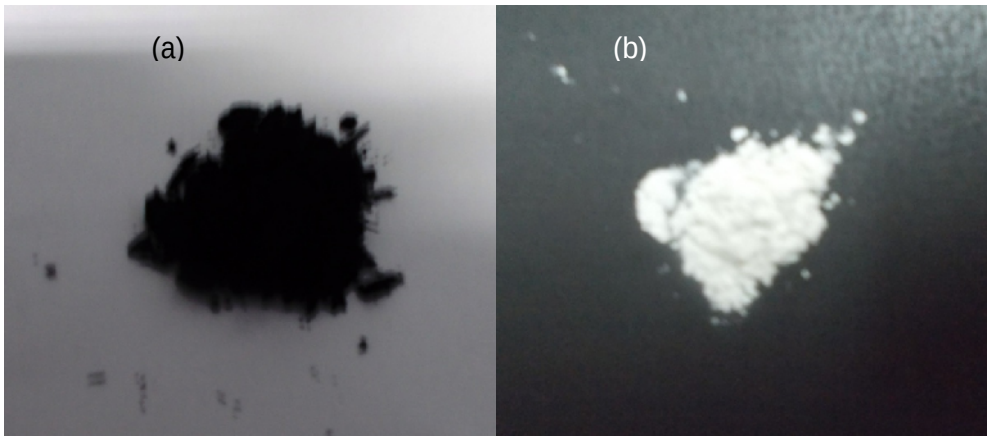


**Figure 1** *(a) Photograph of graphene (b) Photograph of white solid (G-$SO_3H$)*

**Catalytic ability**

The catalytic ability of the acid functionalized graphene was examined through esterification reaction. Esterification was carried out in a mixture of acetic acid (50 mmol) and 1-butanol (50 mmol) at 90 $^{o}$C for 5 h. The catalysts were vacuum dried (10-3 Torr) at 100 $^{o}$C for 1 h before the reactions, and 10 mg catalyst was used for each reaaction. The product was n-butylacetate with a selectivity of nearly 100%. The resulting solution was analyzed by gas chromatography coupled with mass spectroscopy (GC-MS).

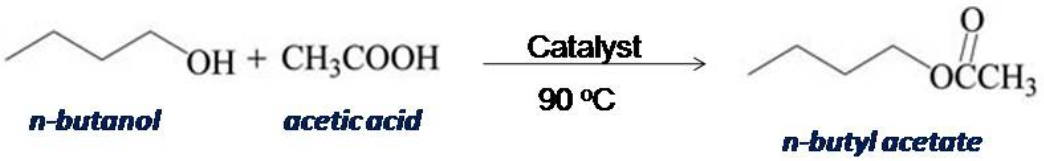

### Characterization techniques

Field emission scanning electron microscope (FESEM) images were recorded with a FEI NOVA NANOSEM 600. Transmission electron microscope (TEM) images were obtained with a JEOL JEM 3010 instrument. Raman spectra were recorded with a LabRAM HR high resolution Raman spectrometer (Horiba Jobin Yvon) using He–Ne Laser (λ=630 nm). X-ray photoelectron spectra was recorded with a Omicron nanotechnology spectrometer.

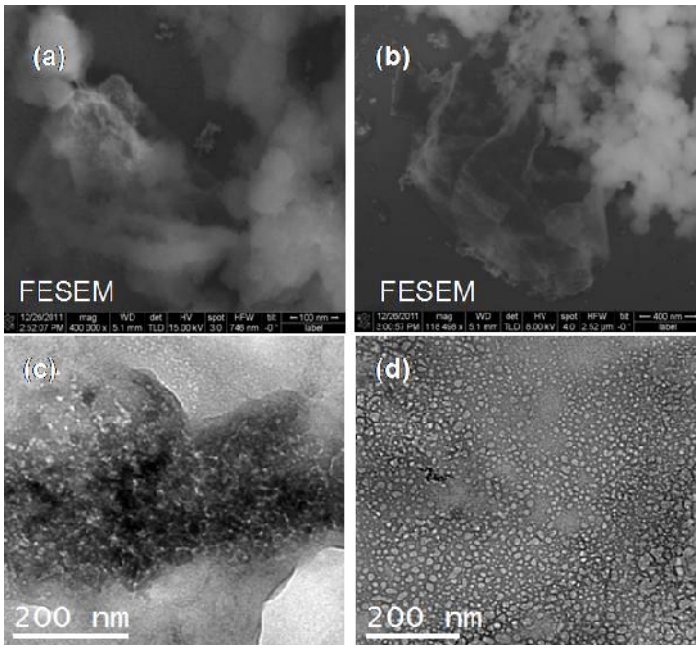


**Figure *2*** *(a & b) FESEM of white solid (c & d) TEM images of the white solid*

### 3.2.4 Results and discussion

FESEM images of the white solid shows the presence of graphene like structures (Figure 2 (a & b). TEM images show the presence of sheets. In Figure 2(c & d), we show typical TEM images of the graphene structures found in the solid. The images do not clearly reveal the graphitic fringes, possibly because of extensive functionalization of the graphene. Acid-base titrations indicated the acid sites present are around 6.7 mmol per gram.

The infrared spectrum of the white solid (Figure 3) show the characteristic band due to -OH (3300 $cm^{-1}$, very broad), $-SO_3H$ (1050, 1350 $cm^{-1}$), C=C/C=O (1600 $cm^{-1}$) and C-S (around 500-700 $cm^{-1}$) groups.

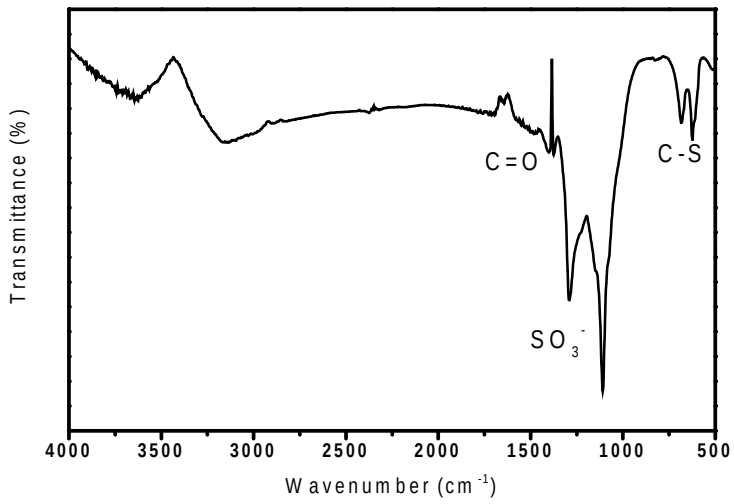


**Figure 3** *The infrared spectrum of the white solid*

Figure 4 shows the TG curves of graphene (G) and G-$SO_3H$ in which acid-functionalized graphene exhibits weight lose centred at 200 $^oC$ to 550 $^oC$ which are assigned to the

decomposition of sulfonic acid groups. These results indicate that sulfonic acid functionalized with graphene has much better thermal stability than the sulfonic acid groups functionalized with organic molecules.

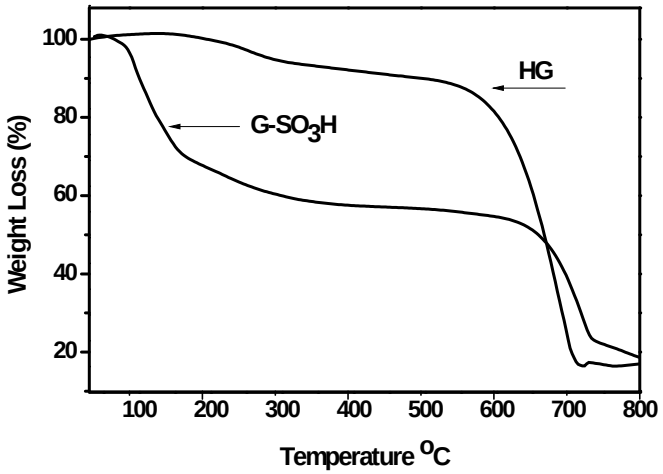


**Figure 4.** *The TG curves of graphene (G) and G-$SO_3H$*

In Figure 5 we show the core level XP spectrum of C 1s, O 1s and S 2p confirming the presence of sulfonic acid groups. XP core level spectra of C 1s (Figure 5(a)) shows peaks centred at 284.5, 286.3 and 288.6 eV, which are corresponding to the non-oxygenated ring carbon, the carbonyl carbon, and the carbon bonded with sulphur respectively. Figure 5(b) shows the core level spectrum of S 2p, which is deconvoluted with four features centered at 167.3, 168.1, 168.4 and 169.2 eV corresponding to C-S and S=O, $-SO_3^-$, C-S and S=O and $-SO_3^-$ respectively. Figure 5(c) shows the core level spectrum of O 1s, which is deconvoluted with three features centred at 529.5, 532.1 and 533.8 eV corresponding to C-O, S=O and O-H respectively.

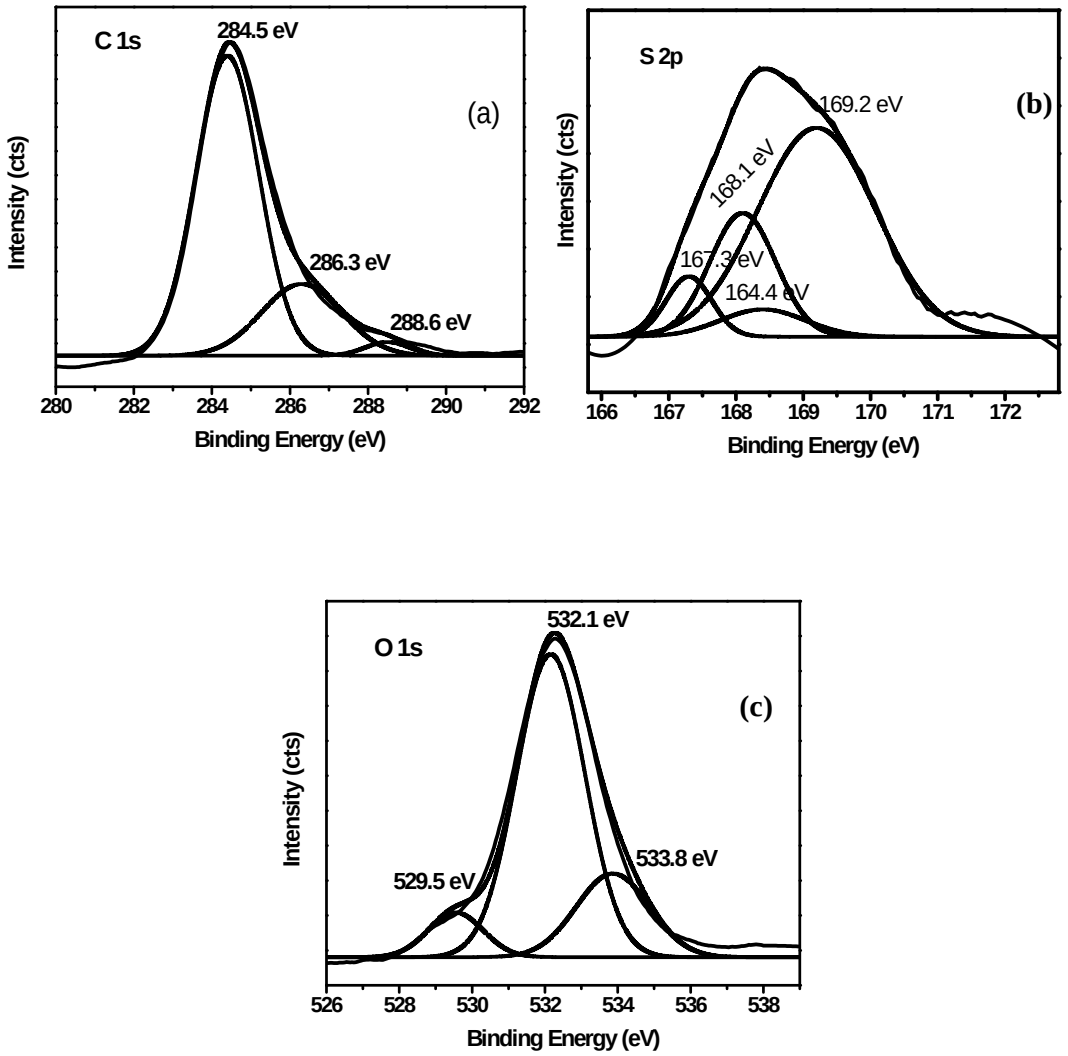


**Figure 6** *XP core level spectrum of (a) C 1s (b) S 2p (c) O1s.*

Table 1 presents the acidic contents and catalytic data for the esterification of acetic acid with 1-butanol to give n-butyl acetate. It is observed that G-$SO_3H$ shows much higher activity that Amberlyst-15 (a commercial catalyst resin). The conversion was around 90 % and 93% for Amberlyst 15 and G-$SO_3H$ respectively for 1 h.

| **Catalyst** | **Acid sites/mmol $g^{-1}$** | **Conversion** | | **Selectivity** |
|---|---|---|---|---|
| | | **1 h** | **5h** | |
| Amberlyst-15 | 4.7 | 90% | 95 % | ~100% |
| HG-$SO_3H$ | 6.7 | 93% | 98% | ~100% |
| Blank | - | 5% | 23% | ~100% |

**Table 1** *The acidic contents and catalytic data for the esterification*

The reactivity is due to the fact that, G-$SO_3H$ has a sheet structure and almost all of the sulfonic groups are exposed to the reactants. In addition to this the structure is also favourable for the high dispersion of sulfonic groups, and most of the sulfonic groups are accessible to reactants.

### 3.2.5 Conclusions

Acid functionalized graphene (G-SO3H) was successfully synthesized by refluxing graphene with sulphuric acid and nitric acid mixture. Catalytic ability was tested using esterification reactions. The higher catalytic activity is attributed to the structure and number of acid sites present in G-$SO_3H$. Thus this catalyst may be used in many other acid-catalysed reactions.

### 3.1.6 References

[1] C. N. R. Rao, A. Govindaraj, in *Nanotubes and Nanowires, RSC nanoscience & Nanotechnology Series*, RSC, Cambridge, UK, 2005.

[2] K. Sumino, M. Imai, *Philos. Mag. A.* 1983, **47**, 753.

[3] K. Sumino, I. Yonenaga, M. Imai, T. Abe, *J. Appl. Phys.* 1983, **54,** 5016.

[4] R. Sen, B. C. Satishkumar, A. Govindaraj, K. R. Harikumar, M. K. Renganathan C. N. R. Rao, *J. Mater. Chem.* 1997, **7**, 2335.

[5] R. Sen, B. C. Satishkumar, A. Govindaraj, K. R. Harikumar, G. Raina, J.-P. Zhang, A. K. Cheetham, C. N. R. Rao, *Chem. Phys. Lett.* 1998, **287**, 671.

[6] M. Terrones, P. M. Ajayan, F. Banhart, X. Blase, D. L. Carroll, J. C. Charlier, R. Czerw, B. Foley, N. Grobert, R. Kamalakaran, P. Kohler-Redlich, M. Ruhle, T. Seeger, H. Terrones, *Applied Physics a-Materials Science & Processing*, 2002, **74**, 355.

[7] Y. Chai, Q. F. Zhang and J. L. Wu, *Carbon*, 2006, **44**, 687.

[8] M. Glerup, J. Steinmetz, D. Samaille, O. Stéphan, S. Enouz, A. Loiseau, S. Roth and P. Bernier, *Chem. Phys. Lett.* 2004, **387**, 193.

[9] Y. S. Min, E. J. Bae, I. P. Asanov, U. J. Kim, W. Park, *Nanotechnology*, 2007, **18**, 4.

[10] P. Ayala, A. Grueneis, T. Gemming, D. Grimm, C. Kramberger, M. H. Ruemmeli, F. L. Freire, H. Kuzmany, R. Pfeiffer, A. Barreiro, B. Buechner and T. Pichler, *J.Phys. Chem. C*, 2007, **111**, 2879.

[11] L. S. Panchalkarla, A. Govindaraj and C. N. R. Rao, *ACS Nano,* 2007, **1**, 494.

[12] S. Y. Kim, J. Lee, C. W. Na, J. Park, K. Seo and B. Kim, *Chem. Phys. Lett.* 2005, **413**, 300.

[13] L. S. Panchakarla, K. S. Subrahmanyam, S. K. Saha, Achutharao Govindaraj, H. R. Krishnamurthy, U. V. Waghmare, C. N. R. Rao, *Adv. Mater*. 2009, **21**, 4726

[14] X. Li, H. Wang, J. T. Robinson, H. Sanchez, G. Diankov and H. Dai, *J. Am. Chem. Soc.*, 2009, **131**, 15939.

[15] D. Genga , S. Yanga,b, Y. Zhanga , J.Yanga , Jian Liua , Ruying Li a , T-K. Shamb, X.Suna, S. Yec and S. Knightsc, *App. Sur. Science*, 2011, **257**, 9193.

[16] D. Wei, Y. Liu, Y. Wang, H. Zhang, L. Huang and G.Yu, *Nano Lett.*, 2009, **9**, 1752.

[17] Y. Shao, S. Zhang, M. H. Engelhard, G. Li, G. Shao, Y. Wang, J. Liu, I. A. Aksay and Y. Lin, *J. Mater. Chem*., 2010, **20**, 7491.

[18] H. M. Jeong, J.W.Lee, W. H. Shin, Y. J. Choi, H. J. Shin, J. K. Kang and J. W. Choi, *Nano Lett.*, 2011, **11**, 2472.

[19] D. Deng, X.Pan, L. Yu, Y. Cui, Y. Jiang, J. Qi§, W.-X.Li, Q. Fu, X. Ma, Q.Xue, G. Sun, X. Bao *Chem. Mater*., 2011, **23**,1188.

[20] Z. Lin , M. Song , Y.Ding , Y. Liu , M. Liu and C. Wong *Phys. Chem. Chem. Phys.*, 2012, **14**, 3381.

[21] Y. Zhang, K. Fugane, T. Mori, L. Niu, and J. Ye, *J. Mater. Chem.*, 2012, **22**, 6575.

[22] Z. Lei, L. Lu and X. S. Zhao, *Energy Environ. Sci.*, 2012, **5**, 6391.

[23] L. Sun, L. Wang, C. Tian, T. Tan, Y. Xie, K. Shi, M. Li, H. Fu, L. Sun, L. Wang, C. Tian , T. Tan, Y. Xie , K. Shi , M. Li and H. Fu, *RSC Adv.*, 2012, **2**, 4498.

[24] D. Usachov, O. Vilkov, A. Grüneis, D. Haberer, A. Fedorov, V. K. Adamchuk, A. B. Preobrajenski, P. Dudin, A. Barinov, M. Oehzelt, C. Laubschat and D. V. Vyalikh, *Nano Lett.*, 2011, **11**, 5401.

[25] W. S. Hummers and R. E. Offeman, *J. Am. Chem. Soc.*, 1958, **80**, 1339.

[26] K. S. Subrahmanyam, L. S. Panchakarla, A. Govindaraj and C. N. R. Rao, *J. Phys. Chem. C*, 2009, **113**, 4257.

[27] K. Wilson, A. F. Lee, D. J. Macquarrie and J. H. Clark, *Applied Catalysis A: General*, 2002, **228**, 127.

[28] D. Margolese, J. A. Melero, S. C. Christiansen, B. F. Chmelka and G. D. Stucky, *Chem. Mater.* 2000**, 12**, 2448.

[29] A. Matsumoto, K. Tsutsumi, K. Schumacher and K. K. Unger, *Langmuir* 2002, **18**, 4014.

**[**30] S. G. Wang and J. L. Li, *Chinese Chemical Letters*, 2006, **17**, 221.

[31] C. W. Jones, M. Tsapatsis, T. Okubo, M. E. Davis *Microporous and Mesoporous Materials* 2001, **42,** 21.

[32] F. Hoffmann, M. Cornelius, J. Morell, and M. Froba, *Angew. Chem. Int. Ed.* 2006, **45**, 3216.

[33] M. Hara, T. Yoshida, A. Takagaki, T. Takata, J. N. Kondo, S. Hayashi and K. Domen, *Angew. Chem., Int. Ed.*, 2004, **43**, 2955.

[34] B. C. Satishkumar, A. Govindaraj, J. Mofokeng, G. N. Subbanna,C. N. R. Rao, *J. Phys. B: At. Mol. Opt. Phys.*, 1996, **29**, 4925.

[35] K. S. Subrahmanyam, L. S. Panchakarla, A. Govindaraj and C. N. R. Rao, *J. Phys. Chem. C*, 2009, **113** ,4257

# CHAPTER 4

# SELECTIVITY IN THE PHOTOCATALYTIC PROPERTIES OF THE COMPOSITES OF $TiO_2$ NANOPARTICLES WITH B- AND N-DOPED GRAPHENES


## Summary*

In this chapter, we show the selectivity in the photocatalytic properties of $TiO_2$-graphene composites with boron and nitrogen doped graphenes. These $TiO_2$-graphene composites also show an excellent enhancement in the photocatalytic activity. We have chosen two different dyes, methylene blue (MB) and rhodamine B (RB) for the photocatalytic studies. These dyes show selectivity towards the nitrogen-doped and boron doped graphenes. Methylene blue being a good electron donor and has a low ionization energy interacts strongly with electron-deficient boron-doped graphene resulting in fast degradation of the dye. On the other hand, RB which is not such a good electron donor and has higher ionization energy interacts strongly with electron-rich nitrogen-doped graphene causing a faster degradation of the dye. Raman spectroscopy was used to understand the interaction between the dye molecules and the graphene composites. The electronic structure of graphene plays an important role in the selectivity as well as the enhancement of the photocatalytic activity.


***** A paper based on this work has been published in *Chemical physics letters (2011).*

## Chapter 4

### 4.1 Introduction

As an important semiconducting material, titanium dioxide ($TiO_2$) has been studied and widely applied in photocatalysis due to its excellent photoelectrochemical properties, including in energy conversion,[1,2] photocatalysis involving photodegradation of organic contaminants [3] and it is widely used as a pigment,[4] in sunscreens,[5] paints,[6] ointments,[7] toothpaste,[8] etc., The capability to utilize $TiO_2$ for these purposes arises from the enhanced reactivity of nanoparticulate $TiO_2$ compared to that of the bulk material and also it is nontoxic, easy to be made, inexpensive and chemically stable. Moreover, $TiO_2$ nanoparticles in the 10-50 nm range take on unusual properties and can be used in various applications, such as self-cleaning window glass, air and water purification systems. $TiO_2$ is a wide band-gap semiconductor and researchers are looking at it as a substitute for silicon to make solar power cells, as well as battery storage media.

In 1972, Fujishima and Honda[9,10] discovered that water can be split, *i.e.*, simultaneously oxidized to oxygen and reduced to hydrogen, when a bias potential is applied to an "*illuminated*" $TiO_2$ single crystal electrode. This remarkable discovery marked the onset of photo induced redox reactions on semiconductor surfaces. It was soon realized that such redox processes could be utilized for environmental cleanup applications, when Frank and Bard,[11] in 1977, showed the photocatalytic oxidation of $CN^-$ and $SO_3^-$ using different semiconductor materials like $TiO_2$, ZnO, CdS, $Fe_2O_3$ and $WO_3$. This was followed by the demonstration of the $TiO_2$ catalyzed photodegradation of chlorinated organic compounds by Ollis,[12,13] and the Pt-loaded-$TiO_2$ catalyzed photochemical sterilization of microorganisms by Matsunaga *et al.*[14] in the early 1980s. Later, O'Regan and Gratzel[15] showed the first high-efficiency solar cell based on dye-sensitized

colloidal $TiO_2$ films for photovoltaic power generation.

Naturally occuring $TiO_2$ has three polymorphs, *i.e.* anatase, brookite, and rutile.[16] Although all three types of polymorphs are expressed using the same chemical formula ($TiO_2$), their crystal structures are different. Rutile is thermodynamically the most stable phase, although the anatase phase forms at lower temperatures. Both of these phases show photocatalytic activity whereas the brookite phase does not. Despite the fact that the band gap values are 3.0 eV for the rutile and 3.2 eV for the anatase phases, both absorb only UV rays. Such characteristics of the rutile phase seem more suitable for use as a photocatalyst because the rutile phase can absorb light of a wider range. However, the anatase phase exhibits higher photocatalytic activity.[17] The most prominent reasons are attributed to the difference in the energy structure between the two phase types and the surface area. In both phases, the position of the valence band is deep, and the resulting positive holes show sufficient oxidative power. Usually, the anatase crystal phase forms at lower temperatures, showing higher surface areas compared to the rutile phase. A larger surface area with a constant surface density of adsorbents leads to faster surface photocatalytic reaction rates. In this sense, the higher the specific surface area, the higher the photocatalytic activity that one can expect. Therefore, the anatase phase exhibits higher overall photocatalytic activity compared to the rutile phase. High temperature treatment usually improves the crystallinity of $TiO_2$ nanomaterials, which can induce the aggregation of small nanoparticles and decrease the surface area. Therefore, it is very difficult to predict the photocatalytic activities from the physical properties of $TiO_2$ nanomaterials.

### 4.1.1 Basics of Photocatalysis

A photocatalytic reaction can be defined as a reaction induced by photoabsorption of a photocatalyst, which remains unchanged during the reaction.[18] Semiconductor photocatalysis is broadly thought of as the catalysis of a photochemical reaction at the surface a solid semiconductor.[19,20] In the semiconductor context, such as concerning $TiO_2$, photocatalysis is usually introduced with respect to a band model (Figure 1), where two reactions occurring simultaneously: (a) oxidation from photogenerated holes, and (b) reduction from photogenerated electrons. These processes must occur at equal rates if the photocatalyst is to remain unchanged.

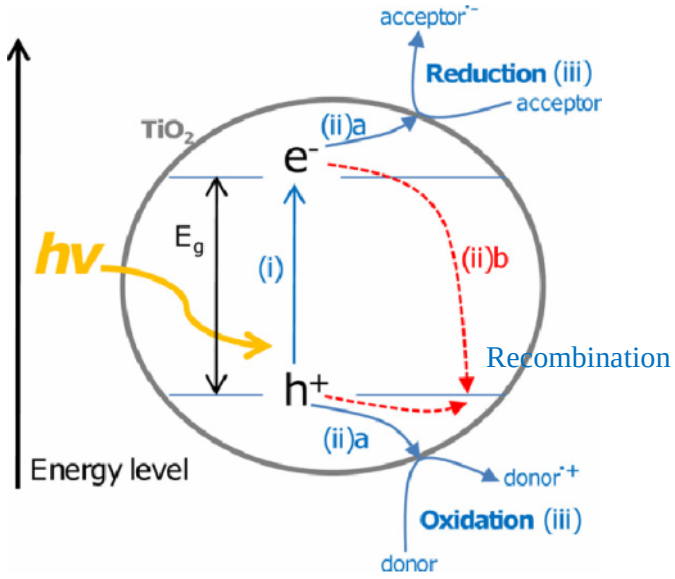


**Figure 1.** *Main processes in semiconductor photocatalysis. (i) Photon absorption and electron–hole pair generation. (ii) Charge separation and migration; (ii)a to surface reaction sites or (ii)b to recombination sites. (iii) Surface chemical reaction at active sites.*

The first process is the absorption of photons to create electron–hole pairs (Figure 1). The energy of the incident light must be greater than the energy difference between the valence and conduction bands, if an electron is to be promoted from the former to the latter. Success of this stage is dependent on the band-gap of the semiconductor. A primary reason for the low solar photoconversion efficiency of $TiO_2$ is because the band-gap of 3.2 and 3.0 eV respectively for the anatase and rutile phases. This means that $TiO_2$ can only be excited under irradiation of UV light at wavelengths <380 nm, which covers only ~5% of the solar spectrum.[21] The development of photocatalysts capable of absorbing light in the visible region of the spectrum requires engineering the band-gap to less than 3.0 eV.

The second process is the separation and migration of the photogenerated electrons and holes (Figure 1). These electron-hole pair can undergo either migration to surface reaction sites or recombination. The time resolved spectroscopic studies shows that the electron-hole trapping or recombination rates are extremely fast (of the order of $10^{-6}$-$10^{-15}$ s), and can substantially lower the photocatalytic activity. The recombination occurs at boundaries and defects, but if the particle size is reduced, the distance that the photogenerated electrons and holes need to travel to surface reaction sites is reduced, thereby reducing the recombination probability.[22] This becomes significant below 2 nm for both the anatase and rutile phases, leading to a blue-shift in the band-gap.[23]

The final process involves the surface chemical reactions, for which active sites and surface area are important (Figure. 1). The surface area can be increased by using highly porous materials or reducing their size.[24] Hence the high surface area-to-volume ratio of nanosized particles, rods, tubes, flakes etc. is another important reason for seeking to

design and engineer photocatalytic materials on the nanoscale**.** Photocatalysts which have a high tendency for trapping of reactants, and which facilitate transfer of reactants to active sites, are also desirable and may be promoted by high-surface area nanostructure and surface chemical modification.

### 4.1.2 Fundamental Approaches for Enhancement of Photocatalytic Activity

There are three fundamental approaches for enhancement of photocatalytic activity:

(i) band-gap tuning or extension of excitation wavelength by the use of photosensitizers,

(ii) minimizing charge carrier recombination,

(iii) promotion of the forward reaction and adsorbance of reactants through the provision of adequate surface area and quantity of active sites.

Carbonaceous nanomaterials have been proposed to enhance $TiO_2$ photocatalysis by addressing these key areas, along with other more novel mechanisms of enhancement. The most fundamental route for the synthesis of carbon-$TiO_2$ nanocomposites involves simple mixing. This is usually performed in solution, and possibly with pre-functionalization of surfaces. These methods have been both promoted for their simplicity[25] and criticized for the low level of interaction, *i.e.* no establishment of intimate contact or chemical bonding.[26] Sol–gel synthesis, hydrothermal synthesis and solvothermal method are some of the methods generally used to make these carbon-$TiO_2$ nanocomposites.

Carbon nanotubes (CNTs) have a variety of applications because of their unique properties structural, chemical, thermal, electrical and more. Catalysis and in particular heterogeneous catalysis has been seen as a possible application.[27] CNTs show the potential to contribute to all three of the routes of increasing photocatalytic activity. It has high-surface area, high quality active sites, helps in retardation of electron–hole recombination as well as visible light catalysis by the modification of band-gap.[28] Thus, CNT–$TiO_2$ mixtures or composites shows enhancement in photocatalytic activity.

Graphene is one of the most exciting materials,[29,30] and continues to receive significant attention due to its promising applications such as nanoelectronics,[31] supercapacitors[32] and more. Graphene has been used as a two-dimensional photocatalyst support in photocatalysis. Exfoliated graphene sheets have a theoretical surface area of ~2600 $m^2$ $g^{-1}$,[33] making graphene highly attractive as a high-surface area 2D photocatalyst support. The application of graphene in combination with $TiO_2$ therefore presents the opportunity to simultaneously cover all three of the mechanisms of photocatalytic enhancement. The newly developed graphene-$TiO_2$ nanocomposites are based on the use of graphene oxide (GO), derived by chemical oxidation of graphene. The first graphene-semiconductor mechanism was demonstrated by Williams *et al*.[34] Zhang *et al*.[35] have reported a hydrothermally prepared GO–$TiO_2$ composite, and assessment of the photocatalytic activity via the degradation of methylene blue. Photocatalytic activity was found to be higher than that of $TiO_2$ alone, or CNT-$TiO_2$ composites with the same carbon content. The enhancement was ascribed to the two-dimensional planar graphene structure favouring dye absorption, and suppressed electron–hole recombination due to the high electrical conductivity. Enhancement was also attributed to extension of light

absorption to longer wavelengths in the visible range due to the high transparency and band-gap narrowing resulting from the presence of Ti–O–C bonds.[35]

## 4.2 Scope of the present investigations

Selective photocatalysis is an interesting field with potential applications in organics separation as well as selective degradation. Most studies of the $TiO_2$-graphene composites have concentrated on electron transfer between $TiO_2$ and graphene oxide or graphene although there are indications that the electronic structure of the nanocarbons may play a crucial role in the photocatalysis. We considered it important to examine the nature of interaction of graphene with $TiO_2$ as well as with adsorbed molecules to understand the photocatalytic properties. Since the electronic properties of graphene can be conveniently tuned chemically by doping with nitrogen and boron, thereby changing the effective band gap of the composites, we have investigated the photocatalytic properties of $TiO_2$ by using chemically doped graphenes as supports. With this purpose, we have studied the interaction of $TiO_2$ nanoparticles with B- and N-doped graphenes and also the interaction of the graphenes with two dye molecules possessing widely different electron-donating abilities or ionization energies. The molecules investigated are methylene blue (I) and rhodamine B (II), the former with a very low ionization energy of 5.3 eV. Rhodamine B has an ionization energy of 6.7 eV. It was felt that the study would show whether the photodegradation of these dye molecule by the $TiO_2$-graphene composites depends on the electronic properties of graphene.

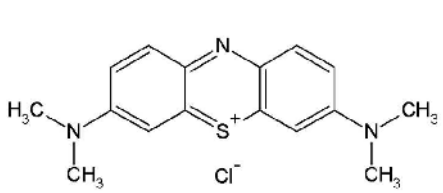


I

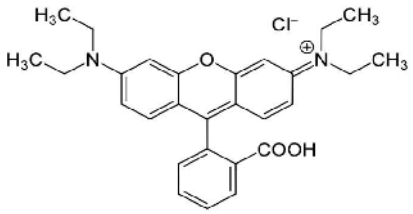


II

## 4.3 Experimental Section

### 4.3.1 Synthesis of graphene and doped graphenes

Graphene with 2-4 layers (HG) was prepared by arc-discharge in the presence of hydrogen (200 Torr) and helium (500 Torr).[36] Boron-doped graphene (BG) was prepared by carrying out the arc-discharge using boron-packed graphite electrodes (3 at. % Boron) in the presence of $H_2$ (200 Torr) and He (500 Torr).[37] Nitrogen-doped graphene (NG) was prepared by carrying out arc-discharge of graphite in the presence of $H_2$ (200 Torr), He (200 Torr), and $NH_3$ (300 Torr).[37]

### 4.3.2 Acidification of graphene and doped graphene

2 mg of graphene was added to a mixture of 1.6 mL of conc. sulfuric acid, 1.6 mL conc. nitric acid and 3.5 mL of distilled water. The mixture was sonicated for 10 min and transferred to a teflon lined autoclave and treated under microwave irradiation at 600 W for 20 min. The graphene samples so obtained were washed several times with distilled water to remove excess acid.[38]

### 4.3.3 Synthesis of $TiO_2$ nanoparticles

$TiO_2$ nanoparticles were prepared as follows. In a typical reaction, a solution of ethanol (25 mL) and water (2.5 mL) was heated to 80 °C with constant stirring.[39] A mixture of 0.18 mL titanium orthobutoxide and 0.045 ml $H_2SO_4$ in 5 mL ethanol was added to the above solution. The resulting mixture was kept stirring at 80 $^oC$ for 12 h. The reaction mixture was then cooled down to room temperature and the solid was collected by centrifugation and washed with distilled water. In the second step of the synthesis, the washed solid was dispersed in water/DMF (12 mL/0.3 mL). The suspension was transferred to a 25 mL teflon-lined stainless steel autoclave for hydrothermal reaction at 180 °C for 16 h. The final product was collected by centrifugation and washed with distilled water. The nanoparticles were examined by electron microscopy.

### 4.3.4 Synthesis of $TiO_2$-Graphene nanocomposites

Composites of $TiO_2$ with undoped graphene (TG), with N-doped graphene (TNG) and with B-doped graphene (TBG) were prepared by the procedure described by Dai *et al.*[39] In a typical reaction, 1.8 mg of acidified graphene (same for doped graphene) was dispersed in EtOH/water (25 mL/2.5 mL) mixture. The suspension was heated to 80 °C with stirring. Mixture of 0.18 mL titanium orthobutoxide and 0.045 mL of $H_2SO_4$ in 5 mL ethanol was added to above solution. The resulting mixture was kept stirring at 80 $^oC$ for 12 h. The reaction mixture was cooled to room temperature, the solid collected by centrifugation and washed with distilled water. In the second step of the synthesis, the washed solid was dispersed in water/DMF (12 mL/0.3 mL). The suspension was transferred to a 25 mL teflon-lined stainless steel autoclave for hydrothermal treatment at

180 °C for 16 h. The final composite material was collected by centrifugation and washed with distilled water.

### 4.3.5 Photocatalytic Study

Photodegradation kinetics were studied as follows. In a typical kinetic study, 4 mg of photocatalyst ($TiO_2$, TG, TNG and TBG) was suspended in 10 mL of 0.015 mmol/L aqueous solution of rhodamine B (RB) or methylene blue (MB). The resulting suspension was sonicated for 10 min followed by 10 min stirring to allow sufficient mixing. Under constant stirring conditions, the mixture RB (or MB) with the photocatalyst was irradiated with a 120 W high pressure mercury lamp which was positioned 30 cm away from the quartz vessel (see Figure 2). Samples were collected after regular intervals and the

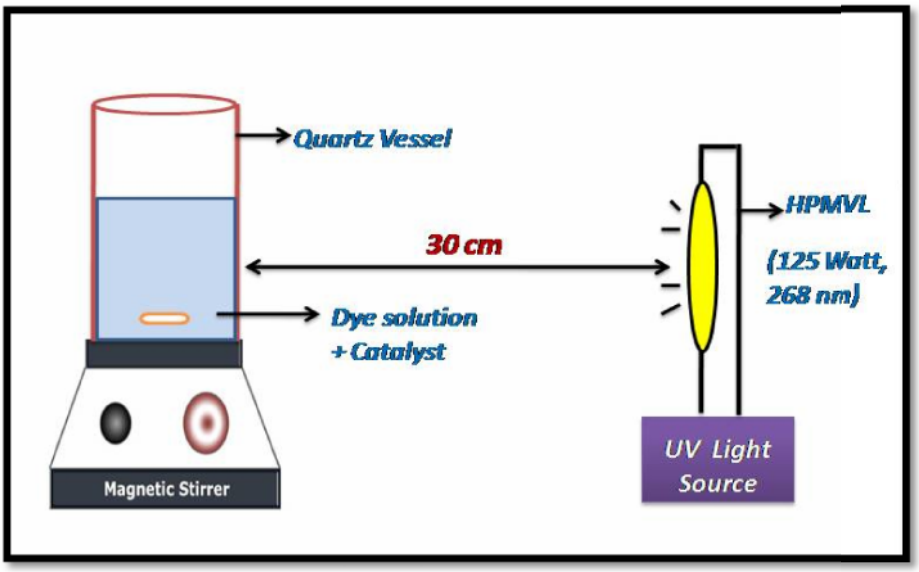


**Figure 2.** *Design of the photocatalytic reactor used for photocatalytic study*

changes in concentration of the organic dye were monitored by measuring UV-Vis absorption spectra. The collected samples were centrifuged for 5 min to remove the $TiO_2$ or $TiO_2$-graphene composites before UV-Vis measurements. The peak maximum of rhodamine B (at 553 nm) was used to determine dye concentration. Photodegradation of methylene blue was conducted in a similar way by using 10 mL portions of a 0.015 mmol/L aqueous solution of methylene blue and 4 mg suspension of $TiO_2$ and other composite materials. The absorption maximum of methylene blue was at 655 nm.[39]

**Characterization techniques**

Field emission scanning electron microscope (FESEM) images were recorded with a FEI NOVA NANOSEM 600. Transmission electron microscope (TEM) images were obtained with a JEOL JEM 3010 instrument. X-ray diffraction (XRD) patterns were recorded in the θ-2θ Bragg–Bretano geometry with a Siemens D5005 diffractometer using CuKα (λ=0.151418 nm) radiation. Raman spectra were recorded with a LabRAM HR high resolution Raman spectrometer (Horiba Jobin Yvon) using He–Ne Laser (λ=632 nm). UV–Vis absorption spectra were recorded using a Perkin-Elmer Lambda 900 UV/Vis/NIR spectrometer.

## 4.4 Results and Discussion

Pure graphene (HG), B-doped (BG) and N-doped (NG) graphenes were prepared by arc-discharge method and these samples were acidified.[38] The $TiO_2$ nanoparticles as well as composites of $TiO_2$ with pure graphene (TG), N-doped graphene (TNG) and

B-doped graphene (TBG) were prepared by the procedure described by Dai *et al.*[39]

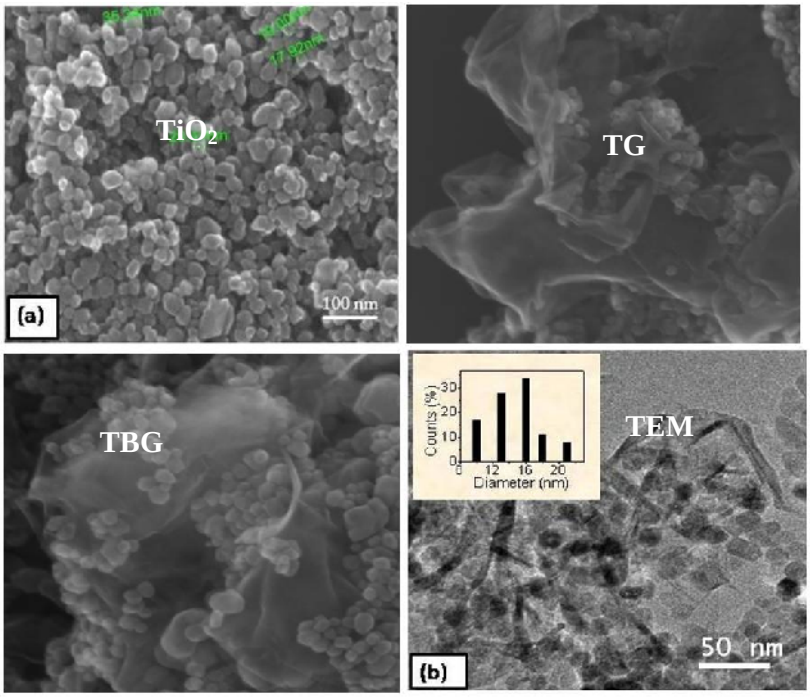


**Figure 3.** *FESEM images of $TiO_2$, TG and TBG and TEM image of TG composite.*

A typical FESEM image of the as-synthesized $TiO_2$ nanoparticles and $TiO_2$-graphene composites is shown in Figure 3. It can be observed from the SEM image that the graphene sheets are covered with $TiO_2$ nanoparticles. The TEM images also present the morphology of the composites, wherein the graphene sheets are decorated with $TiO_2$ particles. The $TiO_2$ particles exhibit a narrow size distribution with an average size of 15 nm. The good distribution of $TiO_2$ particles on graphene will benefit the photocatalysis.

The X-Ray diffraction pattern of the $TiO_2$ nanoparticles could be indexed on the anatase structure (a=3.7852Å, c= 9.5139Å, JCPDS 21-1272). The $TiO_2$ nanoparticles in the composite with graphene also had the anatase structure with presented peak intensities (101), (004), (105), and (211) (see Figure 4).

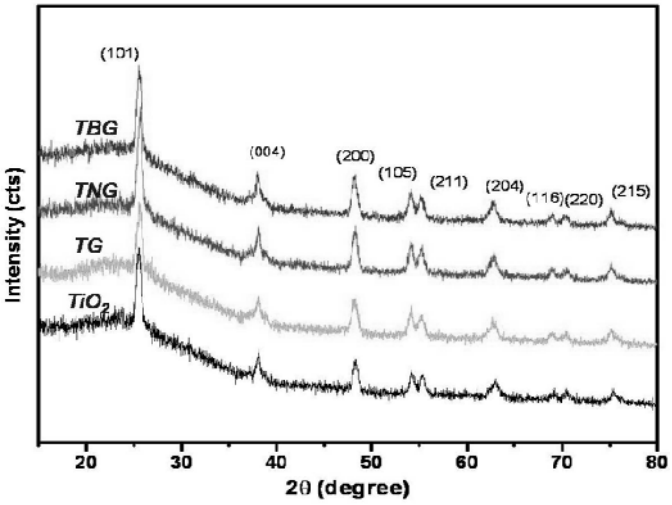


**Figure 4.** *XRD patterns of (a) $TiO_2$ (b) TG (c) TNG (d) TBG.*

Raman spectroscopy is known to be a sensitive tool for characterizing $TiO_2$, graphene and its interaction with other molecules.[40,41] The anatase phase of $TiO_2$ was evidenced from Raman spectroscopy. We show the typical Raman spectra of $TiO_2$ and $TiO_2$-graphene composites in Figure 5(a). We observed four peaks at the low frequency region for both $TiO_2$ and $TiO_2$-graphene composites and are assigned to the $E_{1g}$ (149 $cm^{-1}$), $B_{1g}$ (398 $cm^{-1}$), $A_{1g}$ (516 $cm^{-1}$) and $E_g$ (637 $cm^{-1}$) modes of anatase phase respectively.

(a)

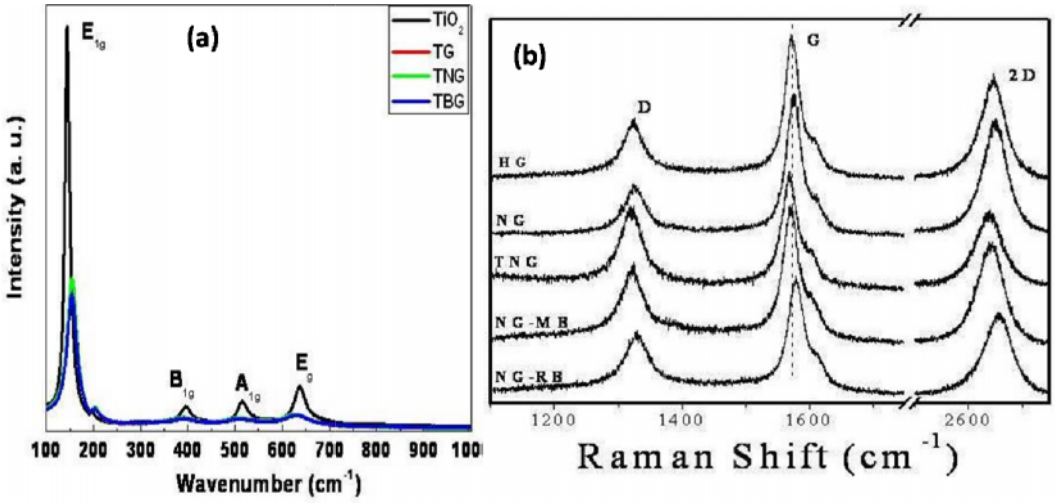


**Figure 5(a)** *Raman spectra for $TiO_2$ nanoparticles with pure and doped graphenes.*

**(b)** *Raman Spectra of G, NG, TNG, NG-MB and NG-RB.*

| Sample | G Band ($cm^{-1}$) | 2D Band ($cm^{-1}$) | $I_{2D}/I_G$ |
|---|---|---|---|
| HG | 1572 | 2645 | 0.73 |
| TG | 1569 | 2640 | 0.55 |
| NG | 1574 | 2649 | 0.66 |
| TNG | 1569 | 2638 | 0.66 |
| BG | 1581 | 2647 | 0.10 |
| TBG | 1574 | 2641 | 0.15 |
| G-RB | 1570 | 2643 | 0.70 |
| NG-RB | 1580 | 2663 | 0.70 |
| BG-RB | 1583 | 2652 | 0.09 |
| G-MB | 1573 | 2646 | 0.61 |
| NG-MB | 1571 | 2443 | 0.76 |
| BG-MB | 1587 | 2614 | 0.17 |

**Table 1.** *Raman data of the graphenes, $TiO_2$-graphene composites and graphene-dye adducts.*

The Raman G-band, characteristic of the $sp^2$ carbon network, and the defect-related 2D band are especially useful in examining effects of doping and charge-transfer interactions. In Figure 5(b), we show typical Raman spectra and list the important Raman results in Table 1. Some interesting conclusions can be drawn regarding the interaction of graphene with $TiO_2$ and with the dye molecules on the basis of the changes in the Raman G and 2D bands. The effect of doping graphene with boron and nitrogen is to shift the Raman G-band slightly to a higher frequency in conformity with the literature[37]. The ratio of the intensity of the 2D band with respect to that of the G-band, $I_{2D}/I_G$, decreases on B- and N-doping. On depositing $TiO_2$ nanoparticles on the graphene samples, the G-band frequency decreases in both the doped and the undoped cases (see Table 1). The $I_{2D}/I_G$ ratio remains around the same value or decreases slightly in the composites. Interaction of rhodamine B (RB) and methylene blue (MB) with the graphene samples causes interesting changes in the G band (see Figure 5(b) and Table 1).

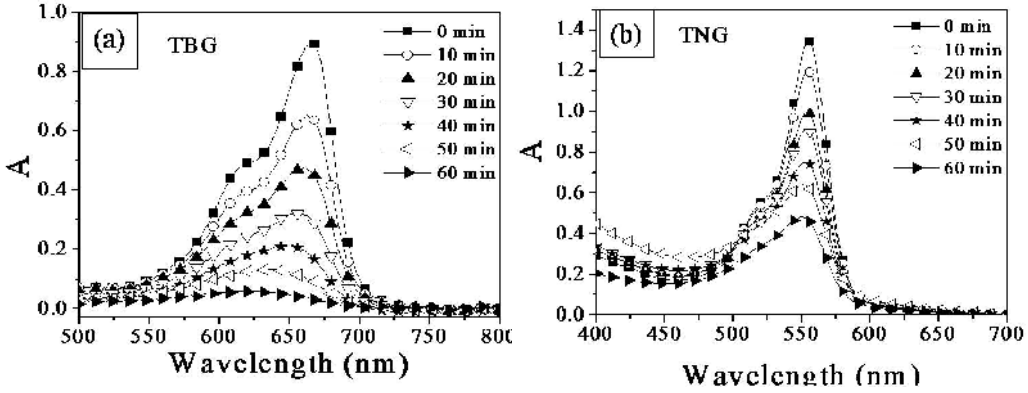


**Figure 6.** *Changes in absorption spectra of (a) methylene blue and (b) rhodamine B deposited on TBG and TNG, respectively, on irradiation.*

The most important observation with regard to the interaction of the dye with graphene from this study is that there is a substantial increase in the G-band frequency of N-doped graphene (NG) on interaction with RB, with the changes in the G-bands of HG and BG being marginal. In the case of MB, the largest shift in the G-band frequency is found in the case of B-doped graphene (BG). We also observe significant changes in the 2D band. Thus, the frequency of the 2D band of NG increases on interaction with RB where as changes in the case of HG and BG are marginal. The 2D band frequency of BG decreases on interaction with MB and the changes in the HG and NG are marginal. These shifts in the G and 2D bands are significant, whereas methylene blue which is a good electron donor with low ionization energy interacts more with the p-type graphene, BG. On the other hand, Rhodamine B with a higher ionization energy interacts strongly with the n-type graphene, NG. Photocatalytic activities of pure $TiO_2$ and of the composites of $TiO_2$ with HG, BG and NG were investigated in the case of rhodamine B and methylene blue by making use of the changes in electronic absorption spectra of the dyes with respect to time. In Figure 6, we show typical changes in the absorbance of the dyes on irradiation with respect to time.

Photodegradation of these dyes appears to follow the Langmuir-Hinshelwood reaction kinetics, which predicts an exponential decrease in the concentration of the dye molecule as a function of time.[28] We have examined the change in the concentration ($C/C_0$) of the dyes with reaction time. In Figure 7(a), we show the time variation of $C/C_0$ of methylene blue. We notice that the degradation rate varies as TBG > TNG > TG > $TiO_2$. In Figure 8(a), we show the time variation of $C/C_0$ of rhodamine B. The degradation rate varies as TNG > TBG > TG > $TiO_2$.

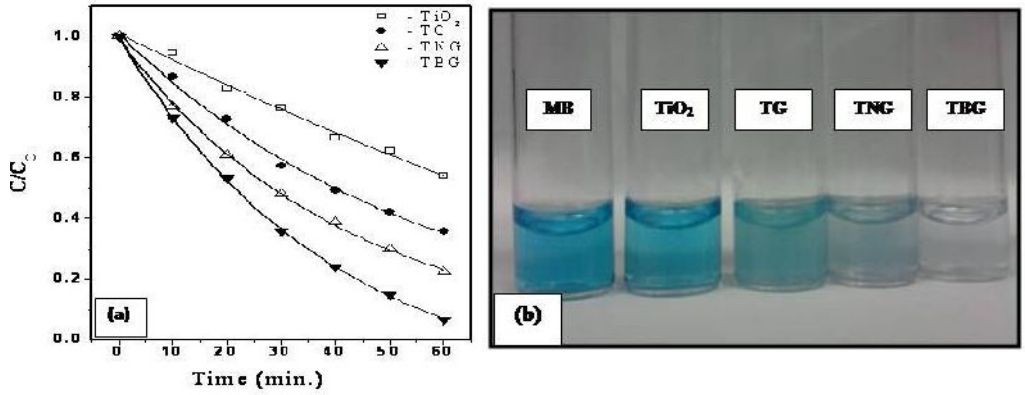


**Figure 7(a)** *Photocatalytic degradation of methylene blue monitored as the variation of normalized concentration with the irradiation time in the presence of $TiO_2$, TG, TNG and TBG.* **(b)** *Photographs showing color variation after 1 h.*

We have shown the photographs of the dye solutions after 1h of irradiation in Figure 7(b) and 8(b). The photographs clearly show how TBG is more effective with MB and TNG with RB. Electron-poor TBG is selective in the degradation of MB because of the higher electron-donating ability of this dye. Similarly, electron-rich TNG is selective in the degradation of RB which is not a good electron donor. The effectiveness TBG in the photodegradation of MB can be understood on the basis of the strong interaction between the two as inferred from Raman spectra. The same is true for the effectiveness of TNG in the case of RB.

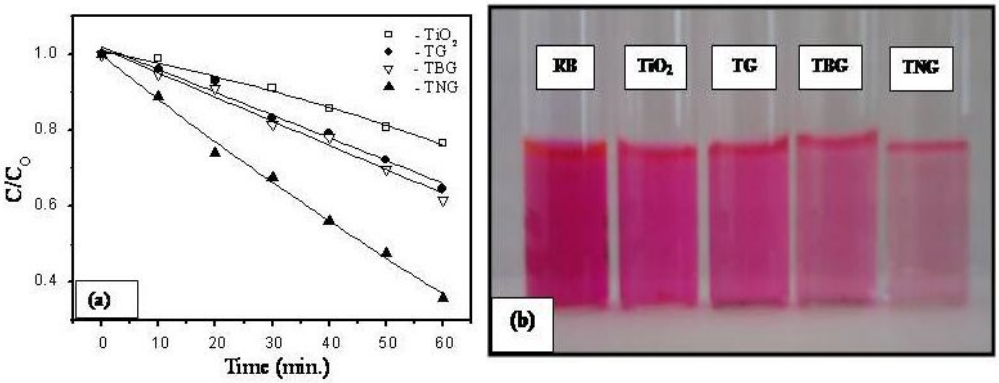


**Figure 8(a)** *Photocatalytic degradation of rhodamine B monitored as the variation of normalized concentration with the irradiation time in the presence of $TiO_2$, TG, TBG and TNG.* **(b)** *Photographs showing color variation after 1 h.*

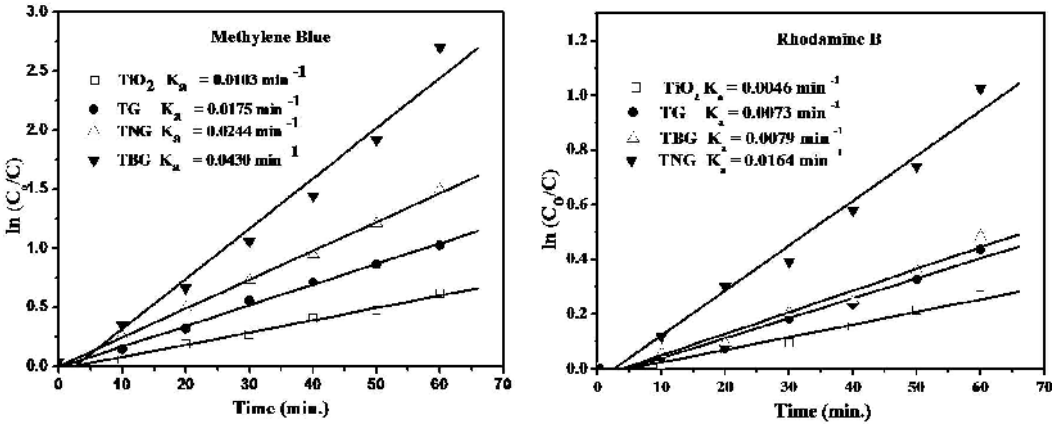


**Figure 9.** *ln($C_0$/C) versus irradiation time for $TiO_2$ and its composites with graphene for (a) Methylene blue and (b) Rhodamine B*

The kinetics of the degradation reaction are fitted to a pseudo first order reaction at low dye concentrations: $\ln(C_0/C) = k_a t$, where $k_a$ is the apparent rate constant, $C_0$ is the initial concentration of the reactant. Under the conditions of the experiments we used here, the initial concentration of methylene blue, $C_0$, is 0.015 mmol/L, which is very small. The $\ln(C_0/C)$ vs $t$ curves for $TiO_2$ and its composites with graphene for methylene blue and rhodamine B are plotted in Figure 9(a) and (b) respectively. The linearity of the curves indicates that the kinetics for the photocatalytic decomposition of MB and RB follows a pseudo first order rate. The rate constant of $TiO_2$ is smaller when compare to its graphene composites. In methylene blue case, the values of $k_a$ for the $TiO_2$, TG, TNG, TBG are 0.010, 0.018, 0.024, 0.043 $min^{-1}$ respectively. The value of $k_a$ for the TBG is found to be more than four times that of $TiO_2$. In rhodamine B case, the value of $k_a$ for the $TiO_2$, TG, TNG, TBG are 0.005, 0.0073, 0.016, 0.008 $min^{-1}$ respectively. The value of $k_a$ for the TNG is found to be nearly three times that of $TiO_2$.

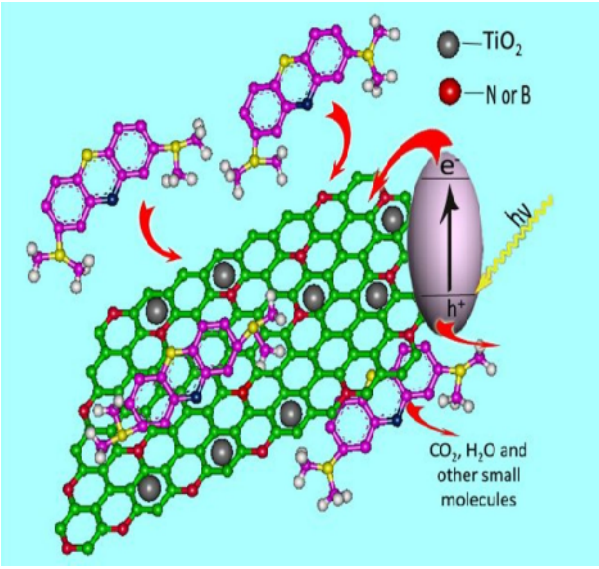


**Scheme I.** *Structure of $TiO_2$- doped graphene and tentative processes of the photodegradation of methylene blue (MB) over $TiO_2$- doped graphene*

## 4.5 Conclusions

The present study clearly establishes selectivity in the interaction of dyes with chemically doped graphenes and the photodegradation of the dyes catalyzed by the $TiO_2$ nanoparticles present on the graphene surface. The mechanism is likely to involve the photoexcitation of electrons in the $TiO_2$ nanoparticles followed by their transfer to graphene (see Scheme I). The adsorbed dye molecules interact with graphene using π-π and charge transfer interaction.[35] Accordingly, a dye which is a good electron donor (MB in present case) interacts more strongly with hole-doped graphene (BG), while a dye which is a poorer electron donor interacts more strongly with electron-doped graphene (NG). This selective interaction is reflected in the photodegradation kinetics as well, since photodegradation occurs through the electrons transferred to graphene from $TiO_2$. The electronic structure of graphene, therefore, plays a significant role in the photodegradation kinetics.

## 4.6 References


[1] A. J. Bard ***J.*** *Phys. Chem.* 1982***, 86,*** 172.

[2] K. Kalyanasundaram, M. Gratzel, E. Pelizzetti. *Coord. Chem. Rev.* 1986**, 69,** 57**.**

[3] S. T. Craig, D. F.Ollis, *Journal of Catalysis* 1990, **122**, 178.

[4] G. Pfaff, P. Reynders, *Chem. Rev.* 1999, ***99***, 1963.

[5] A. Salvador, M. C. Marti, J. R. Adell, R. A. March, J. G. *J. Pharm. Biomed. Anal.* 2000, ***22***, 301

[6] R. Zallen, M. P. Moret, *Solid State Commun.* 2006, ***137***, 154.

[7] J. H. Braun, A. Baidins, R. E. Marganski, *Prog. Org. Coat.* 1992, ***20***, 105.

[8] S. A. Yuan, W. H. Chen, S. S. Hu, *Mater. Sci. Eng. C* ,2005, **25**, 479.

[9] A. Fujishima, K. Honda, *Nature* 1972, ***37***, 238.

[10] A. Fujishima, T. N. Rao, D. A. Tryk, *J. Photochem. Photobiol. C*, 2000, **1**, 1.

[11] S. N. Frank, A. J. Bard , *J Phys Chem,* 1977, **81**, 1484.

[12] A. L. Pruden, D. F. Ollis, *J Catal*, 1983, **82**, 404.

[13] C-Y. Hsiao, C-L. Lee and D. F. Ollis, *J Catal* ,1983, **82**, 418.

[14] T. Matsunaga, R. Tomato, T. Nakajima and H. Wake, *Microbiol Lett.*,1985, **29**, 211.

[15] B. O'Regan, M. Gratzel, *Nature,* 1991, **353**, 737.

[16] U. Diebold, *Surface Science Reports,* 2003, **48**, 53.

[17] J. M. Herrmann, *Topics in Catalysis* 2005**, 34**, 49.

[18] B. Ohtani, *Chem. Lett.* 2008, **37**, 217.

[19] P. V. Kamat, *J. Phys. Chem. C,* 2007, **111,** 2834.

[20] N. Serpone, E. Pelizzetti *Photocatalysis: fundamentals and applications.* New York; Chichester: Wiley; 1989.

[21] S. Malato, P. Fernandez, M. I. Maldonado, J. Blanco, W. Gernjak, *Catal. Today*, 2009,**147**,1

[22] A. Kudo, Y. Miseki, *Chem. Soc. Rev*, 2009, **38**, 253

[23] N. Satoh, T. Nakashima, K. Kamikura, K. Yamamoto, *Nat. Nano.* 2008, **3**, 106.

[24] V. Chhabra,V. Pillai, B. K. Mishra, A. Morrone, D. O. Shah, *Langmuir* 1995,**11**, 3307.

[25] Y. Yao, G. Li, S. Ciston, R. M. Lueptow, K. A. Gray, *Environ. Sci. Technol.* 2008, **42**, 4952.

[26] W. Wang, P. Serp, P. Kalck, J. L. Faria, *J. Mol. Catal. A: Chem*, 2005, **235**, 194.

[27] P. Serp, M. Corrias, P. Kalck, *Appl. Catal. A*, 2003, **253**, 337.

[28] K. Woan, G. Pyrgiotakis, W. Sigmund, *Adv. Mater.* 2009, **21**, 2233.

[29] A. K. Geim, 2009, **324**, 1530.

[30] C. N. R. Rao, A. K. Sood, K. S. Subrahmanyam, A. Govindaraj, *Angew. Chem. Int. Ed*, 2009, **48**, 7752.

[31] D. A. Areshkin, C. T. White, *Nano Lett.* 2007, ***7***, 3253.

[32] S. R. C. Vivekchand, C. S. Rout, K. S. Subrahmanyam, A. Govindaraj, C. N. R. Rao, *J. Chem. Sci.*, 2008, **120**, 9.

[33] S. Stankovich, D. A. Dikin, G. H. B. Dommett, K. M. Kohlhaas, *Nature* 2006, **442**, 282.

[34] G. Williams, B. Seger, P. V. Kamat. *ACS Nano*, 2008, **2**, 1487.

[35] H. Zhang, X. Lv, Y. Li, Y. Wang, J. Li, *ACS Nano*, 2009, **4**, 380.

[36] K.S. Subrahmanyam, L.S. Panchakarla, A. Govindaraj, C.N.R. Rao, *J. Phys. Chem. C* 2009, **113**, 4257.

[37] L. S. Panchakarla, K. S. Subrahmanyam, S. K. Saha, A. Govindaraj, H. R. Krishnamurthy, U. V. Waghmare, C. N. R. Rao, *Adv. Mater*. 2009, **21**, 4726.

[38] K. S. Subrahmanyam, S. R. C. Vivekchand, A. Govindaraj, C.N.R. Rao, *J. Mater. Chem.* 2008, **18,** 1517.

[39] Y. Liang, H. Wang, H.S. Casalongue, Z. Chen, H. Dai., *Nano Res.* 2010, **3,** 701.

[40] C.N.R. Rao, R. Voggu, *Materials Today*, 2010, **13**, 34.

[41] A. Das, S. Pisana, B. Chakraborty, S. Piscanec, S.K. Saha, U.V. Waghmare, K.S. Novoselov, H.R. Krishnamurthy, A.K. Geim, A.C. Ferrari, A.K. Sood, *Nature Nanotech*, 2008, **3**, 210.

# CHAPTER 5

# A RAMAN STUDY OF THE INTERACTION OF ELECTRON-DONOR AND -ACCEPTOR MOLECULES WITH CHEMICALLY DOPED GRAPHENE


## Summary*

Graphene is a fascinating two-dimensional nanomaterial with unique electronic structure and properties. Effects of interaction of nitrogen- and boron-doped few-layer graphene with electron-donor and -acceptor molecules have been investigated by employing Raman spectroscopy and the results compared with those of interaction with few-layer pristine graphene. The G-band position of doped graphene got affected with increasing concentration of tetrathiafulvalene (TTF) which are electron-donors and increasing concentration of tetracynoethylene (TCNE) which are electron-acceptor molecules. The 2D band position is also affected and decreases markedly with the concentration of either. The present study, demonstrates how the electronic structure and phonons of doped graphene are markedly affected by interaction with electron-donor and –acceptor molecules. We have also compared results with nitrogen-doped single walled carbon nanotubes.



***** A paper based on this work has been published in *Journal of Molecular Structure (2012).*

## Chapter 5

### 5.1 Introduction

Graphene, the mother of all graphitic materials exhibits a number of exciting physical properties, previously not observed at nanoscale.[1,2] In particular, the band structure of graphene exhibits two intersecting bands at two in-equivalent K points in the reciprocal space, and its low energy excitations are massless Dirac fermions near these K points because of the linear (photon-like) energy momentum dispersion relationship. This results in very high electron mobility in graphene, which can be further improved significantly, even up to ~$10^5$ $cm^2$/V.s. Electron or hole transport in field-effect devices based on graphene can be controlled by an external electric field. It has been demonstrated theoretically that the chiral massless Dirac fermions of graphene propagate anisotropically in a periodic potential, which suggests the possibility of building graphene based electronic circuits from appropriately engineered periodic surface potential patterns, without the need for cutting or etching. Graphene-based devices can be expected to have many advantages over silicon-based devices. However, precise control of the carrier type and concentration in graphene is not easy. Up to now, most of the graphene samples were either deposited on a $SiO_2$ surface or grown on a SiC surface, and these epitaxial graphenes are usually electron doped by the substrate.[3] To control the n-type carrier concentration in the graphene, alkali metal atoms have been deposited on graphene. The single, open-shell $NO_2$ molecule is found to be a strong acceptor, whereas its equilibrium gaseous state $N_2O_4$ acts as a weak dopant and does not result in any significant doping effect.[4] Thus, it is desirable and crucial to develop new method to precisely control the carrier type and concentration in graphene for further

development of graphene-based nanoelectronics. The control of carrier type and concentration has been achieved in SWNTs by electrochemical doping or chemical doping.

### 5.1.1 Raman spectroscopy

Raman spectroscopy has emerged as an effective probe to characterize graphene sample in terms of the number of layers and their quality.[5,6] Single-layer graphene shows the well-known G-band characteristic of the $sp^2$ carbon network around 1580 $cm^{-1}$. The D band around 1350 $cm^{-1}$ and D' band around 1620 $cm^{-1}$ are defect induced. The 2D band at ~2680 $cm^{-1}$ differs in single and few-layer graphene and can be understood on the basis of the double resonance Raman process involving different electronic dispersion. The 2D band can be employed to determine the number of layers in few-layer graphene. By combining Raman experiments with *in-situ* transport measurements of graphene in field-effect transistor geometry, it has been shown that the G-modes of single- and bi-layer graphenes blue shift on doping with electron as well as holes. On the other hand, the 2D band blue-shifts on hole doping whereas it red shifts on doping with electrons.[7,8] The relative intensity of the 2D band is quite sensitive to doping. Theoretical calculations based on time-dependant perturbation theory have been employed to explain the observed shifts of the G-band. Comparison between theory and experiment, however, is not entirely satisfactory at high doping levels ($>1x10^{13}/cm^2$) and the disagreement is greater for the 2D band. In the case of bi-layer graphene,[8] the blue shift of the G-band with doping has contributions from phonon-induced inter-band and intra-band electronic transitions, thereby giving an experimental measure of the overlap integral between A and B atoms in the two layers.

Furthermore, the in-plane vibration in bi-layer graphene splits into a symmetric Raman active mode ($E_g$) and an anti-symmetric infrared active mode ($E_u$). Doping dependence of these modes has been examined by Raman scattering[9] and infrared reflectivity measurements.[10]

### 5.1.2 Charge-transfer doping of carbon nanotubes

Doping of SWNTs and double-walled carbon nanotubes (DWNTs) with bromine and iodine has been investigated.[11-14] Charge-transfer doping of DWNTs has been used to distinguish between the behavior of the S/M and M/S outer/inner semiconducting (S) and metallic (M) tube configurations. The binding of electron accepting molecules ($F_4$TCNQ (2,3,5,6-tetrafluoro-7,7,8,8-tetracyanoquinodimethane)) and $NO_2$ to SWNTs leads to a threshold voltage shift towards positive gate voltages, while the binding of electron donating molecules ($NH_3$ and polyethylenimine) leads to a shift towards negative gate voltages.[15-17] Field-effect transistor (FET) devices made of semiconducting SWNTs have been used to obtain quantitative information on charge-transfer with aromatic compounds.[18] Stoddart *et al.*[19] have fabricated SWNT/FET devices to investigate the electron/charge-transfer with the donor-acceptor SWNT hybrids. A SWNT/FET device, functionalized non-covalently with a zinc porphyrin derivative shows that SWNTs act as electron donors and that the porphyrin molecules act as the electron acceptors. There are various efforts in the literature to tune the electronic properties of SWNTs. Charge transfer is well known in molecular

transfer pathway. For the intra-molecular case, the donor and/or acceptor molecule has to form a new chemical bond with the nanotubes. Obviously, the formation of new covalent band through functionalization of nanotubes may significantly modify the structure as well as its electronic properties. On contrary to that, one can self assemble some selective donor or acceptor molecules on the surface of SWNTs developing a possibility of charge-transfer. Recently, Voggu *et al*.[20] have investigated the interactions of various electron-withdrawing (chlorobenzene, nitrobenzene, tetracyanoquinodimethane (TCNQ), tetracyanoehtylene (TCNE)) and electron-donating (anisole, aniline, tetrathiafulvalene (TTF)) molecules with SWNTs to determine the sensitivity of their electronic structure and properties to molecular charge-transfer. They have investigate the effect of these donor and acceptor molecules as measured by both electronic and Raman spectra of the SWNTs and found the donor and acceptor molecules induce opposite effects in the electronic and Raman spectra as well as in electrical resistivity.

### 5.1.3 Charge-transfer doping of graphene

Graphene is near nearly semi-metal membrane, whose extreme physical strength and electron mobility at room temperature result from extensive electron conjugation and delocalization.[21] Charge-transfer to and from adsorbed species can shift the graphene Fermi level by a large fraction of an electron volt.[22,23] Such adsorption-induced chemical doping adjusts the Fermi level without introducing substitutional impurities, or basal plane reactions, that interrupt the conjugated network. Adsorption induced chemical doping may well become an important aspect of future graphene technologies. In graphene, consisting of

only a few-layers, chemical doping can result from both surface adsorption and intercalation between layers.

Organic molecules containing aromatic π-systems can be used to solubilize and modify the electronic structure of graphene. Charge-transfer with coronene tetracarboxylate (CT) has been exploited recently to solubilize graphene sheets.[24] It was shown that the CT molecules help to exfoliated few-layer graphene and selectively solubilize single- and double- layer graphenes. Graphene quenches the fluorescence of aromatic molecules, probably due to the electron transfer, feature of possible use in photovoltaics. Charge-transfer from fluorescent molecules to graphene has been utilized in visualization of graphene sheets by fluorescence microscopy[25] and in the use of graphene as a substrate for resonance Raman spectroscopy.[26] This chapter describes our efforts towards understanding the effect of the various electron-donor and acceptor molecules on the electronic structure of doped graphenes.

## 5.2 Scope of the present investigations

Nanocarbons are receiving great attention in the last few years due to their fascinating properties. Among the nanocarbons, carbon nanotubes and graphene have emerged as frontier areas of research, specially because of the novel electronic properties of the latter. The electronic structure of carbon nanotubes and graphene can be modified by electrochemical doping, chemical doping and doping through molecular charge transfer. Doping holes and electrons in single–walled carbon nanotubes (SWNTs) as well as in

graphene affects the Raman spectra markedly. The Raman G-band which corresponds to the tangential mode is highly sensitive to changes in the electronic structure of SWNTs and graphene. The G-band has been shown to stiffen and soften on interaction with electron-acceptor and electron-donor molecules respectively. The intensity and position of the Raman 2D band are also sensitive to doping. Recent studies have demonstrated that electron-donating molecules such as tetrathiafulvalene (TTF) and electron-withdrawing molecules such as tetracyanoehtylene (TCNE) bring about significant changes in the Raman spectra of graphene due to charge-transfer effects. Since the interaction of electron-donating molecules corresponds to electron-doping while interaction with electron-withdrawing molecules corresponds to hole doping, we considered it important to investigate the effect of electron-donor and electron-acceptor molecules on the Raman spectra of boron- and nitrogen-doped graphene which correspond to p- and n-type graphene respectively. For purpose of comparison, we have investigated the interaction of TTF and TCNE on nitrogen doped-SWNTs as well.

## 5.3 Experimental section

### 5.3.1 Synthesis of few-layer graphene

Few-layer graphene (HG) was prepared by the arc evaporation of graphite in a water-cooled stainless steel chamber filled with a mixture of hydrogen (200 Torr) and helium (500 Torr) without using any catalyst.[27] In a typical experiment, a graphite rod (Alfa Aesar with

99.999% purity, 6 mm in diameter and 50 mm long) was used as the anode and another graphite rod (13 mm in diameter and 60 mm in length) was used as the cathode. The discharge current was in the 100-150 A range, with a maximum open circuit voltage of 60 V. The graphene obtained by this method contains 2-4 layers.

### 5.3.2 Synthesis of doped graphenes and SWNTs

Boron-doped graphene (BG) was prepared by carrying out the arc-discharge using boron-packed graphite electrodes (3 at. % Boron) in the presence of $H_2$ (200 Torr) and He (500 Torr).[28] Nitrogen-doped graphene (NG) was prepared by carrying out arc-discharge of graphite in the presence of $H_2$ (200 Torr), He (200 Torr), and $NH_3$ (300 Torr).[28] The boron and nitrogen contents in the doped graphene samples were approximately 3 and 1 at. % respectively as estimated by X-ray photoelectron spectroscopy and electron energy loss spectroscopy. Thus, the BG and NG are lightly doped with the impurity atoms randomly distributed as evidenced from EELS measurements. The number of layers of the doped graphene samples was 2-4 as determined by atomic force microscopy. Nitrogen-doped SWNTs were prepared by arc discharge using the $Y_2O_3$+Ni catalyst with melamine as the nitrogen source.[29] The amount of nitrogen in the N-SWNTs was 2.5 at %.

## Characterization techniques

The number layers in the graphene samples prepared by us was 2-3 as indicated by AFM. TEM images were obtained with a JEOL JEM 3010 instrument fitted with a Gatan CCD camera operating at an accelerating voltage of 300 kV. FESEM images were obtained using a FEI Nova Nanosem 600. For Raman measurements, the graphene or SWNT samples were dispersed in benzene and drop-casted on a glass slide along with the appropriate concentration of TTF and TCNE. The concentration of these donor and acceptor molecules varied between $10^{-6}$ and $10^{-2}$ M. It is difficult to make good measurements beyond this concentration range.

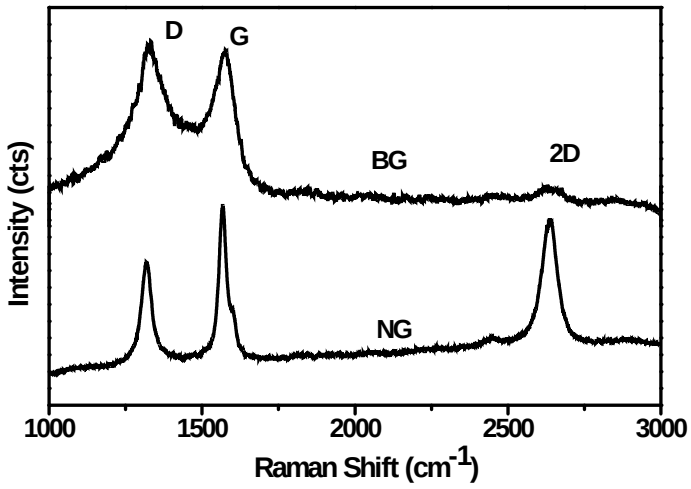


**Figure 1a** *Raman spectra of boron-doped (BG) and nitrogen-doped graphene (NG)*

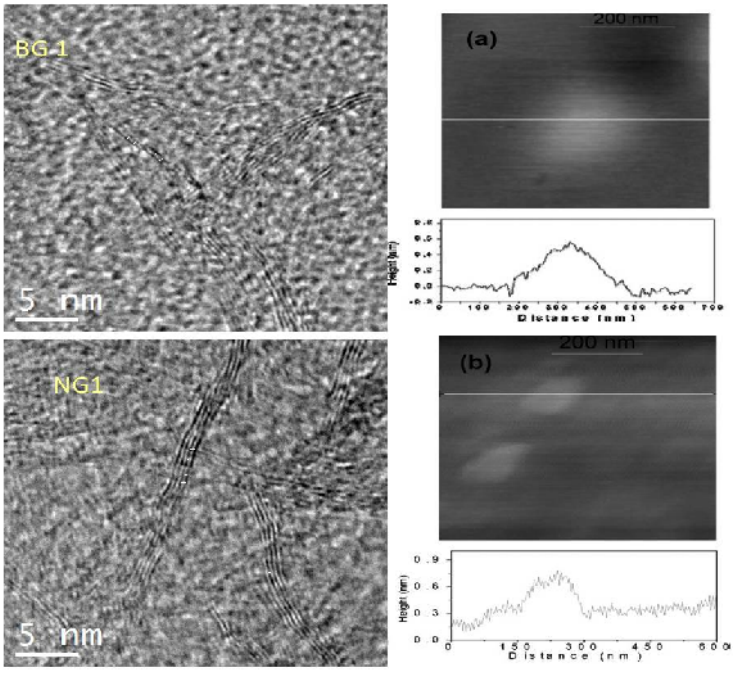


**Figure 1b.** *TEM images of (a)Boron- doped graphene (BG) and (b) Nitrogen-doped graphene (NG). AFM images of these samples are shown alongside*

The films so obtained were dried and Raman spectra recorded with a LabRAM HR high resolution Raman spectrometer (Horiba Jobin Yvon) using He–Ne Laser (λ = 632 nm). Experimental uncertainty in the Raman frequencies is well within ±1 $cm^{-1}$. AFM measurements were performed using a Bruker-Innova atomic force microscope. UV –Visible absorption spectra were recorded with a Perkin-Elmer spectrometer. The absorption spectra of the TCNE-graphene and TTF-graphene systems show clear signatures of TCNE and TTF, thereby confirming that the molecules were adsorbed on the graphene surface. The surfaces can be cleared easily after absorption showing the process to be reversible.

## 5.4 Results and Discussion

We have prepared boron-doped graphene (BG) by arc-discharge between two graphite electrodes was carried out where one of the electrodes was filled with elemental boron. The B-doped graphene sample so obtained also contained 2–4 layers.[28] We prepared nitrogen-doped (NG) graphene with 2–4 layers by carrying out arc discharge in the presence of $H_2$ + ammonia.[28] The samples were characterized Raman spectroscopy (Figure 1a), transmission electron microscopy and atomic force microscopy (Figure 1b) as described in the literature.[28]

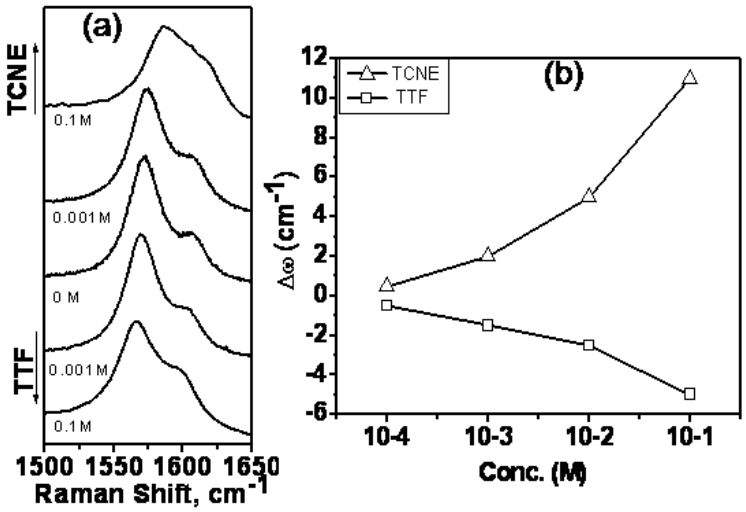


**Figure 2.** *(a) Raman G-band of undoped graphene caused by interaction with TCNE and TTF (b) plots of the G-band shifts against concentrations of TCNE and TTF.*

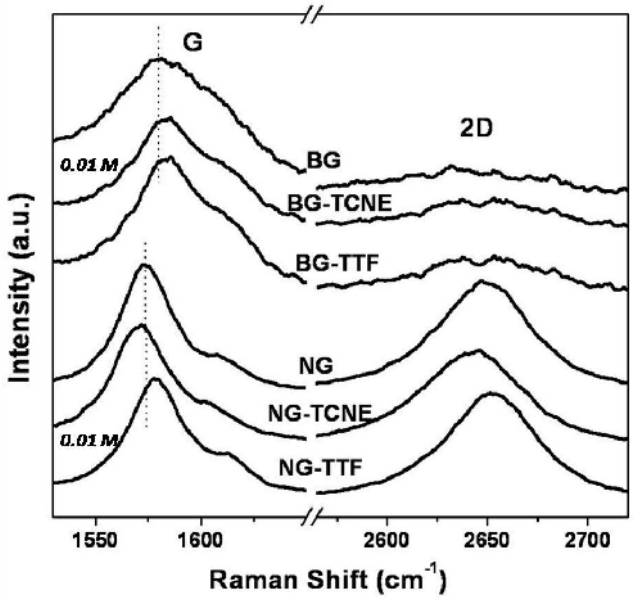


**Figure 3.** *Raman spectra of NG and BG and the effect of TCNE and TTF on the Raman G and 2D bands*

In Figure 2(a) we show the effect of interaction of TCNE and TTF on the Raman G-band of undoped graphene. The G-band is not affected in the absence of dopants. In Figure 2(b), we plot the shifts of the G-band on interaction of TCNE and TTF with undoped graphene. We see that TCNE causes greater shift of the G-band than TTF though in the opposite direction. The stiffening of BG is slightly smaller than in pure graphene.

In Figure 3 we show typical Raman spectra of NG and BG and the effect of TCNE and TTF on the Raman bands. BG shows the Raman G-band at 1581 $cm^{-1}$ and the 2D band at 2636 $cm^{-1}$. NG shows the G-band at 1574 $cm^{-1}$ and the 2D band at 2648 $cm^{-1}$. We first examine the interaction of BG with TTF and TCNE.

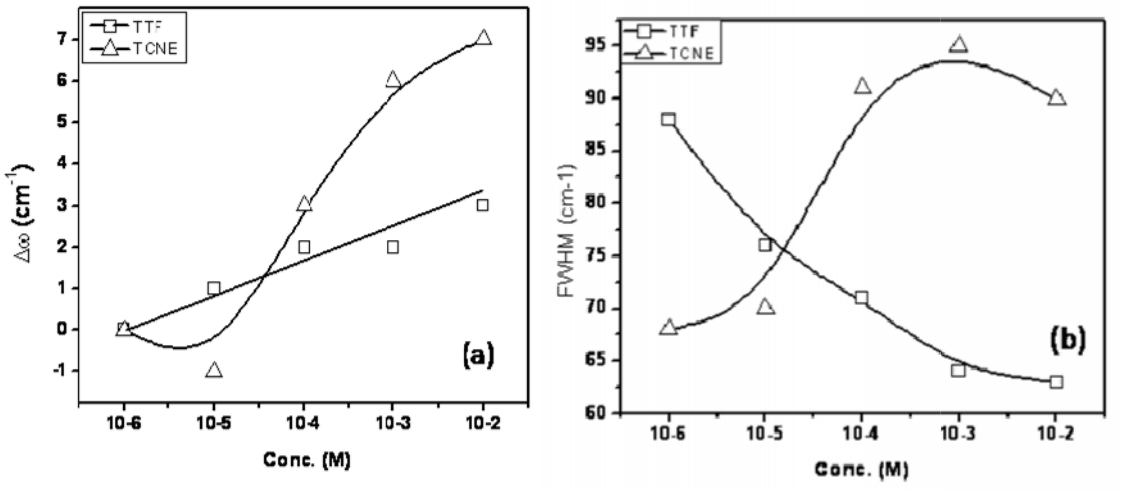


**Figure 4.** *(a) Raman shifts of the G-band of BG on interaction with varying concentrations of TTF and TCNE. (b) Change in the FWHM of G-band with the concentration of TTF and TCNE. The curves are drawn as guides to the eye.*

In Figure 4(a) we show the effect of concentration of TTF and TCNE on the Raman G-band of BG. We observe a significant shift of the G-band to higher frequencies on interaction with TCNE. Doping holes through interaction with TCNE stiffens the G-band significantly in the case of B-doped graphene just as in the case of undoped graphene.[30] Since TTF donates electrons, the G-band shift is negligible. In Figure 4(b), we show the variation of the full-width at half maximum (FWHM) of the G-band on interaction with TTF and TCNE with BG. We see that the FWHM increases with the increase in the concentration of TCNE while there is decrease in FWHM with increase in TTF concentration. Thus, the concentration dependence of the FWHM shows opposite trends in the case of electron-donor and -acceptor molecules.

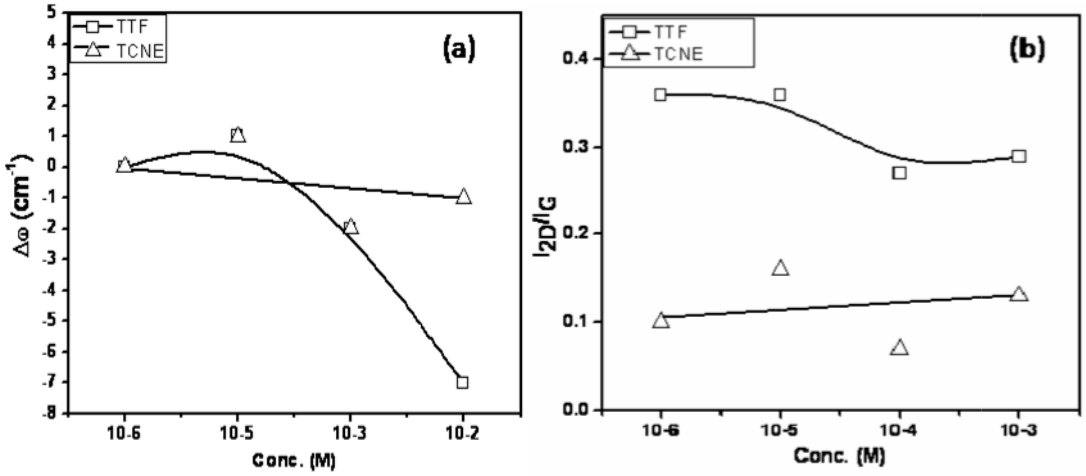


**Figure 5.** (*a) Raman shifts of the 2D band of BG on interaction with varying concentrations of TTF and TCNE. (b) Ratio of the relative intensities of the 2D and G-bands with varying the concentration of TTF and TCNE. The curves are drawn as guides to the eye*

In Figure 5(a) we show the effect of concentration of TTF and TCNE on the 2D band position of BG. There is greater softening of the 2D band in the case of TTF compared to that found with TCNE. In Figure 5(b), we plot the ratio of the intensity of the 2D band with respect to that of the G-band, $I_{2D}/I_{G,}$ as a function of concentration of TTF and TCNE. It is well documented that $I_{2D}/I_G$ ratio is sensitive to doping.[7] We obtained the $I_{2D}/I_G$ ratios, following Das *et al.*[7] TCNE has negligible effect on the $I_{2D}/I_G$ ratio while there is a measurable decrease at moderate concentrations of TTF.

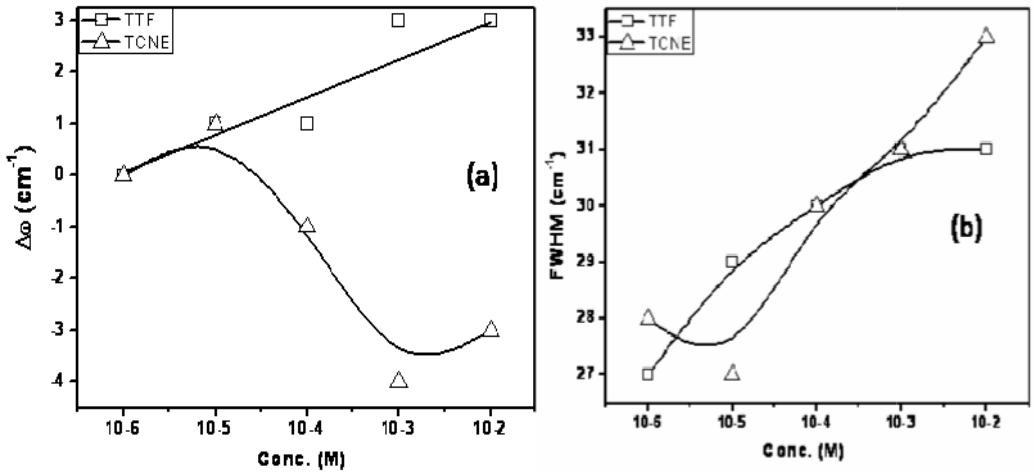


**Figure 6.** *(a) Raman shifts of the G-band of NG on interaction with varying concentrations of TTF and TCNE. (b) Change in the FWHM of the G-band with the concentration of TTF and TCNE. The curves are drawn as guides to the eye.*

In Figure 6(a) we show the variation of the G-band position of NG on interaction with TTF and TCNE. The G-band softens on interaction with TCNE and stiffens in the case of TTF. It is significant that TTF and TCNE shows opposite trends of the shifts of G-band. Undoped graphene shows stiffening of the G-band with TCNE and softening with TTF. This behavior of NG with TCNE is exactly opposite to that of BG. This is understandable since NG is electron doped while BG is hole doped. The FWHM of the G-band increases on interaction

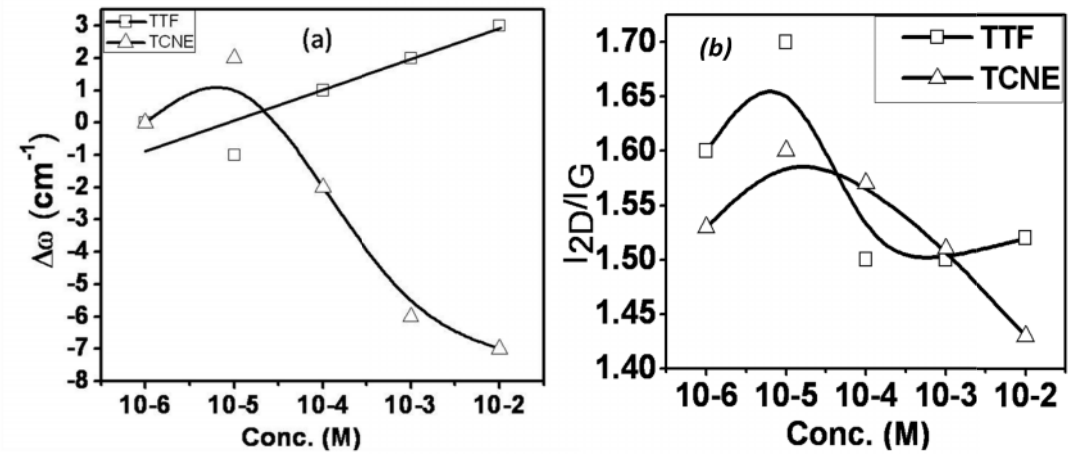


**Figure 7** *(a) Raman shifts of the 2D band of NG on interaction with TTF and TCNE. (b)The ratio of the relative intensities of the 2D and G-bands with varying the concentrations of TTF and TCNE. The curves are drawn as guides to the eye*

with both TTF and TCNE as shown in Figure 6(b), the effect of TCNE being slightly larger. The 2D band of NG shows opposite trends of the shifts on interaction with TTF and TCNE, the directions being similar to those of the G-band as shown in Figure 7 (a). The $I_{2D}/I_G$ ratio decreases sharply on interaction with these molecules (Figure 7 (b)).

We have carried out Raman measurements on N-SWNTs for purpose of comparison. Nitrogen-doped SWNTs shows stiffening of the G-band on interaction with TCNE and almost no effect in the case of TTF as shown in Figure 8(a). The significant effect observed with electron-withdrawing TCNE is what one would except of hole doping in N-SWNTs. The FWHM of the G-band decreases with increase in TCNE concentration while there is

negligible change with TTF concentration. The 2D band of N-SWNTs also shows stiffening on interaction with TCNE and no effect with TTF as shown in Figure 8(b).

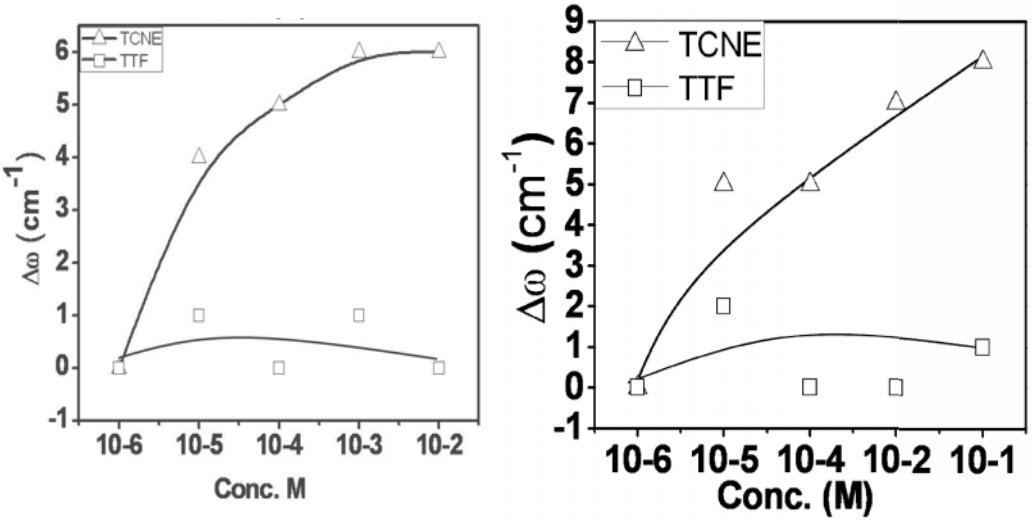


**Figure 8** *(a)Raman shifts of the G-band of N-SWNT on interaction with varying concentrations of TTF and TCNE.*

*(b) The Raman shifts of the 2D band of N-SWNT on interaction with varying concentrations of TTF and TCNE. The curves are drawn as guides to the eye*

It is noteworthy that B- and N-doped graphenes show differences in the Raman spectral changes on interaction with electron-donor and –acceptor molecules. Thus, BG shows a much greater stiffening of the G-band on interaction with TCNE compared to TTF. The change in the FWHM value is in opposite directions. NG shows softening of the G-band with TCNE and slight stiffening with TTF. The FWHM values, however, show similar changes. The 2D band softens significantly on interaction of BG with TTF and a negligible change

with TCNE. NG, on the other hand, shows significant softening of the G-band with TCNE and a little stiffening with TTF. The 2D band of NG becomes somewhat narrower on interaction with TTF and TCNE. That BG and NG show distinctly different Raman shifts due to molecular charge-transfer with donor and acceptor molecules is consistent with the fact that these graphenes have p-type and n-type character respectively. It is gratifying that Raman spectroscopy is such a fine probe to monitor minor changes in the electronic structure of the lightly doped graphenes, brought about by molecular charge-transfer (see Scheme I). A complete understanding of the nature of charge-transfer induced changes in the Raman spectra requires theoretical study.

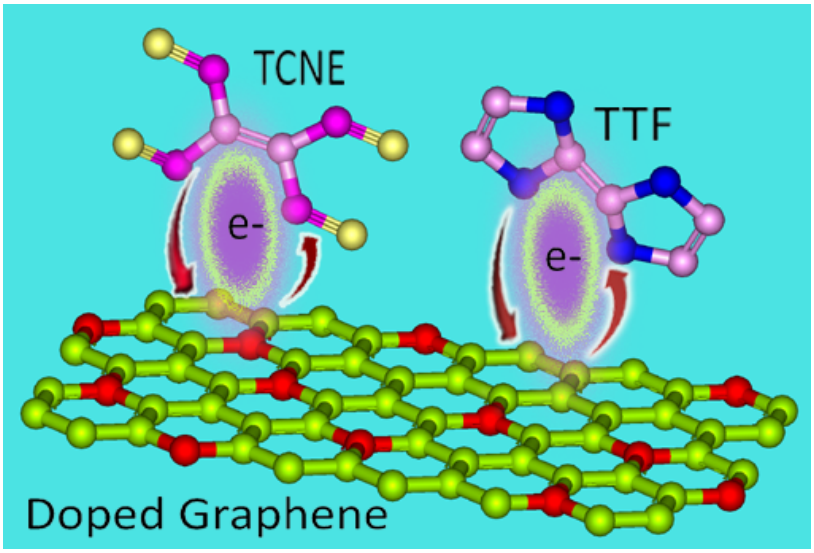


**Scheme I.** *Interaction of electron-donor (TTF) and -acceptor molecule (TTF) with chemically doped graphene.*

The changes in the Raman spectra of chemically doped graphenes observed on interaction with electron donor and acceptor molecules reflect the changes in the electronic structure on electron-phonon interaction. The G-band is a doubly degenerate phonon mode ($E_g$) of the $sp^2$ carbon network and stiffening of this band arises from the non-adiabatic removal of Kohn anomaly at r-point. Broadening of the G-band occurs due to the absence of blockage of the decay channels of the phonons into electron-hole pairs. Changes in the Raman spectrum by molecular doping would involve local structural changes and inhomogeneities arising from the interaction of the adsorbed molecules and randomness in the position, in addition to the changes in the Fermi energy caused by the charge transfer. These different channels of interaction of the donor and acceptor molecules can have effects on the G-band frequency of graphene that are opposite in sign, which is further effected by chemical doping of graphene. It is clear that interaction of electron donating molecules such as TTF (n-type doping) is weaker than that of electron accepting molecules such as TCNE (p-type doping). Thus, TCNE would have greater effect on the G-band frequency as reflected in a larger shift in the Fermi energy. Dynamical corrections to the G-band frequency dominate in this case, compensating the effects of opposite sign arising from any changes in structure. Such effects due to adsorbed molecules are further influenced by chemical doping of graphene. One, would, therefore, expect differences in the effects of molecular charge transfer between N- and B- doped graphenes.

## 5.5 Conclusions

The present study demonstrates that Raman spectra of chemically doped graphenes are sensitive to molecular charge-transfer with electron-donor and acceptor molecules. Not only do nitrogen- and boron-doped graphenes exhibit different changes in the Raman spectra on interaction with these molecules, but also the donor and acceptor molecules themselves have different effects on the Raman spectra of both n- and p-type graphenes. The observed changes are consistent with expectations based on theoretical considerations.

## 5.6 References

[1] A. K. Geim, K. S. Novoselov, *Nat. Mater.* 2007, **6**, 183.

[2] A. K. Geim, *Science* 2009, **324,** 1530.

[3] S. Y. Zhou, G. H. Gweon, A. V. Fedorov, P. N. First, W. A. de Heer, D. H. Lee, F. Guinea, A. H. Castro Neto, A. Lanzara, *Nat. Mater.* 2007, **6**, 770.

[4] T. O. Wehling, K. S. Novoselov, S. V. Morozov, E. E. Vdovin, M. I. Katsnelson, A. K. Geim, A. I. Lichtenstein, *Nano Lett.* 2007, **8**, 173.

[5] A. C. Ferrari, J. C. Meyer, V. Scardaci, C. Casiraghi, M. Lazzeri, F. Mauri, S. Piscanec, D. Jiang, K. S. Novoselov, S. Roth, A. K. Geim, *Phys. Rev. Lett.* 2006, **97**, 187401.

[6] A. Gupta, G. Chen, P. Joshi, S. Tadigadapa, Eklund, *Nano Lett.* 2006, **6,** 2667.

[7] A. Das, S. Pisana, B. Chakraborty, S. Piscanec, S. K. Saha, U. V. Waghmare, K. S. Novoselov, H. R. Krishnamurthy, A. K. Geim, A. C. Ferrari, A. K. Sood, *Nat. Nanotechnol.* 2008, **3,** 210.

[8] A. Das, B. Chakraborty, S. Piscanec, S. Pisana, A. K. Sood, A. C. Ferrari, *Phys. Rev. B* 2009, **79**, 155417.

[9] L. M. Malard, D. C. Elias, E. S. Alves, M. A. Pimenta, *Phys. Rev. Lett.* 2008, **101**, 257401.

[10] A. B. Kuzmenko, L. Benfatto, E. Cappelluti, I. Crassee, D. van der Marel, P. Blake, K. S. Novoselov, A. K. Geim, *Phys. Rev. Lett.* 2009, **103**, 116804.

[11] A. M. Rao, P. C. Eklund, S. Bandow, A. Thess, R. E. Smalley, *Nature* 1997, **388**, 257.

[12] J. Chen, M. A. Hamon, H. Hu, Y. Cheng, A. M. Rao, P. C. Eklund, R. C. Haddon, *Science* 1998, **282**, 95.

[13] G. M. do Nascimento, T. Hou, Y. A. Kim, H. Muramatsu, T. Hayashi, M. Endo, N. Akuzawa, M. S. Dresselhaus, *Nano Lett.* 2008, **8**, 4168.

[14] G. M. do Nascimento, T. Hou, Y. A. Kim, H. Muramatsu, T. Hayashi, M. Endo, N. Akuzawa, M. S. Dresselhaus, *J. Phys. Chem. C* 2009, **113**, 3934.

[15] M. Shim, A. Javey, N. W. Shi Kam, H. Dai, *J. Am. Chem. Soc.* 2001, *123*, 11512.

[16] J. Kong, N. R. Franklin, C. Zhou, M. G. Chapline, S. Peng, K. Cho, H. Dai, *Science* 2000, **287**, 622.

[17] T. Takenobu, T. Kanbara, N. Akima, T. Takahashi, M. Shiraishi, K. Tsukagoshi, H. Kataura, Y. Aoyagi, Y. Iwasa, *Adv. Mater.* 2005, **17**, 2430.

[18] A. Star, T.-R. Han, J.-C. P. Gabriel, K. Bradley, G. Gruner, *Nano Lett.* 2003, *3*, 1421.

[19] D. S. Hecht, R. J. A. Ramirez, M. Briman, E. Artukovic, K. S. Chichak, J. F. Stoddart, G. Gruner, *Nano Lett.* 2006, **6**, 2031.

[20] R. Voggu, C. S. Rout, A. D. Franklin, T. S. Fisher, C. N. R. Rao, *J. Phys. Chem. C* 2008, **112**, 13053.

[21] C. Lee, X. Wei, J. W. Kysar, J. Hone, *Science* 2008, **321**, 385.

[22] X. Wang, X. Li, L. Zhang, Y. Yoon, P. K. Weber, H. Wang, J. Guo, H. Dai, *Science* 2009, **324**, 768.

[23] F. Schedin, A. K. Geim, S. V. Morozov, E. W. Hill, P. Blake, M. I. Katsnelson, K. S. Novoselov, *Nat. Mater.* 2007, **6**, 652.

[24] A. Ghosh, K. V. Rao, S. J. George, C. N. R. Rao, *Chem. Eur. J.* 2010, **16**, 2700.

[25] J. Kim, L. J. Cote, F. Kim, J. Huang, *J. Am. Chem. Soc.* 2009, **132**, 260.

[26] L. Xie, X. Ling, Y. Fang, J. Zhang, Z. Liu, *J. Am. Chem. Soc.* 2009, **131**, 9890.

[27] K. S. Subrahmanyam, L. S. Panchakarla, A. Govindaraj and C. N. R. Rao, *J. Phys. Chem. C*, 2009, **113** ,4257

[28] L. S. Panchakarla, K. S. Subrahmanyam, S. K. Saha, A. Govindaraj, H. R. Krishnamurthy, U. V. Waghmare, C. N. R. Rao, *Adv. Mater.* 2009, **21**, 4726.

[29] L. S. Panchakarla, A. Govindaraj, C. N. R. Rao, *Inorg. Chim. Acta*, 2010, **363**, 4163.

[29] B. Das, R. Voggu, C. S. Rout, C. N. R Rao, *Chem. Commun.* 2008, **41**, 5155.